EPFL

Thèse n° 7230

Optimization-based Control, Estimation, and Identification of Urban Road Transport Systems

Présentée le 31 janvier 2020

à la Faculté de l'environnement naturel, architectural et construit
Laboratoire de systèmes de transports urbains
Programme doctoral en génie électrique

pour l'obtention du grade de Docteur ès Sciences

par

Isik Ilber SIRMATEL

Acceptée sur proposition du jury

Prof. C. N. Jones, président du jury
Prof. N. Geroliminis, directeur de thèse
Prof. M. Papageorgiou, rapporteur
Prof. B. De Schutter, rapporteur
Prof. J. Lygeros, rapporteur

École polytechnique fédérale de Lausanne

2020

Es ist des Lernens kein Ende.
— Robert Schumann

Ülkeme ve aileme...

Acknowledgments

I am extremely grateful to my supervisor Nikolas Geroliminis for his wise guidance, uplifting enthusiasm, and boundless support. I am particularly thankful to him for offering me an opportunity to pursue a Ph.D. at LUTS, placing confidence in me for so many years, and letting me explore many research directions freely without losing focus on the big picture. I consider it a privilege to have known him and worked with him, as he is both a great scientist and a good friend.

I would like to thank my committee members John Lygeros, Markos Papageorgiou, Bart De Schutter, and Colin Neil Jones, for taking the time to review this dissertation, the interesting discussion, and their valuable comments.

Being a member of the LUTS team was a great pleasure. I have enjoyed the good mood, the friendly atmosphere, and the motivating environment. Special thanks go to our dear secretary Christine Debossens for keeping the administrative side of the lab running smoothly, and her friendly and cheerful attitude. I would like to thank previous and current LUTS colleagues Anastasios Kouvelas, Caio Beojone, Claudia Bongiovanni, Dimitrios Tsitsokas, Emmanouil Barmpounakis, Leonardo Bellocchi, Martí Ferrer, Martin Repoux, Mehmet Yıldırımoğlu, Mikhail Murashkin, Mohammadreza Saeedmanesh, Mor Kaspi, Nan Zheng, Patrick Stokkink, Raphaël Lamotte, Semin Kwak, and Wei Liu. It has been a great pleasure to know you and work with you.

Moreover, I would like to express my sincere gratitude to Petros Ioannou for providing me with the opportunity of a productive three months research stay in his lab at the University of Southern California, and to Mehmet Yıldırımoğlu, with whom I had the opportunity to have a close and fruitful collaboration on some parts of this thesis.

My deepest gratitude goes to my parents, Rukiye Senem and Cihan, for their unconditional love and support for my whole life. To them I owe everything.

Lausanne, November 4, 2019 I. İ. S.

Abstract

Urbanization intensifies as a global trend, exposing transportation networks to ever increasing levels of congestion. As network usage increases with available infrastructure, building new roads is not a solution. Design of intelligent transportation systems, involving identification, estimation, and feedback control methods with dynamical traffic models, is emerging as a feasible way to improve operation of existing infrastructure. Nevertheless, complexity of large-scale networks, spatiotemporal propagation of congestion, and uncertainty in traveler choices present considerable challenges for modeling, estimation, and control of road transport systems. This dissertation focuses on development of novel and practicable optimization-based traffic control and estimation methods for improving mobility in large-scale urban road networks.

Part I is dedicated to identification, estimation, and control methods based on macroscopic traffic dynamics for perimeter controlled urban networks. Obtaining accurate estimates of model parameters and traffic states is critical for feedback perimeter control systems. In chapter 2, a nonlinear moving horizon estimation (MHE) scheme is proposed for combined state and demand estimation for a two-region urban network with dynamical modeling via macroscopic fundamental diagram (MFD). A traffic control framework consisting of identification, state estimation, and control methods is developed in chapter 3, enabling model-based feedback perimeter control of city-scale traffic.

Part II focuses on traffic management methods considering regional route guidance. Equipping traffic controllers with route guidance carries potential for high performance congestion management. Chapter 4 contains model predictive control (MPC) schemes integrating route guidance and perimeter control actuators, capable of superior performance compared to using only perimeter control. A hierarchical traffic controller is designed in chapter 5, employing a path assignment mechanism to realize macroscopic route guidance commands of a network-level MPC.

Keywords: traffic control, large-scale urban road networks, macroscopic fundamental diagram, perimeter control, route guidance, model predictive control, moving horizon estimation, model-based parameter estimation.

Zusammenfassung

Verstädterung verstärkt sich als globaler Trend und setzt Verkehrsnetze einem immer höheren Niveau von Stauung. Da Netzwerknutzung mit der verfügbaren Infrastruktur zunimmt, ist der Bau neuer Strassen keine Lösung. Der Entwurf intelligenter Transportsysteme, der Identifikation, Schätzung und Regelung mit dynamischen Verkehrsmodellen beinhaltet, erweist sich als praktikabler Weg zur Verbesserung des Betriebs der vorhandenen Infrastruktur. Dennoch stellen die Komplexität grosser Netzwerke, die räumlich-zeitliche Ausbreitung von Verkehrsstaus und die Ungewissheit bei der Wahl der Reisenden erhebliche Herausforderungen für die Modellierung, Schätzung und Regelung der Strassenverkehrssysteme dar. Diese Dissertation richtet sich auf die Entwicklung neuartiger und praktikabler optimierungsbasierter Verkehrsregelungs- und -schätzungsmethoden zur Verbesserung der Mobilität in grossen städtischen Strassennetzen.
Teil I befasst sich mit Identifikations-, Schätzungs- und Regelungsmethoden, die auf makroskopischer Verkehrsdynamik für perimetergesteuerte Stadtnetze basieren. Das Abrufen genauer Schätzungen von Modellparametern und Verkehrszuständen ist für Regelungssysteme mit Perimetersteuerung von entscheidender Bedeutung. In Kapitel 2 wird eine nichtlineare Zustandsschätzungsmethode auf bewegtem Horizont für die kombinierte Zustands- und Bedarfsschätzung für ein Stadtnetz mit zwei Regionen mit dynamischer Modellierung über ein makroskopisches Fundamentaldiagramm vorgeschlagen. In Kapitel 3 wird eine Verkehrsregelungsstruktur entwickelt, die aus Methoden zur Identifikation, Zustandsschätzung und Regelung besteht und die modellbasierte Regelung des Stadtverkehrs ermöglicht.
Teil II befasst sich mit Verkehrsleitungsmethoden unter Berücksichtigung der regionalen Routenführungssystemen. Die Ausstattung von Verkehrsreglern mit Routenfährung besitzt das Potenzial für ein leistungsstarkes Stauungsmanagement. Kapitel 4 enthält modellprädiktive Regelungsmethoden, die Aktuatoren für Routenführung und Perimetersteuerung integrieren und im Vergleich zur reinen Perimetersteuerung eine überlegene Leistung bieten. In Kapitel 5 wird eine hierarchische Verkehrsregelungsmethode entworfen, die einen Wegzuweisungsmechanismus verwendet, um makroskopische Routenführungsbefehle eines modellprädiktiven Reglers auf Netzwerkebene zu realisieren.

Schlüsselwörter: Verkehrsregelung, grosse städtische Strassennetze, makroskopisches Fundamentaldiagramm, Perimetersteuerung, Routenführung, modellprädiktive Regelung, Zustandsschätzung auf bewegtem Horizont, modellbasierte Parameterschätzung.

Contents

Chapter 1

Introduction

1.1 Background and motivation

Modeling and control of road traffic in large-scale urban road networks present considerable challenges. Large network size, inadequate infrastructure and coordination, spatiotemporal propagation of congestion, and the interaction between driver decisions and the traffic control system contribute to the difficulties faced when creating realistic models and designing effective control schemes for urban networks. Although considerable research has been directed towards designing efficient real-time traffic control schemes in the last decades (see [1] for a review), dynamical modeling and control design for heterogeneously congested networks at the city level remains a challenging problem. Traditional methods face difficulties when used for large-scale urban networks. As the system size increases, approaches based on centralized computations requiring a global system model become intractable.

Substantial research effort has been directed towards modeling and control of urban traffic, which usually focus on mesoscopic models keeping track of link-level dynamics with local control strategies. Based on the linear-quadratic regulator (LQR) problem, traffic-responsive urban control [2] represents a multivariable feedback regulator approach for network-wide urban traffic control, which has been tested both via simulations and field implementations (see [3], [4]). Inspired by the max pressure routing scheme for wireless networks [5], many local traffic control schemes have been proposed for networks of signalized intersections (see [6], [7]), which involve evaluations at each intersection requiring information exclusively from adjacent links. Although the high level of detail in mesoscopic traffic models is desirable for simulation purposes, the increased model complexity results in complications for large-scale control, whereas local control strategies might not be able to operate properly under heavily congested conditions, as they do not protect the congested regions downstream. In fact, a local controller will send more vehicles towards congested city centers as this will locally decrease queue lengths in major

directions. Thus, strategies that might penalize a few intersections locally to get better global system performance should be investigated. Another disadvantage of sophisticated local controllers is the need for detailed information on link traffic states, which can be difficult to estimate or measure.

Considering severe model uncertainty, difficulty of instrumentation, and excessive computational burden associated with detailed link-level modeling and control methods that need to consider all intersections and traffic lights for managing traffic in the entire city, such traffic management approaches appear to be practically infeasible. As an alternative to these link-level approaches, network-level methods employing perimeter control (i.e., control with actuation over a set of traffic lights on the perimeter between two neighborhood-sized areas) are receiving increasing attention as practicable approaches for city-wide traffic control. Based on macroscopic modeling of heterogeneously congested urban road networks, perimeter control involves manipulation of macroscopic traffic flows (i.e., rate of vehicles transferring between neighborhood-sized areas). However, employing aggregated modeling and control approaches using only a small subset of all intersections as actuators, the perimeter control method shows substantial promise in alleviating congestion and improving mobility in large-scale urban networks.

In the first step of the method, a heterogeneously congested city-sized road network is partitioned into a set of regions with homogeneous distribution of congestion, enabling development of trustworthy and low-error macroscopic traffic models. Then, a set of traffic lights on the boundaries (i.e, at the perimeters of the regions) between the regions are instrumented to be used as the actuators that can manipulate vehicle flows between the regions. After installing sensors over the city to measure the number of vehicles in each region (possibly also their destination regions), it is possible to construct feedback perimeter control systems for managing traffic and improving mobility at the city scale. Using various control design techniques, many perimeter control (or gating) methods have been developed for single-region [8]–[10] and multi-region [11]–[14] urban networks.

Macroscopic fundamental diagram (MFD) of urban traffic emerged as the primary modeling tool enabling aggregated modeling and control approaches for large-scale traffic management. An urban region with roughly homogeneous accumulation (i.e., small spatial link density heterogeneity) can be modeled using the MFD, which provides a unimodal, low-scatter, and demand-insensitive relationship between accumulation and trip completion flow. MFD as a concept was first proposed in [15], and experimentally proven to exist with dynamic features for urban areas in [16].

Although a powerful modeling tool, the MFD has also complications that might undermine its accuracy in expressing urban traffic dynamics: (a) Heterogeneous distribution of accumulation, especially in congested conditions, leads to the loss of a well-defined MFD for the urban region (see [17]–[20]), (b) hysteresis phenomena leading to different behaviors in the MFD shape for the onset and offset of congestion (see [21], [22]). While

heterogeneously congested networks do not exhibit well-defined MFDs, using clustering methods the network can be partitioned into a set of homogeneously congested (i.e., with low link density variance) regions, which can result in a set of well-defined MFDs for each region (see [23]–[25]). Proper treatment of boundary queues with MFD-based dynamics also necessitates considering multi-region models. Despite its shortcomings, the MFD substantially reduces the complexity of traffic models by avoiding the need for considering the densities of individual links of the network, which number in the thousands for city-scale systems. Appearing thus as an efficient modeling tool for expressing aggregated traffic dynamics, the MFD enables estimation and control design for network-level urban road traffic management.

Design of MFD-based controllers and state estimators requires consideration of the following points: (a) Constraints on the traffic states and control inputs, (b) multivariable nonlinear dynamics of the MFD-based network model, (c) possibility of having access to future information (e.g., estimates of the trip demands based on historical data), (d) relatively large sampling times (around 1-2 minutes). These points strongly suggest the suitability of using optimization-based control and estimation methods, namely model predictive control (MPC) and moving horizon estimation (MHE).

MPC is an advanced control technique based on real-time repeated optimal control, having a critical advantage over other control methods with its ability to handle constraints systematically. A computationally efficient method for tackling infinite horizon, constrained optimal control problems (OCPs), MPC provides approximate solutions to such problems via solving a series of finite horizon open-loop OCPs in receding horizon fashion. At each sampling instant, using the current state of the system as initial state, the finite horizon OCP is solved to obtain a sequence of optimal controls, the first of which is applied to the system and the whole procedure is repeated in the next sampling instant. Discussions on important issues of MPC can be found in [26] and an overview of theoretical aspects is given in [27]. Employing a dynamical model and past measurements to optimize over state trajectories in a finite horizon window, the MHE method (see, e.g., [28]) is the state estimation counterpart to MPC, specifying an advanced state estimation technique involving constrained nonlinear optimization.

Application of MPC to traffic control problems saw increased interest in the ITS literature in the last decades. Many MPC based methods for various settings of traffic control have been proposed: Ramp metering for freeway networks, variable speed limits, integrated route guidance and variable speed limits for freeway networks, and signal control for urban networks [29]–[33].

MPC schemes with MFD-based prediction models for urban networks began to appear only recently in the literature. In the first work on this direction, a nonlinear MPC design is given for a two-region urban network equipped with perimeter control actuation [13]. For the cooperative control of a mixed transportation network consisting of a freeway and

two urban regions, an MPC scheme is proposed in [34]. A hybrid MPC formulation is developed in [35] for an urban network equipped with both perimeter control systems and switching signal timing plans. A model with heterogeneity dynamics is described in [36] together with a hierarchical control system with MPC on the upper level. Considering performance constraints on travel time and delay metrics, a model predictive perimeter controller is designed in [37]. A multi-scale stochastic MPC is proposed in [38], with connected vehicles as sensors. In [39] a two-level hierarchical MPC is designed, with an MFD-based network-level centralized controller at the upper level and a distributed control system with link-based models at the lower level.

Feedback controllers are usually combined with state estimators for enabling closed-loop operation with noisy and indirect measurements on the system state. Literature on state estimation for road traffic focuses mainly on freeway networks: A mixture Kalman filter based on the cell transmission model is proposed in [40]. In [41], an extended Kalman filter is designed for real-time state and parameter estimation for a freeway network with dynamics described by the METANET model [42]. A particle filtering framework is proposed in [43] for a second order freeway traffic model that is efficiently parallelizable. Superiority of Lagrangian state estimation formulations over the Eulerian case using extended Kalman filters for the Lighthill-Whitham and Richards (LWR) model is reported in [44]. There is also some literature on urban traffic state estimation: In [45] an unscented Kalman filter is designed based on a kinematic wave model modified for urban traffic. An approach integrating the Kalman filter with advanced data fusion techniques is taken by [46] for urban network state estimation. A data fusion based extended Kalman filter is proposed in [47] for urban corridors based on the LWR model.

Works exploring actuation via route guidance with MFD-based models started appearing relatively recently in the literature. Considering two-route network abstractions, simple routing strategies are studied in [48]. MFD-based routing strategies are proposed in [20] for grid network management without traffic lights. In [49] an MFD-based taxi dispatch system is designed for improving taxi service quality. A route reservation method for minimizing travel times is developed in [50]. Based on the assignment model in [51], an iterative route guidance strategy is proposed in [52].

Considering the aforementioned works on traffic estimation and control, the following directions can be identified that are not well explored in the literature: (i) Development of state and parameter estimation methods considering large-scale traffic dynamics, (ii) integration of feedback perimeter control methods with MFD-based state estimation, (iii) evaluation of MFD-based estimation and control schemes on detailed microscopic simulations, (iv) integration of regional route guidance with perimeter control and path assignment. The work contained in this dissertation is motivated by the possibility of addressing these points by developing optimization-based identification, estimation, and control methods using MFD-based models, which are detailed in the objectives.

1.2 Objectives

The overarching objective is to design road traffic control systems for improving mobility in large-scale urban networks. Aiming to provide high performance yet practicable solutions for city-scale congestion management, the dissertation contains approaches integrating macroscopic dynamical traffic modeling with optimization-based estimation and control.

The objectives can be categorized into two distinct groups: (i) Development of estimation and control methods for perimeter controlled urban networks, (ii) design of traffic management schemes employing regional route guidance actuation. Objectives of individual chapters according to dissertation structure are listed as follows:

Part I Optimal Perimeter Control and Estimation for Urban Networks

Chapter 2 Nonlinear MHE for a two-region MFDs system The objective is to introduce a nonlinear MHE scheme for a two region large-scale urban road network with dynamics described via MFD. Various measurement configurations (i.e., types of sensors) likely to be encountered in practice are considered, such as measurements on regional accumulations and transfer flows without origin-destination information, and results of their observability tests are presented. By providing accurate estimates of accumulation states and inflow demands, the proposed state estimator is expected to enable operation of feedback perimeter control schemes under situations of noisy and incomplete measurements.

Chapter 3 Identification, estimation, and control for large-scale networks The chapter involves designing a traffic management framework consisting of model-based identification, estimation, and control for city-scale road networks. The identification method should enable computation of the MFD parameters leading to small prediction errors for the network model. Furthermore, extending the work in chapter 2, nonlinear MHE and economic MPC schemes for a four region network are developed, making use of the MFD parameters obtained by the proposed identification method. The framework should enable designing city-level traffic control systems based on macroscopic dynamics, yielding both a method for obtaining the model parameters, and a combined estimation-control scheme capable of operation under noisy measurements.

Part II Large-scale Traffic Management via Regional Route Guidance

Chapter 4 Integration of route guidance and perimeter control The aim is to develop economic MPC schemes integrating perimeter control and regional route guidance actuation, which distributes traffic flows exiting a region over its neighboring regions. The MPC schemes should improve mobility in

heterogeneously congested large-scale urban road networks, and adding route guidance is expected to yield improvements over using only perimeter control.

Chapter 5 Integration of route guidance and path assignment A hierarchical traffic management scheme is proposed for large-scale congestion control by integrating route guidance with assignment of vehicles to specific paths. Extending the work in chapter 4, an economic MPC with route guidance actuation at the upper-level is integrated with a path assignment mechanism recommending sub-regional paths for vehicles to follow at the lower-level. The scheme is expected to provide a practicable congestion management approach for improving mobility in urban networks.

1.3 Contributions

Main contributions

Considering the motivation and objectives, main contributions of the dissertation for each chapter can be listed as follows:

Part I Optimal Perimeter Control and Estimation for Urban Networks

Chapter 2 Nonlinear MHE for a two-region MFDs system A nonlinear MHE scheme capable of OD inflow demand and accumulation state estimation is proposed for a two-region large-scale urban network model with MFD-based dynamics, together with four practically motivated measurement compositions. Observability tests reveal that observability is retained for compositions with limited or no measurements on OD-based information. This has practical significance, since OD-based measurements are usually not available or difficult to obtain in real-time. Extensive macroscopic simulations show that the estimation performance of the proposed MHE scheme is fairly insensitive to increasing noise variance, and is superior to an extended Kalman filter (EKF). An important result is that the control performance of the combined MHE-MPC scheme is virtually insensitive to increasing variance in measurement noise, which is a practically relevant finding considering that perimeter control schemes have to operate under noisy conditions in the field. Further simulations revealed that assuming constant future demands in the MPC formulation yields control performances practically identical to the case with perfect demand information. Overall, the results indicate a strong potential towards implementation of MFD-based perimeter control, since the proposed MHE-MPC scheme is capable of high performance congestion management under severe conditions of measurement noise, limited or no OD-based information, and unknown future inflow demands.

Chapter 3 Identification, estimation, and control for large-scale networks A system identification method employing MFD-based dynamical model is introduced for model-based parameter estimation (MBPE) of large-scale urban networks. The method is based on the least squares prediction error approach, where the parameter estimation problem is cast as an optimization problem aiming to minimize the weighted least squares difference between the measurements and model predictions. Furthermore, MFD-based nonlinear MHE and economic MPC formulations are developed yielding a combined estimation and control framework for perimeter-controlled urban networks. The methods are applied to a four region urban network using detailed microscopic simulation experiments, with good estimation and control performance. These results specify the first application of optimization-based identification, estimation, and control methods in microscopic simulation tests involving MFD-based models with traffic states containing current and destination region information.

Part II Large-scale Traffic Management via Regional Route Guidance

Chapter 4 Integration of route guidance and perimeter control Economic MPC schemes using route guidance actuation are designed, together with a novel MFD-based urban network model. The chapter contains contributions in two aspects: (i) In the traffic modeling side a cyclic behavior prohibiting dynamic urban network model is proposed, with the potential of yielding more realistic simulation results compared to current MFD-based urban network models in the literature, (ii) in the control design aspect, integrating perimeter control and route guidance type actuators, economic nonlinear MPC schemes are developed for improving mobility in urban networks. Macroscopic simulation studies show the potential for substantial improvement in mobility through the use of route guidance, in comparison to control via perimeter control only. The results also reveal that since route guidance actuation cannot restrict flows, unlike perimeter control, it is unable to protect urban regions from severe congestion especially for cases with imperfect driver compliance.

Chapter 5 Integration of route guidance and path assignment A hierarchical traffic management scheme based on path assignment and route guidance is proposed, together with MFD-based regional and sub-regional dynamical traffic models. The chapter involves contributions in two aspects: (i) Based on integer linear programming (ILP), a path assignment mechanism is proposed that can translate upper-level and aggregated control actions (i.e. route guidance commands) into lower-level and disaggregated traffic decisions, (ii) heterogeneity effect and variable trip lengths are incorporated into the regional route guidance MPC framework. The proposed hierarchical scheme is evaluated in macroscopic simulations using a 49 sub-region network. The results indicate a great potential in making efficient use of network capacity via actuation over

paths and achieving improved mobility. Such a hierarchical traffic management scheme can potentially be implemented in real life applications for realizing macroscopic route guidance actuation.

Other contributions

In the period of the work towards the dissertation, a novel modeling and control approach for public transport operations was developed alongside the aforementioned main body of contributions on traffic estimation and control. A summary of the work is provided in the following.

Bus transport systems cannot retain scheduled headways without feedback control due to their unstable nature, leading to irregularities such as bus bunching, and ultimately to increased service times and decreased bus service quality. Traditional anti-bunching methods considering only regularization of spacings might unnecessarily slow down buses en route. Motivated by the importance of developing efficient modeling and control methods for public transport operations, in this work a mixed logical dynamical (MLD) systems approach is taken for developing bus speed control systems. The work contains contributions in two aspects: (i) For modeling, a computationally efficient MLD model is proposed, capable of capturing detailed dynamics of single line bus operations, involving interactions of bus motion and passenger flows between buses and stops. Taking 1 milliseconds per iteration, this bus system model can be used for simulation-based in-depth analyses of bus networks for evaluation of bus system management schemes. (ii) In the control aspect, a novel hybrid MPC is designed based on a simplified MLD bus system model for computational tractability. The hybrid MPC achieves consistently high bus system performance with a dual objective of spacing regularity and fast operation, by coordinating the buses operating on the line via manipulating their speeds in real time. By construction, the proposed MPC formulation results in convex mixed integer quadratic programming problems, enabling real-time feasible solutions with computation times less than 0.7 seconds. Performance of the hybrid MPC is compared to classical I- and PI-controllers from literature via simulations using the proposed MLD model. Results indicate the potential of the hybrid MPC in decreasing service times and improving headway regularity, even for decreased bus capacity values. Performance and real-time tractability of the proposed hybrid MPC suggest high value for practical applications. Preliminary results of this work are presented in:

- I. I. Sirmatel and N. Geroliminis, “Hybrid modeling and predictive control of bus transport systems”, in *Transportation Research Board 96th Annual Meeting*, 2017. [Online]. Available: https://trid.trb.org/view/1439090 [53]

- I. I. Sirmatel and N. Geroliminis, “Dynamical modeling and predictive control of bus transport systems: A hybrid systems approach”, *IFAC-PapersOnLine*, vol. 50,

no. 1, pp. 7499 –7504, 2017, Proceedings of the 20th IFAC World Congress. DOI: 10.1016/j.ifacol.2017.08.1067 [54]

- I. I. Sirmatel and N. Geroliminis, "Hybrid model predictive control of bus transport systems", in *17th European Control Conference (ECC)*, IEEE, 2018, pp. 1660–1665. DOI: 10.23919/ECC.2018.8550489 [55]

The study is published as a stand-alone article as:

- I. I. Sirmatel and N. Geroliminis, "Mixed logical dynamical modeling and hybrid model predictive control of public transport operations", *Transportation Research Part B: Methodological*, vol. 114, pp. 325–345, 2018. DOI: 10.1016/j.trb.2018.06.009 [56]

1.4 Structure

This dissertation consists of 6 chapters, which are briefly described in the following. The main 4 chapters (excluding chapters 1 and 6) are organized into 2 parts. Part I includes chapters 2 and 3, focusing on optimization-based control, estimation, and identification methods employing macroscopic traffic models for mobility improvement in perimeter controlled urban road networks. Part II includes chapters 4 and 5, containing development of large-scale traffic management schemes integrating route guidance-based economic MPC with perimeter control and path assignment, respectively. Each chapter is a complete stand-alone research article including an abstract, introduction, methodology, results, and conclusion with its own notation.

Chapter 2 contains a nonlinear MHE design for a perimeter controlled urban network with dynamics described as a two-region MFDs system. Various practical measurement configurations are presented, along with results of their observability tests. Extensive macroscopic simulations are used to compare the proposed method with an EKF with respect to state estimation and control performance. Preliminary results of this work are presented in:

- I. I. Sirmatel and N. Geroliminis, "Moving horizon estimation for model predictive perimeter control of multi-region MFD networks", in *Transportation Research Board 98th Annual Meeting*, 2019. [Online]. Available: https://trid.trb.org/view/1572773 [57]
- I. I. Sirmatel and N. Geroliminis, "Moving horizon demand and state estimation for model predictive perimeter control of large-scale urban networks", in *18th European Control Conference (ECC)*, IEEE, 2019, pp. 3650–3655. DOI: 10.23919/ECC.2019.8795828 [58]

Chapter 2 is a stand-alone article published as:

- I. I. Sirmatel and N. Geroliminis, "Nonlinear moving horizon estimation for large-scale urban road networks", *IEEE Transactions on Intelligent Transportation Systems*, 2019. DOI: 10.1109/TITS.2019.2946324 [59]

In chapter 3 a traffic management framework consisting of optimization-based identification, estimation, and control methods is developed for large-scale urban networks using MFD-based dynamical models. The identification procedure is used to obtain MFD parameters, which are then used in the dynamical models embedded in the combined state estimation and control scheme. Microscopic simulation studies on a four region urban network demonstrate operation of the framework. Chapter 3 is the last study performed during the work towards the dissertation. Preliminary results of the study are under review as:

- I. I. Sirmatel and N. Geroliminis, "Model-based identification, estimation, and control for large-scale urban road networks", in *19th European Control Conference (ECC)*, IEEE, under review [60],

while a journal article is under preparation.

Chapter 4 includes economic MPC designs integrating perimeter control with route guidance, and a cyclic behavior prohibiting MFD-based urban network model. Macroscopic simulation studies are used to demonstrate control performance of the various actuation schemes and effect of driver compliance to route guidance commands. Preliminary results of this work are presented in:

- I. I. Sirmatel and N. Geroliminis, "Model predictive control of large-scale urban networks via perimeter control and route guidance actuation", in *55th IEEE Conference on Decision and Control (CDC)*, IEEE, 2016, pp. 6765–6770. DOI: 10.1109/CDC.2016.7799311 [61]
- I. I. Sirmatel and N. Geroliminis, "Integration of perimeter control and route guidance in large-scale urban networks via model predictive control", in *Transportation Research Board 96th Annual Meeting*, 2017. [Online]. Available: https://trid.trb.org/view/1438872 [62]

Chapter 4 is a stand-alone article published as:

- I. I. Sirmatel and N. Geroliminis, "Economic model predictive control of large-scale urban road networks via perimeter control and regional route guidance", *IEEE*

Transactions on Intelligent Transportation Systems, vol. 19, no. 4, pp. 1112–1121, 2018. DOI: 10.1109/TITS.2017.2716541 [63]

In chapter 5 a hierarchical traffic control scheme is developed, integrating regional route guidance-based economic MPC and a sub-regional path assignment mechanism, for improving mobility in large-scale networks, together with MFD-based regional and sub-regional traffic models. Operation of the hierarchical scheme is demonstrated by macroscopic simulations with a network containing 49 sub-regions. In this study, the first author contributed the low-level modeling and path assignment approaches, while the second author contributed the economic MPC method. Preliminary results of this work are presented in:

- M. Yildirimoglu, I. I. Sirmatel, and N. Geroliminis, "Hierarchical management of heterogeneous large-scale urban networks via path assignment and regional route guidance", in *Transportation Research Board 97th Annual Meeting*, 2018. [Online]. Available: https://trid.trb.org/view/1495726 [64]

Chapter 5 is a stand-alone article published as:

- M. Yildirimoglu, I. I. Sirmatel, and N. Geroliminis, "Hierarchical control of heterogeneous large-scale urban road networks via path assignment and regional route guidance", *Transportation Research Part B: Methodological*, vol. 118, pp. 106–123, 2018. DOI: 10.1016/j.trb.2018.10.007 [65]

Finally, chapter 6 contains conclusions of the dissertation together with the summaries of the main contributions, discussions on potential practical applications, and directions for future research.

Part I

Optimal perimeter control and estimation for urban networks

Chapter 2

Nonlinear MHE for a two-region MFDs system

2.1 Introduction

Most works in the literature on perimeter control assume that: a) Current values of accumulations $n_{ij}(t)$ and inflow demands $q_{ij}(t)$ (with i and j denoting the current and destination regions, respectively) are known (i.e., measured perfectly), b) future trajectories of inflow demands $q_{ij}(t)$ are available. Such assumptions are problematic for practice due to following reasons: 1) Measurements are corrupted by noise, 2) measuring $n_{ij}(t)$ or $q_{ij}(t)$ might be impossible, costly, or problematic due to privacy reasons, as they require information on the origins and destination of drivers, 3) assuming that future values of $q_{ij}(t)$ are known is unrealistic, as it is impossible to know OD demands exactly in advance. We address the first two shortcomings directly in this chapter by a nonlinear MHE scheme. Employing a dynamical model and past measurements to optimize over state trajectories in a finite horizon window, the MHE method specifies an advanced state estimation technique involving constrained nonlinear optimization. The method is integrated with a model predictive perimeter control scheme to provide a practicable traffic management framework, able to deal with cases of noisy measurements and lack of availability of information on $n_{ij}(t)$ and/or $q_{ij}(t)$.

Literature review is not included here; it is given for the whole dissertation in chapter 1.

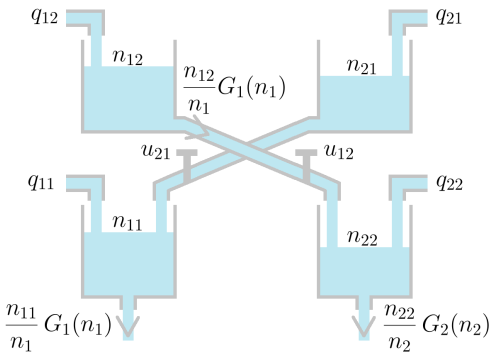

Figure 2.1 – Four reservoirs representation of an urban network with 2 regions.

2.2 Modeling of a two-region urban network

Consider a heterogeneous urban road network that can be partitioned into 2 homogeneous regions (see fig. 2.1). Each region i, with $i \in \{1, 2\}$, has a well-defined outflow MFD $G_i(n_i(t))$ (veh/s), which is the outflow (i.e., trip completion flow) at accumulation $n_i(t)$. The flow of vehicles appearing in region i and demanding trips to destination j (i.e., origin-destination (OD) inflow demand) is $q_{ij}(t)$ (veh/s), whereas $n_{ij}(t)$ (veh) is the accumulation in region i with destination j, while $n_i(t)$ (veh) is the regional accumulation at time t; $n_i(t) = \sum_{j=1}^{2} n_{ij}(t)$. Between the two regions there exists perimeter control actuators $u_{12}(t)$ and $u_{21}(t) \in [u_{\min}, u_{\max}]$ (with $0 \leq u_{\min} < u_{\max} \leq 1$), that can restrict transfer flows. Dynamics of a 2-region MFDs network is [13]:

$$\dot{n}_{11}(t) = q_{11}(t) + M_{21}(t) - M_{11}(t) \tag{2.1a}$$
$$\dot{n}_{12}(t) = q_{12}(t) - M_{12}(t) \tag{2.1b}$$
$$\dot{n}_{21}(t) = q_{21}(t) - M_{21}(t) \tag{2.1c}$$
$$\dot{n}_{22}(t) = q_{22}(t) + M_{12}(t) - M_{22}(t), \tag{2.1d}$$

while $M_{ii}(t)$ and $M_{ij}(t)$ express the exit (i.e., vehicles disappearing from the network) and transfer flows (i.e., vehicles transferring between regions), respectively:

$$M_{ii}(t) = \frac{n_{ii}(t)}{n_i(t)} G_i(n_i(t)) \quad \forall i \in \{1, 2\} \tag{2.2a}$$
$$M_{ij}(t) = u_{ij}(t) \frac{n_{ij}(t)}{n_i(t)} G_i(n_i(t)) \quad \forall i \in \{1, 2\},\ j \neq i. \tag{2.2b}$$

It is important to note here that the above expressions for $M_{ii}(t)$ and $M_{ij}(t)$ involve approximating the outflow MFD $G_i(n_i(t))$ as the ratio of a production MFD $P_i(n_i(t))$ (veh.m/s) and a regional average trip length l_i (m) (that is assumed to be constant and OD-independent). Accumulation-based models can be improved using flows involving

OD-dependent trip lengths, which can be done, e.g., by rewriting eq. (2.2b) as follows:

$$M_{ij}(t) = \frac{n_{ii}(t)}{n_i(t)} \frac{P_i(n_i(t))}{l_{ij}}, \tag{2.3}$$

where l_{ij} (m) is the average trip length traveled inside region i for trips from i to j. Details of such models (and their extensions) can be found in [52] and [36]. In [16] the assumption of outflow being approximately equal to production divided by trip length was tested with real data without any OD information. Although the $P_i(n_i(t))/l_i$ approximation for outflow yields accumulation-based models that are adequate for control design with simplified system dynamics without delays, it should not be considered as a universal law. For example, strong demand fluctuations forming fast evolving transients can affect the distribution of trip lengths in a region at a specific time, possibly creating inaccuracies in $P_i(n_i(t))/l_i$ approximation of outflow.

All trips inside a region are assumed to have similar trip lengths (i.e., the origin and destination of the trip does not affect the distance traveled by a vehicle). Simulation and empirical results [16] suggest the possibility of approximating the MFD by an asymmetric unimodal curve skewed to the right (i.e., the critical accumulation n_i^{cr}, for which $G_i(n_i(t))$ is at maximum, is less than half of the jam accumulation n_i^{jam} that puts the region in gridlock). Thus, $G_i(n_i(t))$ can be expressed using a third degree polynomial in $n_i(t)$:

$$G_i(n_i(t)) = a_i n_i^3(t) + b_i n_i^2(t) + c_i n_i(t), \tag{2.4}$$

where a_i, b_i, and c_i are known parameters (which are to be extracted from historical data in practice). Multi-region dynamical modeling formulations for urban networks with more than two regions can be found in [36], [63].

2.3 Optimal estimation and control

2.3.1 Modeling for demand estimation

Obtaining accurate real-time information on inflow demands $q_{ij}(t)$ is difficult in practice; such measurements are either unavailable or highly noisy. Circumventing this problem is possible through including inflow demands in the state estimation procedure. Towards this end we define the inflow demand terms $q_{ij}(t)$ as state variables, yielding the augmented dynamical system:

$$\begin{bmatrix} \dot{n}(t) \\ \dot{u}(t) \\ \dot{q}(t) \end{bmatrix} = \begin{bmatrix} f_n(n(t), q(t), u(t)) \\ \delta(t) \\ \mathbf{0} \end{bmatrix}, \tag{2.5}$$

where $n(t)$ contains the accumulations $n_{ij}(t)$

$$n(t) = [n_{11}(t)\ n_{12}(t)\ n_{21}(t)\ n_{22}(t)]^{\mathrm{T}}, \tag{2.6}$$

$q(t)$ contains the inflow demands $q_{ij}(t)$

$$q(t) = [q_{11}(t)\ q_{12}(t)\ q_{21}(t)\ q_{22}(t)]^{\mathrm{T}}, \tag{2.7}$$

$u(t)$ contains the perimeter controls

$$u(t) = [u_{12}(t)\ u_{21}(t)]^{\mathrm{T}}, \tag{2.8}$$

whereas $f_n(\cdot)$ is the dynamics given in eq. (2.1), while $\mathbf{0}$ is a vector of zeros (expressing that the inflow demands are assumed to be constant in time).

Note that, to facilitate formulations related to state estimation, the perimeter controls $u_{12}(t)$ and $u_{21}(t)$ are defined here as state variables, with the actual control input vector being $\delta(t) = [\delta_{12}(t)\ \delta_{21}(t)]^{\mathrm{T}}$. The reason is that, state estimation is assumed to be conducted before computing the control input, thus during state estimation at time step t it is impossible to access $u(t)$ as it is not available yet.

Considering additive process noise $w(t)$, and measurements $y(t)$ corrupted by noise $v(t)$, we can write the dynamics and measurement as:

$$\dot{x}(t) = f(x(t), \delta(t)) + w(t) \tag{2.9}$$
$$y(t) = h(x(t)) + v(t), \tag{2.10}$$

where $x(t)$ is the augmented state

$$x(t) = [n(t)^{\mathrm{T}}\ u(t)^{\mathrm{T}}\ q(t)^{\mathrm{T}}]^{\mathrm{T}}, \tag{2.11}$$

$f(\cdot)$ is the augmented dynamical system given in eq. (2.5), $h(\cdot)$ is the measurement equation, while $w(t)$ contains unknown disturbances (i.e., process noise) expressing plant-model mismatch:

$$\begin{aligned} w(t) &= [w_n(t)^{\mathrm{T}}\ \mathbf{0}^{\mathrm{T}}]^{\mathrm{T}} \\ w_n(t) &= [w_{n_{11}}(t)\ w_{n_{12}}(t)\ w_{n_{21}}(t)\ w_{n_{22}}(t)]^{\mathrm{T}}, \end{aligned} \tag{2.12}$$

where $w_{n_{ij}}(t) \sim \mathcal{N}(0, \sigma^2_{w,n})$ is white Gaussian noise, modeling uncertainty in the dynamics $f_n(\cdot)$. As the inflow demands are modeled as constant parameters, their dynamics are assumed to be unaffected by process noise, whereas perimeter controls are directly manipulated by the controller without any associated uncertainty, thus these two terms have their associated process noise terms equal to 0.

2.3.2 Measurement compositions and observability

Measurement configurations

Measurements available in an application dictate which state variables can be included in the dynamical model that is used to design model-based estimation and control schemes. In this section we present some measurement configurations likely to be encountered in practice of large-scale urban road network management. The important question of whether the traffic state can be determined from available measurements (i.e., observability) will be tackled in the next section.

Measurements on accumulations $n_{ij}(t)$

One straightforward measurement configuration involves simply measuring all accumulations $n_{ij}(t)$:

$$\begin{aligned} y_\alpha(t) &= h_\alpha(x(t)) + v_\alpha(t) \\ h_\alpha(x(t)) &= n(t) \\ v_\alpha(t) &= [v_{n_{11}}(t)\ v_{n_{12}}(t)\ v_{n_{21}}(t)\ v_{n_{22}}(t)]^{\mathrm{T}}, \end{aligned} \tag{2.13}$$

where $v_{n_{ij}}(t) \sim \mathcal{N}(0, \sigma^2_{v,n_{ij}})$ is white Gaussian noise, modeling measurement noise of $n_{ij}(t)$. While in most works on MFD-based control it is assumed that measurements on $n_{ij}(t)$ are available, this might be difficult in practice with conventional sensors, since measuring $n_{ij}(t)$ requires drivers to report their destination at the start of the trip.

Measurement on regional accumulations $n_i(t)$ and transfer flows $M_{ij}(t)$

Compared to $n_{ij}(t)$, regional accumulations $n_i(t)$ and transfer flows $M_{ij}(t)$ are easier to measure as they require loop detectors only (dispersed inside a region for $n_i(t)$ and placed at the boundary between regions for $M_{ij}(t)$). Thus, a more practical measurement configuration involves measuring $M_{ij}(t)$ and $n_i(t)$:

$$\begin{aligned} y_\beta(t) &= h_\beta(x(t)) + v_\beta(t) \\ h_\beta(x(t)) &= [n_1(t)\ n_2(t)\ M_{12}(t)\ M_{21}(t)]^{\mathrm{T}} \\ v_\beta(t) &= [v_{n_1}(t)\ v_{n_2}(t)\ v_{M_{12}}(t)\ \ v_{M_{21}}(t)]^{\mathrm{T}}, \end{aligned} \tag{2.14}$$

where $v_{n_i}(t) \sim \mathcal{N}(0, \sigma^2_{v,n_i})$ and $v_{M_{ij}}(t) \sim \mathcal{N}(0, \sigma^2_{v,M_{ij}})$ are white Gaussian noise terms, modeling measurement noise of $n_i(t)$ and $M_{ij}(t)$, respectively.

Measurements on inflow demands $q_{ij}(t)$

In some well-instrumented applications it might be possible to measure all $q_{ij}(t)$ terms:

$$\begin{aligned} y_\gamma(t) &= h_\gamma(x(t)) + v_\gamma(t) \\ h_\gamma(x(t)) &= q(t) \\ v_\gamma(t) &= v_q(t), \end{aligned} \tag{2.15}$$

where $v_\gamma(t)$ is the noise associated with $q_{ij}(t)$:

$$v_q(t) = [v_{q_{11}}(t)\ v_{q_{12}}(t)\ v_{q_{21}}(t)\ v_{q_{22}}(t)]^{\mathrm{T}}, \tag{2.16}$$

where $v_{q_{ij}}(t) \sim \mathcal{N}(0, \sigma^2_{v_q})$ is white Gaussian noise, modeling measurement noise of $q_{ij}(t)$.

Measurements on regional inflow demands $q_i(t)$

Some applications might involve access to measurements on $q_i(t)$ instead of $q_{ij}(t)$ (e.g., when GPS information is collected for a sample of vehicles):

$$\begin{aligned} y_\zeta(t) &= h_\zeta(x(t)) + v_\zeta(t) \\ h_\zeta(x(t)) = \begin{bmatrix} q_{11}(t) + q_{12}(t) \\ q_{21}(t) + q_{22}(t) \end{bmatrix} &\quad v_\zeta(t) = \begin{bmatrix} v_{q_1}(t) \\ v_{q_2}(t) \end{bmatrix}, \end{aligned} \tag{2.17}$$

where $v_{q_i}(t) \sim \mathcal{N}(0, \sigma^2_{v,q_i})$ is white Gaussian noise, modeling measurement noise of $q_i(t)$.

Measurement compositions and observability test

Availability of measurements affects the possibility of observing the system state, which is related to the observability property of a dynamical system. Roughly stated, observability is about whether the state can be uniquely determined based on the measurements or not. A dynamical system (i.e., $f(\cdot)$ and $h(\cdot)$) has to be observable in order to do estimation. Observability of nonlinear systems can be checked using the *observability rank condition* developed in [66]. For input-affine systems (such as eq. (2.5)), which can be written as:

$$\begin{aligned} \dot{x}(t) &= f(x) + \sum_{j=1}^{m} g_j(x(t))u_j(t) \\ y_i(t) &= h_i(x(t)),\ i = 1, \ldots, p, \end{aligned}$$

where $x \in \mathbb{R}^l$ is the state, $u_j \in \mathbb{R}$ (with $j = 1, \ldots, m$) are control inputs, and $y_i \in \mathbb{R}$ (with $i = 1, \ldots, p$) are the measurements, it is possible to use a simpler form of the rank condition, as included in the software package developed in [67] or presented in an algorithm given in [68]. This observability test involves constructing the *observability*

codistribution [67]:

$$\Omega_O = \langle f, g_1, \ldots, g_m \mid \text{span}\{dh_1, \ldots, dh_p\}\rangle, \tag{2.18}$$

and checking its rank. If the rank of Ω_O is equal to l (i.e., dimension of the state x), then the observability rank condition is satisfied [67], [68], indicating that the system is locally weakly observable (see §3 in [66] for details).

To check observability of the two-region MFD-based urban network dynamics, we conducted tests for four measurement compositions based on the configurations given earlier:

$$\begin{aligned} h_1(x(t)) &= \begin{bmatrix} h_\alpha(x(t)) \\ h_\gamma(x(t)) \\ u(t) \end{bmatrix} \quad h_2(x(t)) = \begin{bmatrix} h_\alpha(x(t)) \\ h_\zeta(x(t)) \\ u(t) \end{bmatrix} \\ h_3(x(t)) &= \begin{bmatrix} h_\beta(x(t)) \\ h_\gamma(x(t)) \\ u(t) \end{bmatrix} \quad h_4(x(t)) = \begin{bmatrix} h_\beta(x(t)) \\ h_\zeta(x(t)) \\ u(t) \end{bmatrix}, \end{aligned} \tag{2.19}$$

where the compositions are: a) h_1 (with accumulations $n_{ij}(t)$ and inflow demands $q_{ij}(t)$), b) h_2 (with accumulations $n_{ij}(t)$ and regional inflow demands $q_i(t)$), c) h_3 (with regional accumulations $n_i(t)$, transfer flows $M_{ij}(t)$, and inflow demands $q_{ij}(t)$), d) h_4 (with regional accumulations $n_i(t)$, transfer flows $M_{ij}(t)$, and regional inflow demands $q_i(t)$). Note that the perimeter controls $u(t)$ are included in all compositions; they are known and thus need not be measured. Observability tests are done using the ProPac package [67] of the computer algebra tool Mathematica, where observability rank condition is checked for the dynamics eq. (2.5) and each measurement composition. In all four cases the observability rank condition is satisfied according to the results obtained from ProPac.

Since measurement configurations involving limited (i.e., h_2 and h_3) or no OD-based information (i.e., h_4) still yield observability, it is possible to design state estimators to reconstruct $n_{ij}(t)$ and $q_{ij}(t)$ from measurements. Deployment of traffic control schemes involving feedback on $n_{ij}(t)$ and $q_{ij}(t)$ is thus possible with state estimation even if these cannot be measured. This has important implications for practice, since $n_{ij}(t)$ and $q_{ij}(t)$ are difficult to measure.

2.3.3 Moving horizon estimation

We formulate the problem of finding state estimate trajectories for a moving time horizon extending a fixed length into the past, striking a trade-off between measurements and

the prediction model, as the following nonlinear MHE problem:

$$\underset{w_k}{\text{minimize}} \quad \sum_{k=-N_\text{e}}^{-1} \|w_k\|_Q^2 + \sum_{k=-N_\text{e}}^{0} \|v_k\|_R^2 \tag{2.20}$$

$$\text{subject to} \quad \text{for } k = -N_\text{e}, \ldots, 0: \tag{2.21}$$

$$v_k = y_{t+k}(t) - h(x_k) \tag{2.22}$$

$$\text{for } k = -N_\text{e}, \ldots, -1: \tag{2.23}$$

$$x_{k+1} = F(x_k, \delta_{t+k}(t), T_\text{e}) + w_k \tag{2.24}$$

$$\text{for } k = 1, \ldots, N_\text{e}: \tag{2.25}$$

$$\text{a) } 0 \leq n_{ij,k} \quad \forall i, j \in \{1, 2\} \tag{2.26}$$

$$\text{b) } n_{i,k} \leq n_{i,\text{jam}} \quad \forall i \in \{1, 2\} \tag{2.27}$$

$$\text{c) } 0 \leq q_{ij,k} \leq \bar{q}_{ij} \quad \forall i, j \in \{1, 2\}, \tag{2.28}$$

where k is the time interval counter internal to the MHE, N_e is the horizon of the MHE (i.e., estimation horizon), t is the current time step, Q and R are weighting matrices on the process and measurement noise, respectively, w_k, v_k, and x_k are the process noise, measurement noise, and state vectors, for the time interval k, respectively, $h(\cdot)$ is the measurement equation (one of the four given in eq. (2.19)), F is the discrete-time version of the dynamics given in eq. (2.9) with MHE sampling time T_e, whereas $\{y_{t+k}(t)\}_{k=-N_\text{e}}^{0}$ and $\{\delta_{t+k}(t)\}_{k=-N_\text{e}}^{-1}$ are past measurement and control input trajectories available at time step t, respectively, while $n_{ij,k}$, $n_{i,k}$, and $q_{ij,k}$ are the accumulation, regional accumulation, and inflow demand state variables internal to the MHE, respectively, with the constraints expressing their physical or known limits: a) accumulations are non-negative, b) regional accumulations cannot exceed jam accumulation, c) inflow demands are non-negative and cannot exceed some known upper bound $\bar{q}_{ij}$.

2.3.4 Model predictive control

We formulate the problem of finding the control inputs that minimize total time spent (TTS) for a finite horizon as the following economic MPC problem (based on [13]):

$$\begin{aligned}
\underset{\delta_k}{\text{minimize}} \quad & T \cdot \sum_{k=0}^{N_\text{c}} \sum_{i=1}^{2} \sum_{j=1}^{2} n_{ij,k} && (2.29)\\
\text{subject to} \quad & n_0 = \hat{n}_t(t) && (2.30)\\
& u_0 = u(t - T_\text{c}) && (2.31)\\
& |\delta_0| \leq \Delta_u && (2.32)\\
& \text{for } k = 0, \ldots, N_\text{c} - 1 : && (2.33)\\
& \quad n_{k+1} = F_n(n_k, \hat{q}_t(t), u_k, T_\text{c}) && (2.34)\\
& \quad u_{k+1} = F_u(\delta_k, T_\text{c}) && (2.35)\\
& \quad u_\text{min} \leq u_k \leq u_\text{max} && (2.36)\\
& \text{for } k = 1, \ldots, N_\text{c} : && (2.37)\\
& \quad 0 \leq n_{ij,k} \quad \forall i \in \{1, 2\} && (2.38)\\
& \quad \sum_{j=1}^{2} n_{ij,k} \leq n_{i,\text{jam}} \quad \forall i \in \{1, 2\}, && (2.39)
\end{aligned}$$

where k is the time interval counter internal to the MPC, N_c is the horizon of the MPC (i.e., prediction horizon), $\hat{n}_t(t)$ and $\hat{q}_t(t)$ are the information (either measured or estimated) available at time step t on the states $n(t)$ and $q(t)$ (with t being the current time step), Δ_u is the rate limiting parameter on control inputs, n_k, u_k, and δ_k, the accumulation state, perimeter control state, and control input vectors internal to the MPC, respectively, F_n and F_u are the discrete-time version of the corresponding dynamics given in eq. (2.5) with MPC sampling time T_c, whereas $n_{ij,k}$ and $n_{i,k}$ are the accumulation and regional accumulation state variables internal to the MPC. Note that future inflow demands for the prediction horizon are assumed to be constant and fixed to their estimated value. This assumption is analyzed in a later section.

The optimization problems given in eqs. (2.20) and (2.29) are nonconvex nonlinear programs, which can be solved efficiently via, e.g., sequential quadratic programming or interior point solvers (for details, see [69]).

Integrated state estimation and control

For the combined state estimation and perimeter control of large-scale urban networks, we propose a traffic management scheme integrating MHE and MPC, given in eqs. (2.20) and (2.29). Operation of the scheme is formalized in algorithm 1. We are interested in investigating how measurement errors, types of measurement and quality of estimation

(or even no estimation) influence performance of the MFD-based controllers. This is clearly an important aspect that deserves investigation before moving to field applications of MFD-based control.

Algorithm 1 Operation of state estimation and control.

At plant time step $t_\mathrm{p} = 0$, initialize simulation from $x(0)$.

1) At each MHE time step t_e (with $t_\mathrm{e} \in T_\mathrm{e} \cdot \mathbb{Z}_{\geq 0}$), given past measurements $\{y(t_\mathrm{e}-k)\}_{k=N_\mathrm{e}}^{0}$ and control inputs $\{\delta(t_\mathrm{e}-k)\}_{k=N_\mathrm{e}}^{1}$, solve the MHE problem (2.20) to obtain the state estimates $\{\hat{x}_{t_\mathrm{e}-k}(t_\mathrm{e})\}_{k=N_\mathrm{e}}^{0}$.
2) At each MPC time step t_c (with $t_\mathrm{c} \in T_\mathrm{c} \cdot \mathbb{Z}_{\geq 0}$), given the most current state estimate $\hat{x}_{t_\mathrm{c}}(t_\mathrm{c})$, solve the MPC problem (2.29) to obtain control inputs $\{\delta_{t_\mathrm{c}+k}(t_\mathrm{c})\}_{k=0}^{N_\mathrm{c}-1}$.
3) At each plant time step t_p (with $t_\mathrm{p} \in T_\mathrm{p} \cdot \mathbb{Z}_{\geq 0}$), apply the most current control input $\delta_{t_\mathrm{c}}(t_\mathrm{c})$ (with $t_\mathrm{c} \leq t_\mathrm{p}$) to the plant; if simulating, evolve system dynamics given in eq. (2.5) discretized in time with plant sampling time T_p.

Repeat steps 1, 2, and 3 for $t_\mathrm{p} \in T_\mathrm{p} \cdot \mathbb{Z}_{\geq 0}$ up to t_final.

2.4 Results

2.4.1 Congested scenario

All simulations are conducted on a 2-region urban network with the simulation model given in eq. (2.9) for representing the reality. The regions have the same MFD, with the parameters $a_i = 4.133 \cdot 10^{-11}$, $b_i = -8.282 \cdot 10^{-7}$, $c_i = 0.0042$, jam accumulation $n_{i,\mathrm{jam}} = 10^4$ (veh), critical accumulation $n_{i,\mathrm{cr}} = 3.4 \cdot 10^3$ (veh), maximum outflow $G(n_{i,\mathrm{cr}}) = 6.3$ (veh/s), for $i = \{1, 2\}$, which are consistent with the MFD observed in a part of downtown Yokohama (see [16]).

The dynamics are discretized with the Runge–Kutta method with a plant sampling time of $T_\mathrm{p} = 5$ s for simulation, while the sampling times of estimation and control are $T_\mathrm{e} = 10$ s and $T_\mathrm{c} = 90$ s, respectively (with the control sampling time reflecting a realistic value for traffic light cycle time). The MHE and MPC schemes are built using direct multiple shooting [70], while implementation is done using MPCTools [71], which is an interface to CasADi [72], with IPOPT [73] as solver, in MATLAB 8.5.0 (R2015a), on a 64-bit Windows PC with 3.6-GHz Intel Core i7 processor and 16-GB RAM. Horizons MHE and MPC are both chosen as 30 minutes, following the MPC tuning results [13]. Tuning for MHE is given in a later section. The perimeter controls are bounded as $0.1 \leq u_{ij}(t) \leq 0.9$, with a rate limit of $\Delta_u = 0.1$. Simulation length is $t_\mathrm{final} = 240$ minutes.

Standard deviations of the process and measurement noise are chosen as $\sigma_{w,n} = 0.5$ veh/s, $\sigma_{v,n_{ij}} = 1000$ veh, $\sigma_{v,q_{ij}} = 0.5$ veh/s, $\sigma_{v,n_i} = 1000$ veh, $\sigma_{v,M_{ij}} = 1$ veh/s, $\sigma_{v,q_i} = 0.5$ veh/s, specifying severe measurement and process noise conditions. Weighting matrices of the MHE (i.e., Q and R) contain the inverses of these values, to reflect the fact that the stage cost terms related to the process and measurement noises should be weighted inversely

proportional to the associated amount of uncertainty (that is, e.g., the measurements should be trusted more if the measurement noise has a lower variance).

Control performance is evaluated using average time spent per vehicle (TSPV), defined for a single experiment as:

$$\text{TSPV} = \sum_{t=1}^{t_{\text{final}}} \sum_{i=1}^{2} \sum_{j=1}^{2} \frac{n_{ij}(t)}{q_{ij}(t)}, \tag{2.40}$$

while for estimation performance we define two metrics based on the root-mean-square estimation error, one for $n_{ij}(t)$ and the other for $q_{ij}(t)$:

$$\text{RMSE}_n = \frac{1}{4} \sum_{i=1}^{2} \sum_{j=1}^{2} \sqrt{\frac{\sum_{t=1}^{t_{\text{final}}} (n_{ij}(t) - \hat{n}_{ij}(t))^2}{t_{\text{final}}}} \tag{2.41}$$

$$\text{RMSE}_q = \frac{1}{4} \sum_{i=1}^{2} \sum_{j=1}^{2} \sqrt{\frac{\sum_{t=1}^{t_{\text{final}}} (q_{ij}(t) - \hat{q}_{ij}(t))^2}{t_{\text{final}}}} \tag{2.42}$$

where $\hat{n}_{ij}(t)$ and $\hat{q}_{ij}(t)$ are the estimates computed by the MHE at time t, for $n_{ij}(t)$ and $q_{ij}(t)$, respectively.

In the congested scenario, the network is uncongested at the beginning, but faces increased inflow demands as time progresses. For the four measurement compositions with the proposed MHE-MPC method (with inflow demands fixed to their estimated values at time t for the prediction horizon of the MPC), the results are given in figs. 2.2 to 2.6, which contain the true, estimated, and when applicable, measured trajectories of accumulations $n_{ij}(t)$, inflow demands $q_{ij}(t)$, regional accumulations $n_i(t)$, transfer flows $M_{ij}(t)$, and regional inflow demands $q_i(t)$, true trajectories of regional accumulations $n_i(t)$, regional outflows $G_i(t)$, trip completion flows $M_{ii}(t)$, and perimeter controls $u_{ij}(t)$, together with the active parts of the outflow MFDs. A summary of more detailed results is given in table 2.1, which shows control and estimation performance metrics together with CPU times for the MHE and MPC, for the four measurement composition cases comparing an extended Kalman filter (EKF) with the proposed MHE method (both using MPC as the controller), together with a no control case (with perimeter controls fixed to their maximum value of 0.9), and a y-MPC case representing MPC directly using measurements of $n_{ij}(t)$ (i.e., without state estimation).

The results in figs. 2.2 to 2.6 suggest that the proposed MHE-MPC scheme is successful in managing congestion even under severe noise conditions with measurements having partial information (i.e., h_2, h_3, and h_4, given in eq. (2.19)). For the h_1 case depicted in fig. 2.2, despite the significant measurement noise present in both in $q_{ij}(t)$ and $n_{ij}(t)$ (with $\sigma_{v,q_{ij}} = 0.5$ veh/s and $\sigma_{v,n_{ij}} = 1000$ veh), the estimation errors are small resulting in high control performance. From the y-MPC results (i.e., MPC without MHE) in figures (i) and (j) in fig. 2.2, it can be observed that without estimation the network reaches congested

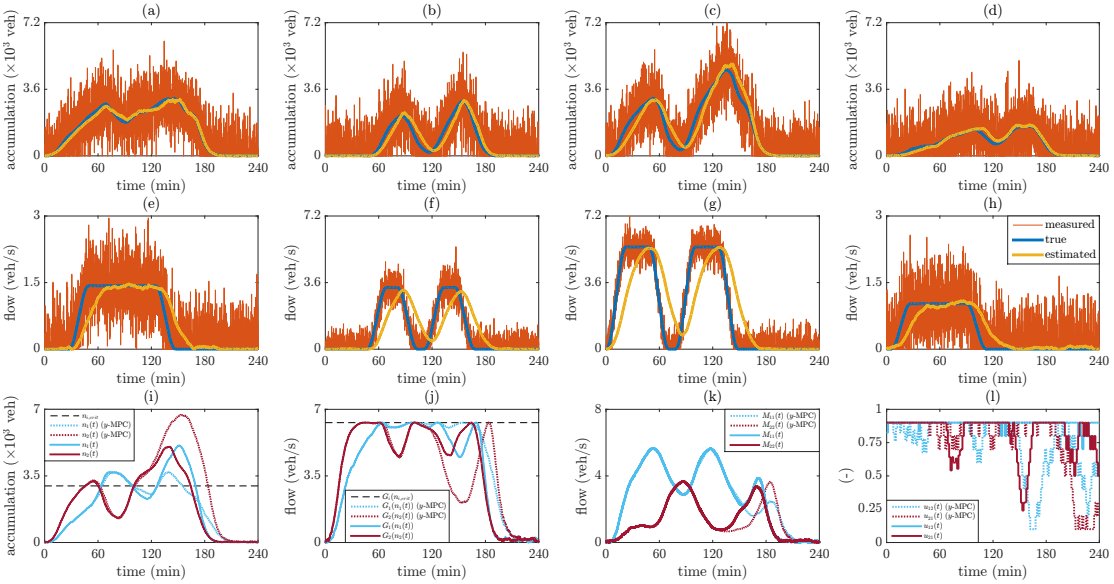

Figure 2.2 – Results of the congested scenario using h_1 with the combined MHE-MPC scheme: Accumulations (a) $n_{11}(t)$, (b) $n_{12}(t)$, (c) $n_{21}(t)$, (d) $n_{22}(t)$; inflow demands (e) $q_{11}(t)$, (f) $q_{12}(t)$, (g) $q_{21}(t)$, (h) $q_{22}(t)$; regional accumulations (i) $n_1(t)$ and $n_2(t)$; regional outflows (j) $G_1(n_1(t))$ and $G_2(n_2(t))$; trip completion flows (k) $M_{11}(t)$ and $M_{22}(t)$; perimeter controls (l) $u_{12}(t)$ and $u_{21}(t)$, with dashed lines in (i) to (l) denoting y-MPC results.

states and there is a significant loss of capacity for region. This is evidenced also by the network experiencing near-gridlock conditions for the no control (in region 1) and y-MPC (in region 2) cases, as can be seen in fig. 2.6. This indicates the importance of estimation for high performance congestion management. Interestingly, as seen from figures (i) and (l) in fig. 2.2, the MPC decides to let region 2 reach congested states before restricting flows by decreasing u_{12}. This highlights that due to the high level of complexity of urban networks, standard and simple control approaches (e.g., keeping the city center at the critical accumulation) might have counter-productive or non-intuitive results with worse performance. Similar conclusions can be drawn for the control actions for measurement types h_2 to h_4 as shown in figs. 2.3 to 2.5. From fig. 2.3 it can be seen for h_2 that since $q_{ij}(t)$ is not measured, there is clearly higher error in the estimation of $q_{ij}(t)$ compared to the h_1 case (where $q_{ij}(t)$ are measured). Nevertheless, the control performance is similar quality, as $n_{ij}(t)$ and $n_{ij}(t)$ are estimated with a level of accuracy similar to h_1. An interesting observation based on fig. 2.5 is that even with the very limited information present in h_4 involving only $n_i(t)$, $M_{ij}(t)$, and $q_i(t)$ measurements, it is still possible to estimate $n_{ij}(t)$ with high accuracy, and despite the increased estimation errors in $q_{ij}(t)$, the control performance is similar to h_1. Overall, the results indicate substantial potential towards real-world implementation of model predictive perimeter control schemes, where OD-based information and future demands might be unavailable and measurements might be corrupted with large amounts of noise. Furthermore, from the results in table 2.1 it

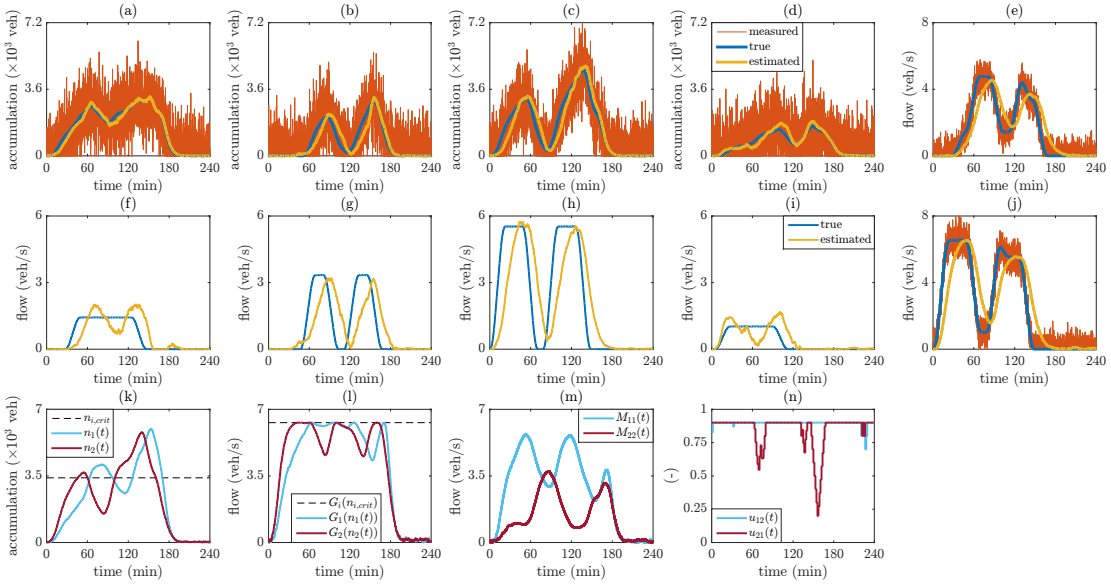

Figure 2.3 – Results of the congested scenario using h_2 with the combined MHE-MPC scheme: Accumulations (a) $n_{11}(t)$, (b) $n_{12}(t)$, (c) $n_{21}(t)$, (d) $n_{22}(t)$; regional inflow demands (e) $q_1(t)$, (j) $q_2(t)$; inflow demands (f) $q_{11}(t)$, (g) $q_{12}(t)$, (h) $q_{21}(t)$, (i) $q_{22}(t)$; regional accumulations (k) $n_1(t)$ and $n_2(t)$; regional outflows (l) $G_1(n_1(t))$ and $G_2(n_2(t))$; trip completion flows (m) $M_{11}(t)$ and $M_{22}(t)$; perimeter controls (n) $u_{12}(t)$ and $u_{21}(t)$.

can be observed that while EKF performance (both estimation and control) suffers from measurement compositions with limited information (i.e., especially h_2 and h_4), MHE seems to be insensitive to the effects of limited information. Furthermore, the results indicate real-time feasibility of the MHE and MPC schemes, as their CPU times of about 1.2 and 0.5 seconds are roughly negligible compared to their sampling times of 10 and 90 seconds, respectively. It is important to note here that a direct quantitative comparison between the four measurement compositions is impossible simply because they involve different measurements, the noise levels of which are not comparable. We also tested accumulation-based models using eq. (2.3), the results of which are omitted since they yielded results similar to those presented here.

2.4.2 Sensitivity to noise intensity

Changing measurement noise intensity is expected to affect estimation and control performance. This effect is examined by a sensitivity analysis, where a set of 50 randomly generated scenarios (each with a different inflow demand profile with moderate to high demands) is tested under the same conditions with the congested scenario (with the exception of sampling times, which are all chosen as 90), varying only the standard deviations of measurement noise: $\sigma_{v,n_{ij}}$ from 100 veh to 1000 veh for the h_1 and h_2 cases; σ_{v,n_i} from 100 veh to 1000 veh and $\sigma_{v,M_{ij}}$ from 0.1 veh/s to 1 veh/s (σ_{v,n_i} and $\sigma_{v,M_{ij}}$

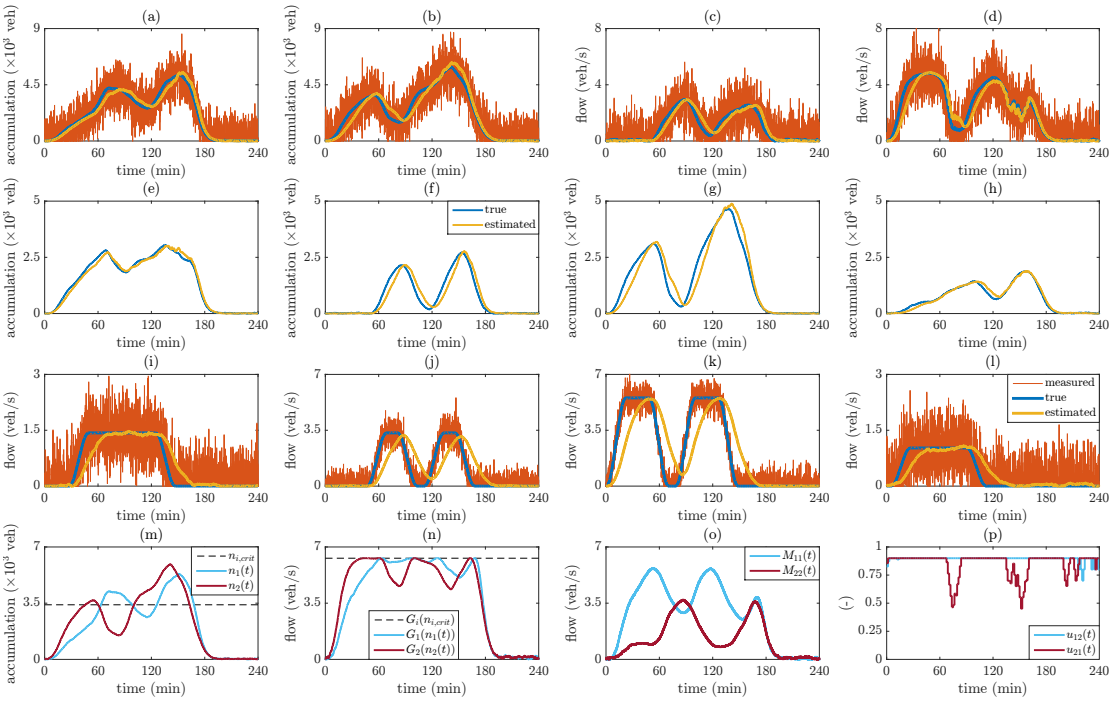

Figure 2.4 – Results of the congested scenario using h_3 with the combined MHE-MPC scheme: Regional accumulations (a) $n_1(t)$, (b) $n_2(t)$; transfer flows (c) $M_{12}(t)$, (d) $M_{21}(t)$; accumulations (e) $n_{11}(t)$, (f) $n_{12}(t)$, (g) $n_{21}(t)$, (h) $n_{22}(t)$; inflow demands (i) $q_{11}(t)$, (j) $q_{12}(t)$, (k) $q_{21}(t)$, (l) $q_{22}(t)$; regional accumulations (m) $n_1(t)$ and $n_2(t)$; regional outflows (n) $G_1(n_1(t))$ and $G_2(n_2(t))$; trip completion flows (o) $M_{11}(t)$ and $M_{22}(t)$; perimeter controls (p) $u_{12}(t)$ and $u_{21}(t)$.

changed together) for h_3 and h_4.

The results are shown in figs. 2.7 to 2.9, depicting RMSE_n, RMSE_q, and TSPV, respectively, as a function the measurement noise standard deviations. As expected, the results suggest degradation in estimation performance with increasing noise levels. Inflow demand estimation performance (i.e., RMSE_q), for the cases of h_1 and h_3, seems to be insensitive to increasing noise levels, which can be attributed to the fact that the inflow demands $q_{ij}(t)$ are measured directly in these two cases, which (unlike the cases of h_2 and h_4) do not rely on the rest of the measurements for reconstructing the inflow demands. Furthermore, it can be observed that for all metrics the MHE is much less sensitive to changes in noise levels compared to the EKF. This is especially pronounced for the TSPV metric, where MHE is almost completely insensitive to increasing noise for all measurement compositions, while the EKF shows substantial degradations for the cases of h_2 and h_4. This can be attributed to features of MHE: (a) it employs a nonlinear model directly (i.e., without any approximations, as in the case of linearization in EKF), (2) it optimizes over state trajectories considering known measurement trajectories inside a finite horizon window into the past (while EKF uses only the last measurement),

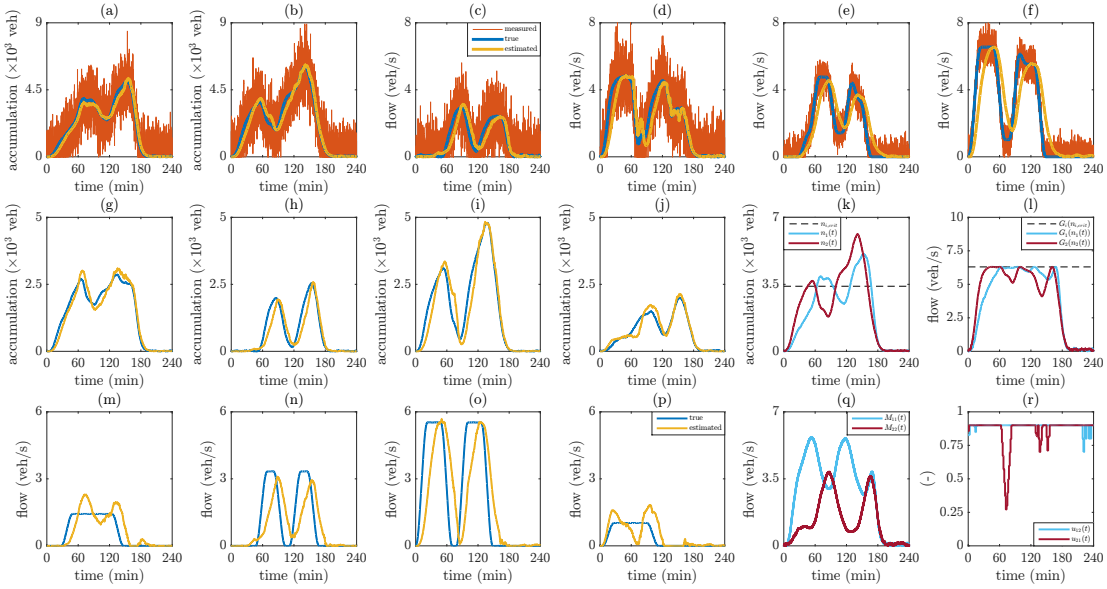

Figure 2.5 – Results of the congested scenario using h_4 with the combined MHE-MPC scheme: Regional accumulations (a) $n_1(t)$, (b) $n_2(t)$; transfer flows (c) $M_{12}(t)$, (d) $M_{21}(t)$; regional inflow demands (e) $q_1(t)$, (f) $q_2(t)$; accumulations (g) $n_{11}(t)$, (h) $n_{12}(t)$, (i) $n_{21}(t)$, (j) $n_{22}(t)$; regional accumulations (k) $n_1(t)$ and $n_2(t)$; regional outflows (l) $G_1(n_1(t))$ and $G_2(n_2(t))$; inflow demands (m) $q_{11}(t)$, (n) $q_{12}(t)$, (o) $q_{21}(t)$, (p) $q_{22}(t)$; trip completion flows (q) $M_{11}(t)$ and $M_{22}(t)$; perimeter controls (r) $u_{12}(t)$ and $u_{21}(t)$.

(3) unlike EKF, it can handle state constraints systematically (see [74] for a detailed discussion comparing MHE and EKF).

Sensitivity to noise intensity without state estimation

Deploying controllers using noisy measurements without state estimators is expected to have adverse affects on control performance, since the controller has to rely on information with a large amount of corruption by noise. To further investigate this point a sensitivity analysis is performed, where a set of 50 randomly generated scenarios (each with a different inflow demand profile with high demands) is tested under the same conditions with the congested scenario, varying only the standard deviations of measurement noise ($\sigma_{v,n_{ij}}$ from 100 veh to 1000 veh). The results of an MPC scheme directly using the measurements (i.e., y-MPC) are compared with MPC schemes using EKF and MHE as state estimator, with the h_1 measurement composition. This is done for fair comparison since y-MPC requires the h_1 measurement composition as it does not have access to a state estimator or observer to extract the state from the measurement.

The results are shown in fig. 2.10, depicting TSPV and improvement in TSPV, respectively, as a function $\sigma_{v,n_{ij}}$. As expected, without a state estimator to filter out noise in the measurement, the control performance shows severe degradations with increasing levels

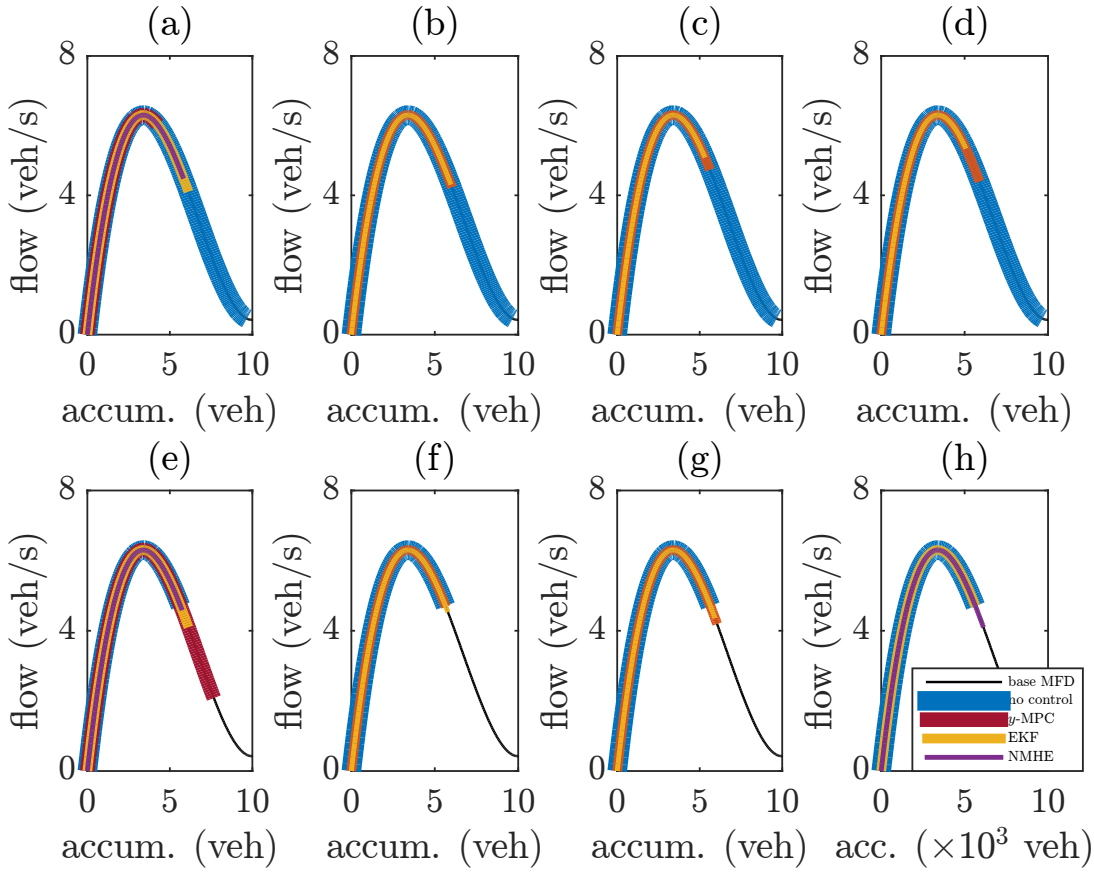

Figure 2.6 – Outflow MFDs for the congested scenario comparing the no control case, y-MPC, and all measurement configurations with the combined EKF-MPC and MHE-MPC schemes: (a) Region 1 with h_1, (b) region 1 with h_2, (c) region 1 with h_3, (d) region 1 with h_4, (e) region 2 with h_1, (f) region 2 with h_2, (g) region 2 with h_3, (h) region 2 with h_4.

of noise. However, using the EKF or MHE, it is possible to keep control performance insensitive to measurement noise, which can yield performance improvements up to 15%. These results emphasize the importance of using state estimation jointly with feedback controllers for efficient operation under situations of measurement noise.

2.4.3 Horizon length tuning for MHE

Similar to the case with MPC where its prediction horizon N_c influences control performance (see [13] and [63] for MPC tuning results for a two-region and seven-region urban network, respectively), MHE performance is strongly influenced by the estimation horizon N_e. To study how changing N_e affects estimation and control performance for the combined MHE-MPC scheme, a series of simulation experiments (with a set of 50 randomly generated scenarios) is conducted with varying values of N_e from 1 to 60 (with

prediction horizon N_c fixed to 20).

The results are shown in fig. 2.11, showing RMSE_n, RMSE_q, and TSPV, as functions of N_e. As expected, estimation performance increases with increasing N_e, especially in the interval $1 \leq N_e \leq 20$, while for $N_e > 20$ the performance increase is not pronounced. It is interesting to note that for measurement compositions h_2 and h_4, RMSE_q decreases with increasing N_e for the whole interval of $1 \leq N_e \leq 30$. This is associated with the fact that these compositions involve measurements on $q_i(t)$ instead of $q_{ij}(t)$, and thus, compared to h_1 and h_3, require more information (i.e., longer horizons) to be able to reconstruct $q_{ij}(t)$. Furthermore, control performance seems to be roughly insensitive to estimation horizon, showing only minor improvement for increasing N_e, suggesting that the MPC is capable of managing congestion when coupled with an MHE, even when said MHE has a short horizon and thus limited estimation performance. Nevertheless, lack of state estimation is catastrophic for the MPC performance when measurement errors are large.

2.4.4 Analysis of constant future inflow demands assumption

Model predictive perimeter control schemes require inflow demand trajectories for the duration of the prediction horizon into the future (i.e., from time step t to time step $t + N_c - 1$). However, it is exceedingly difficult to know future demands accurately in practice. In order to obtain a practicable MPC scheme, in the formulation given in eq. 2.29 it is assumed that the inflow demands are constant and fixed to their estimated values, which is only a rough approximation since demands vary with time. To examine how assuming constant future demands in the MPC formulation affects control performance of the combined MHE-MPC scheme, a set of 50 randomly generated scenarios is evaluated under the same conditions with the congested scenario, varying only the standard deviations of measurement noise associated with the inflow demands: $\sigma_{v,q_{ij}}$ from 0.1 veh/s to 1 veh/s for the h_1 and h_3 cases; σ_{v,q_i} from 0.1 veh/s to 1 veh/s for the h_2 and h_4 cases. Three different cases are compared (all with the combined MHE-MPC scheme): (a) Future demands are assumed constant and fixed to 0, (b) future demands are assumed constant and fixed to the values estimated by the MHE at time t, (c) future demands are fixed to their true values (i.e., perfect knowledge of demands).

The results are shown in fig. 2.12, depicting RMSE_q, RMSE_{fq}, and TSPV as functions of standard deviations associated with inflow demand measurement noise, where RMSE_{fq} is the root-mean-square error expressing the difference between the true inflow demands and the constant trajectories used by the MPC that are fixed to the estimated values at time t, defined for a single simulation experiment as follows:

$$\text{RMSE}_{fq} = \frac{1}{4}\sum_{i=1}^{2}\sum_{j=1}^{2}\sqrt{\frac{\sum_{t=1}^{t_{\text{final}}}\sum_{k=0}^{N_c-1}(q_{ij}(t+k) - \hat{q}_{ij}(t))^2}{t_{\text{final}} \cdot N_c}}. \tag{2.43}$$

From the figures it can be observed that the combined MHE-MPC scheme is fairly insensitive to changing noise intensity associated with inflow demand measurements, since both RMSE_{fq} and TSPV metrics show limited degradation against increasing noise intensity. Furthermore, the figures comparing TSPV of the three cases show that although assuming constant future inflow demands in the MPC is a rough approximation, it yields control performances that are virtually identical to those obtained by having perfect information on inflow demands. These results suggest that a combined MHE-MPC scheme with an MPC formulation having constant future inflow demands fixed to their estimated values represents a practicable traffic control system that is capable of congestion management without having information on future inflow demands.

2.5 Conclusion

In this chapter we proposed a nonlinear MHE scheme capable of OD inflow demand and accumulation state estimation for a two-region large-scale urban network model with MFD-based dynamics. Four practically motivated measurement compositions were described, with varying levels of OD information of drivers. Observability tests, conducted using the MFD-based dynamical model with each of the four compositions, revealed that observability is retained for compositions with limited or no measurements containing OD information. Considering that OD-based real-time measurements are usually not available or difficult to obtain in practice, the possibility of extracting OD-based traffic state and inflow demand from limited measurements is of critical importance for field implementations of MFD-based feedback perimeter control.

Extensive simulations show that the estimation performance of the proposed MHE scheme is fairly insensitive to increasing noise intensity, and is generally superior to an EKF. An important result is that the control performance of the combined MHE-MPC scheme is virtually insensitive to increasing intensity in measurement noise, which is another practically relevant finding considering that perimeter control schemes have to operate under noisy conditions in the field. Further simulations revealed that assuming constant future demands in the MPC formulation yields control performances practically identical to the case with perfect demand information. Overall, the results indicate a strong potential towards implementation of MFD-based perimeter control, since the proposed MHE-MPC scheme is capable of high performance congestion management under severe conditions of measurement noise, limited or no OD-based information, and unknown future inflow demands.

Although the results in this chapter indicate good performance for MFD-based estimation and control methods in macroscopic simulations, more detailed experiments via microscopic simulations are expected to yield more realistically grounded evaluations concerning how such methods would perform in practical implementations of perimeter control in the field. We seek the answers to this question in the next chapter.

Table 2.1 – Performance Evaluation for Congested Scenario

meas. comp. - st. est.	TSPV (min)	RMSE_n (veh)	RMSE_q (veh/s)	mean/max CPU time MHE (s)	mean/max CPU time MPC (s)
no control	26.1	-	-	-	-
y-MPC	20.8	-	-	-	0.30/0.41
h_1-EKF	18.7	349.1	0.80	-	0.32/0.47
h_1-MHE	18.4	228.7	0.75	0.72/1.13	0.33/0.46
h_2-EKF	18.8	584.2	1.24	-	0.31/0.44
h_2-MHE	18.1	265.8	0.89	0.75/1.19	0.33/0.46
h_3-EKF	18.3	318.9	0.80	-	0.32/0.47
h_3-MHE	18.1	218.0	0.75	0.75/1.19	0.33/0.46
h_4-EKF	18.7	583.6	1.11	-	0.31/0.43
h_4-MHE	17.7	277.4	0.91	0.80/1.22	0.33/0.50

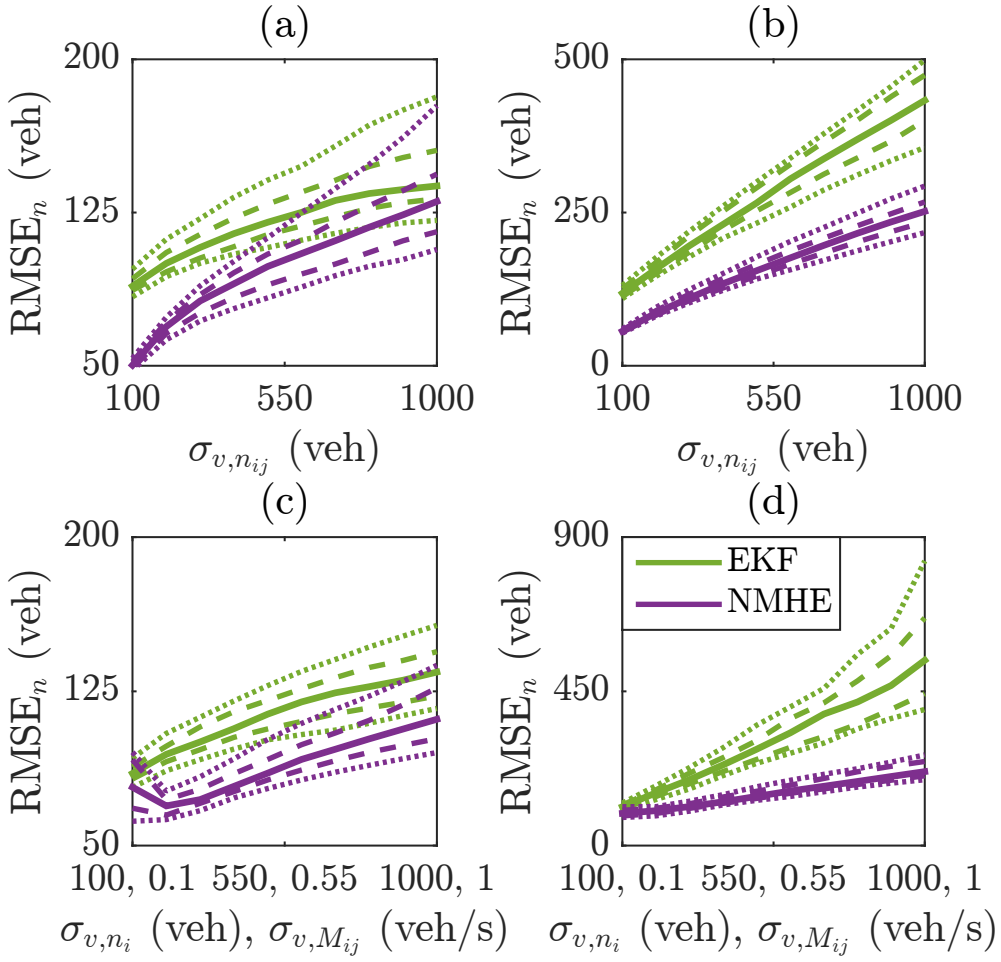

Figure 2.7 – Sensitivity of accumulation state $n_{ij}(t)$ estimation performance to changes in measurement noise intensity, showing the 10th and 90th (dotted), 25th and 75th (dashed), and 50th (solid) percentiles of RMSE$_n$, for a set of 50 randomly generated scenarios and the four measurement compositions: (a) h_1, (b) h_2, (c) h_3, (d) h_4.

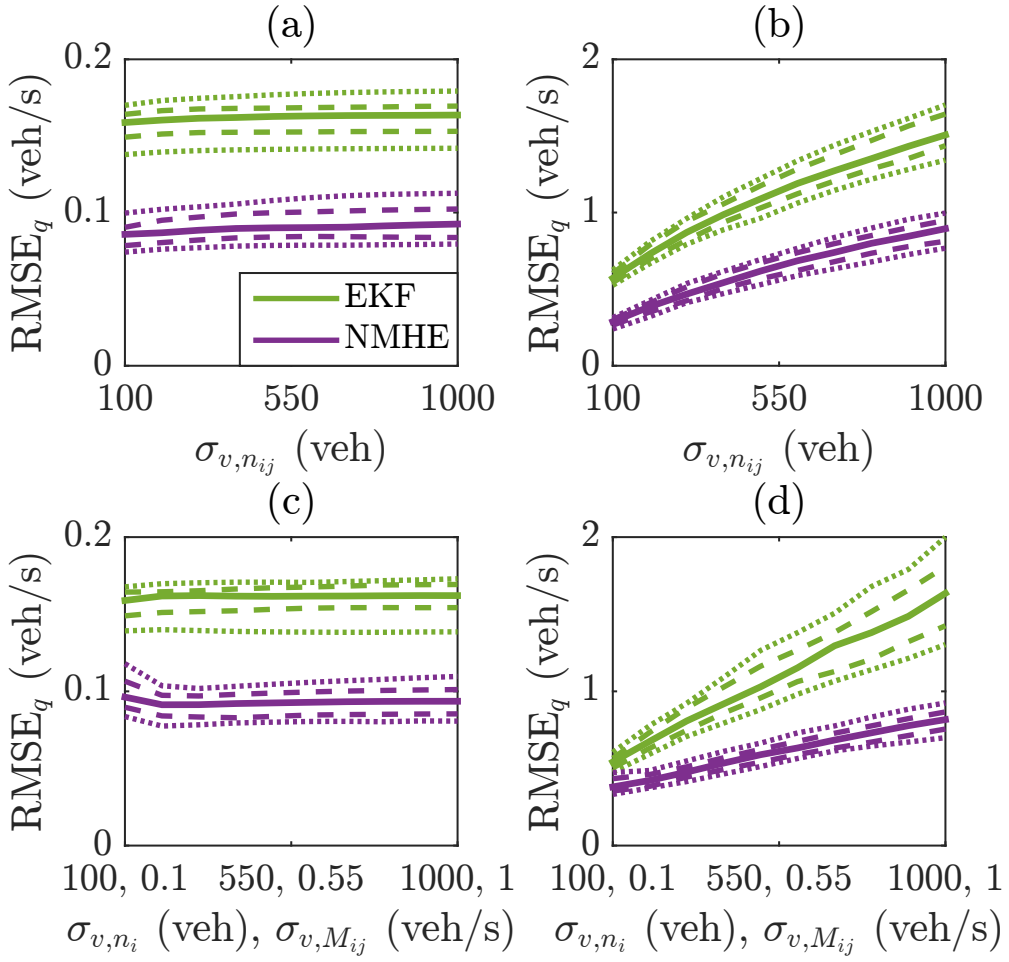

Figure 2.8 – Sensitivity of inflow demand $q_{ij}(t)$ estimation performance to changes in measurement noise intensity, showing the 10th and 90th (dotted), 25th and 75th (dashed), and 50th (solid) percentiles of RMSE$_q$, for a set of 50 randomly generated scenarios and the four measurement compositions: (a) h_1, (b) h_2, (c) h_3, (d) h_4.

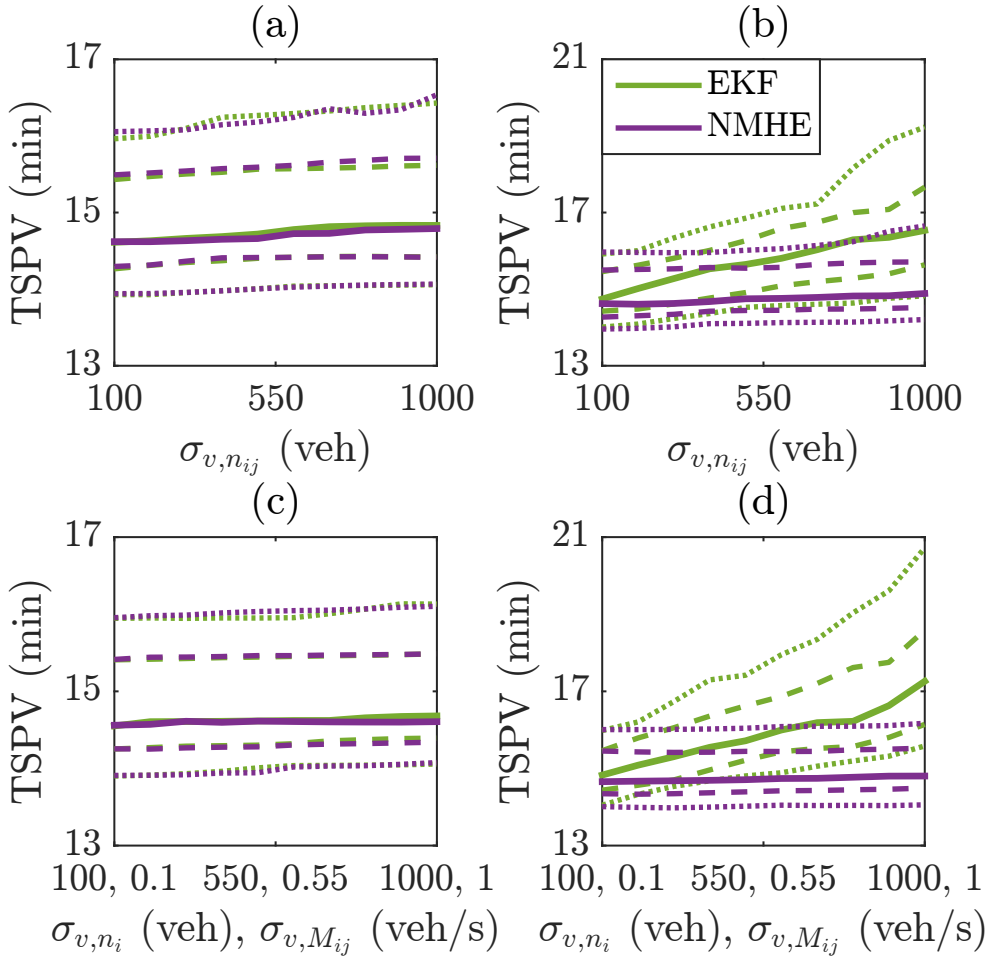

Figure 2.9 – Sensitivity of control performance to changes in measurement noise intensity, showing the 10th and 90th (dotted), 25th and 75th (dashed), and 50th (solid) percentiles of TSPV, for a set of 50 randomly generated scenarios and the four measurement compositions: (a) h_1, (b) h_2, (c) h_3, (d) h_4.

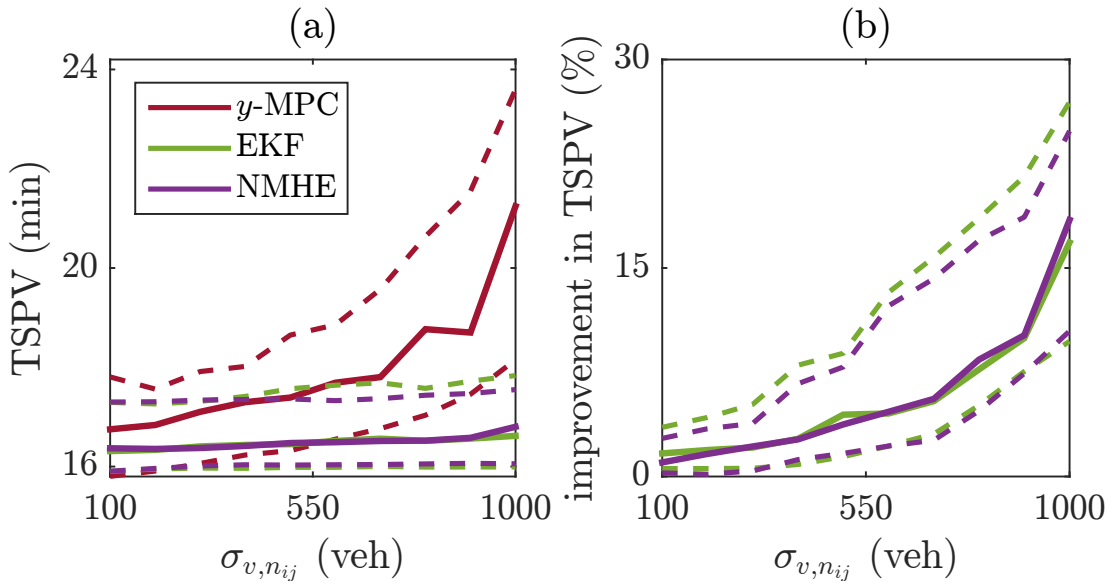

Figure 2.10 – Sensitivity of control performance to changes in measurement noise intensity, showing the 25th and 75th (dashed), and 50th (solid) percentiles of TSPV and improvement in TSPV, for a set of 50 randomly generated scenarios with high demand: (a) TSPV, (b) improvement in TSPV.

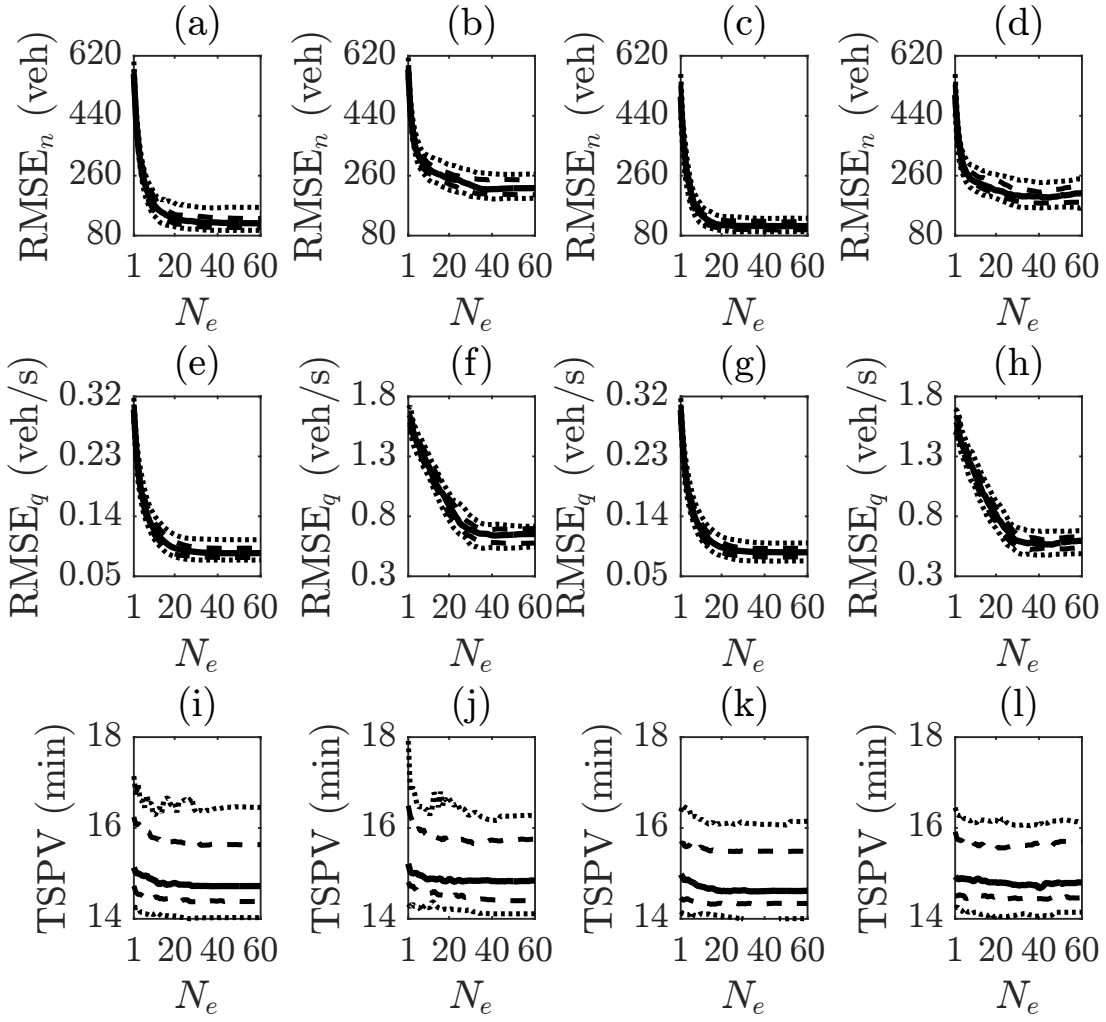

Figure 2.11 – Estimation and control performance of the combined MHE-MPC scheme as functions of estimation horizon N_e, showing the 10th and 90th (dotted), 25th and 75th (dashed), and 50th (solid) percentiles of (a)-(d) RMSE$_n$, (e)-(h) RMSE$_q$, and (i)-(l) TSPV, for a set of 50 randomly generated scenarios and the four measurement compositions: (a), (e), (i) h_1; (b), (f), (j) h_2; (c), (g), (k) h_3; (d), (h), (l) h_4.

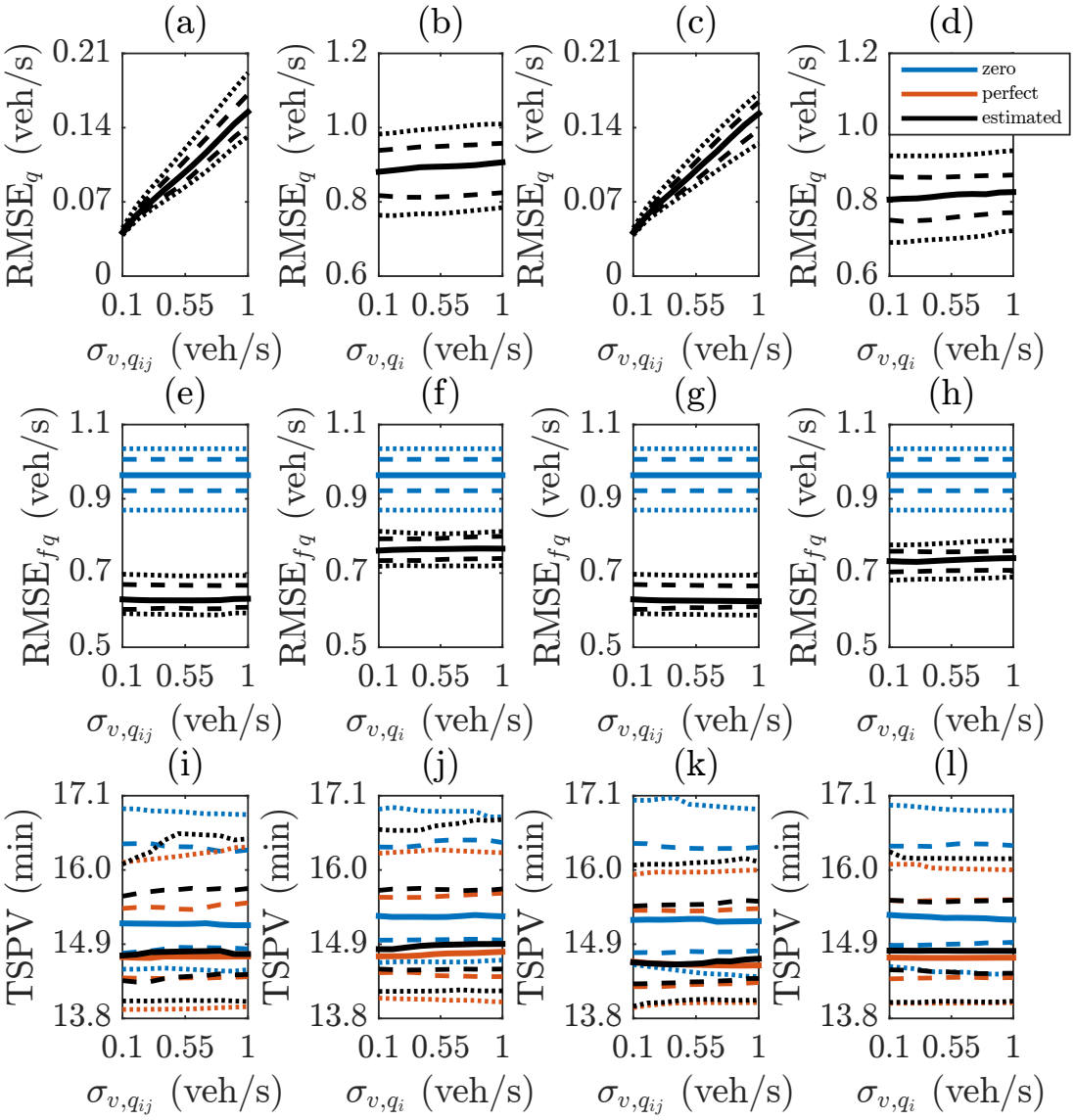

Figure 2.12 – Inflow demand estimation performance, accuracy of constant future inflow demands assumption, and control performance of the combined MHE-MPC scheme as functions of measurement noise intensity, showing the 10th and 90th (dotted), 25th and 75th (dashed), and 50th (solid) percentiles of (a)-(d) RMSE$_q$, and (e)-(h) RMSE$_{fq}$, and TSPV (i)-(l), for a set of 50 randomly generated scenarios and the four measurement compositions: (a), (e), (i) h_1; (b), (f), (j) h_2; (c), (g), (k) h_3; (d), (h), (l) h_4.

Chapter 3

Identification, estimation, and control for large-scale networks

3.1 Introduction

Network-level road traffic control remains a challenging problem. MFD-based dynamical traffic models enable design of model-based estimation and control methods, which represent efficient congestion management solutions with substantial potential for practical implementation. In this chapter we develop a large-scale traffic control framework consisting of optimization-based identification, estimation, and control methods, intended for perimeter controlled multi-region urban networks. Firstly a system identification method is proposed for computing the MFD parameters given measurements on historical trajectories of the accumulation state and inflow demand. The method involves formulating the problem of finding the MFD parameters yielding the best fit between measurements and model predictions as an optimization problem. Furthermore, nonlinear MHE and economic MPC formulations employing MFD-based dynamics are presented, which enable high-performance traffic control under measurement noise. Case studies conducted using detailed microscopic simulation experiments considering an urban network with around 1500 links and 600 intersections, where the MFD parameters obtained by the identification method are used in MHE and MPC design, demonstrate the operation of the proposed framework.

This chapter is based on the work in [60]. Literature review is not included here; it is given for the whole dissertation in chapter 1.

3.2 Modeling of a multi-region urban network

Consider a city-scale road traffic network, consisting possibly of hundreds of links and intersections, with heterogeneous distribution of accumulation (i.e., number of vehicles) on its links. Using the MFD of urban traffic, it is possible to express the rate of vehicles exiting traffic in a region (either through ending the trip inside the region or transferring to an adjacent region) as a function of the region accumulation [16]. Clustering algorithms developed for such large-scale networks (see, e.g., [24]) can be used to partition the network into regions (i.e., a set of links) to obtain low intraregional heterogeneity of accumulation. As shown in [18], [19], a homogeneous distribution of congestion leads to an MFD that is well-defined, i.e., a low scatter of flows is observed for the same accumulation (see fig. 3.1a). Empirical results indicate that the MFD can be approximated by an asymmetric unimodal curve skewed to the right [16], which can, for example, be chosen as a third degree polynomial:

$$g_i(n_i(t)) = a_i n_i^3(t) + b_i n_i^2(t) + c_i n_i(t), \tag{3.1}$$

where $n_i(t)$ (vehicles; abbreviated henceforth as veh) is the accumulation of region i, $g_i(n_i(t))$ (veh/s) is the trip completion flow of the region (i.e., rate of vehicles exiting traffic), whereas a_i, b_i, and c_i are model parameters.

Given a network $\mathcal{R}$ consisting of a set of R regions ($\mathcal{R} = \{1, 2, \ldots, R\}$) (see, e.g., fig. 3.1b), each with a well-defined MFD, aggregated dynamical models of large-scale road traffic networks can be developed based on interregional traffic flows as the following vehicle conservation equations:

$$\dot{n}_{ii}(t) = q_{ii}(t) - m_{ii}(t) + \sum_{h \in \mathcal{N}_i} u_{hi}(t) m_{hii}(t) \tag{3.2a}$$

$$\dot{n}_{ij}(t) = q_{ij}(t) - \sum_{h \in \mathcal{N}_i} u_{ih}(t) m_{ihj}(t) + \sum_{h \in \mathcal{N}_i; h \neq j} u_{hi}(t) m_{hij}(t), \tag{3.2b}$$

where $n_{ii}(t)$ (veh) and $n_{ij}(t)$ (veh) are state variables expressing the accumulation in region i with destination region i and j, respectively (with $n_i(t) = \sum_{j=1}^{R} n_{ij}(t)$), $q_{ii}(t)$ (veh/s) and $q_{ij}(t)$ (veh/s) are disturbances expressing the rate of vehicles appearing in region i demanding trips to destination region i and j, respectively, $u_{ih}(t) \in [\underline{u}, \bar{u}]$ (with $0 \leq \underline{u} < \bar{u} < 1$) are control inputs between each pair of adjacent regions i and h expressing actions of perimeter control actuators (with $h \in \mathcal{N}_i$; where $\mathcal{N}_i$ is the set of regions adjacent to i) that can manipulate vehicle flows transferring between the regions, $m_{ihj}(t)$ (veh/s) is the vehicle flow attempting to transfer from i to h with destination j:

$$m_{ihj}(t) \triangleq \theta_{ihj}(t) \frac{n_{ij}(t)}{n_i(t)} g_i(n_i(t)), \tag{3.3}$$

where $\theta_{ihj}(t) \in [0, 1]$ is the route choice term expressing, for the vehicles exiting region i

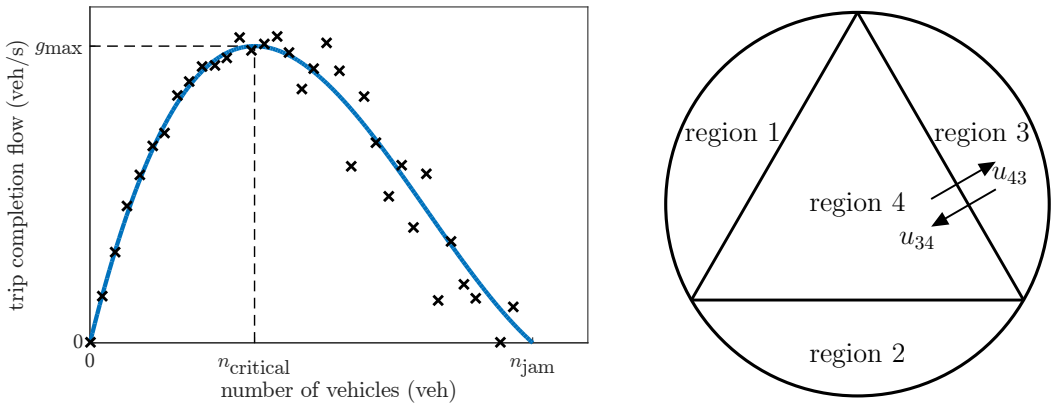

Figure 3.1 – (a) A well-defined macroscopic fundamental diagram. (b) A four region network without route choice.

with destination j, the ratio that is transferring to region h (with $m_{hii}(t)$ and $m_{hij}(t)$ defined similarly), whereas $m_{ii}(t)$ (veh/s) is the exit (i.e., internal trip completion) flow of region i:

$$m_{ii}(t) \triangleq \frac{n_{ii}(t)}{n_i(t)} g_i(n_i(t)). \tag{3.4}$$

Route choice effect can be omitted in modeling if the network topology leads to a single obvious route choice, in which case $\theta_{ihj}(t) = 1$ for all time for only one region $h \in \mathcal{N}_i$ for each i-j pair (with $j \neq i$). For example, for the network depicted in fig. 3.1b, $\theta_{4hj}(t) = 1$ if $h = j$ and $\theta_{4hj}(t) = 0$ otherwise. The focus in this chapter is on those networks where route choice can be omitted (see [63] for a study where it is included).

Assuming additive process and measurement noise, the dynamics (3.2) and measurement can be written as:

$$\dot{n}(t) = f(n(t), q(t), u(t), p) + w(t), \tag{3.5}$$
$$y_n(t) = n(t) + v_n(t) \tag{3.6}$$
$$y_q(t) = q(t) + v_q(t) \tag{3.7}$$

where $n \in \mathbb{R}^{R^2}$ (state) and $q \in \mathbb{R}^{R^2}$ (measured disturbance) are the vectors of accumulations and inflow demands, respectively, $u \in \mathbb{R}^{2 \cdot m_a}$ (control input) is the vector of transferring flow restrictions between adjacent regions via perimeter control actuators (with m_a the number of adjacent region pairs), $p \in \mathbb{R}^{R \cdot m_p}$ is the model parameters vector (with m_p the number of parameters associated with the MFD of one region), $w \in \mathbb{R}^{R^2}$ is the process noise expressing uncertainty in the dynamics (with $w \sim \mathcal{N}(0, \Sigma_w)$), $y_n \in \mathbb{R}^{R^2}$ and $y_q \in \mathbb{R}^{R^2}$ are measurements on n and q, respectively, whereas $v_n \in \mathbb{R}^{R^2}$ and $v_q \in \mathbb{R}^{R^2}$

are measurement noise vectors (with $v_n \sim \mathcal{N}(0, \Sigma_{v_n})$ and $v_q \sim \mathcal{N}(0, \Sigma_{v_q})$).

3.3 Identification, estimation, and control

3.3.1 System identification

Based on the prediction error approach [75], we can formulate the problem of obtaining the MFD parameters with the best least squares fit between the measured and predicted trajectories of $n(t)$ and $q(t)$ as the following MBPE problem:

$$\underset{p,n_k,q_k}{\text{minimize}} \sum_{k=0}^{K-1} \|w_k\|_Q^2 + \sum_{k=0}^{K} \left(\|v_{n,k}\|_{R_n}^2 + \|v_{q,k}\|_{R_q}^2 \right) \tag{3.8}$$

$$\text{subject to for } k = 0, \ldots, K: \tag{3.9}$$

$$y_n(kT) = n_k + v_{n,k} \tag{3.10}$$

$$y_q(kT) = q_k + v_{q,k} \tag{3.11}$$

$$0 \leq n_k \leq \bar{n} \tag{3.12}$$

$$0 \leq q_k \leq \bar{q} \tag{3.13}$$

$$\text{for } k = 0, \ldots, K-1: \tag{3.14}$$

$$n_{k+1} = F(y_n(kT), y_q(kT), u(kT), p) + w_k \tag{3.15}$$

where k is the time interval counter of the MBPE, K is the identification horizon, w_k, $v_{n,k}$, and $v_{q,k}$ are vectors of auxiliary variables internal to the MBPE representing the process noise, and measurement noises associated with the accumulation state and inflow demand, respectively, T is the sampling time, $y_n(t)$ and $y_q(t)$ are measurements on the accumulation state $n(t)$ and inflow demand $q(t)$, respectively, n_k and q_k are the accumulation state and inflow demand vectors internal to the MBPE, respectively, $\bar{n}$ and $\bar{q}$ are upper bounds on the accumulation state and inflow demand (possibly obtained from an analysis on historical data), respectively, F is the discrete-time version of the dynamics given in (3.5), whereas $u(t)$ is the known (recorded in the recent past) vector of perimeter control inputs.

Owing to the prediction error method involving one-step ahead predictions, and the dynamics (3.5) being linear in the MFD parameters, the MBPE problem (3.8) is a convex optimization problem that can be solved reliably and efficiently.

3.3.2 Moving horizon estimation

We formulate the problem of finding state estimate trajectories for a moving time horizon extending a fixed length into the past, striking a trade-off between measurements and the prediction model, as the following nonlinear MHE problem (extending the work in

[58] and [59]):

$$\underset{w_k}{\text{minimize}} \quad \sum_{k=-N_\text{e}}^{-1} \|w_k\|_Q^2 + \sum_{k=-N_\text{e}}^{0} \left(\|v_{n,k}\|_{R_n}^2 + \|v_{q,k}\|_{R_q}^2 \right) \tag{3.16}$$

$$\text{subject to for } k = -N_\text{e}, \ldots, 0: \tag{3.17}$$

$$y_n(t + kT) = n_k + v_{n,k} \tag{3.18}$$

$$y_q(t + kT) = q_k + v_{q,k} \tag{3.19}$$

$$0 \leq n_k \leq \bar{n} \tag{3.20}$$

$$0 \leq q_k \leq \bar{q} \tag{3.21}$$

$$\text{for } k = -N_\text{e}, \ldots, -1: \tag{3.22}$$

$$n_{k+1} = F(n_k, q_k, u(t + kT), \hat{p}) + w_k \tag{3.23}$$

where k is the time interval counter of the MHE, N_e is the estimation horizon, w_k, $v_{n,k}$, and $v_{q,k}$ are vectors of auxiliary variables internal to the MHE representing the process noise, and measurement noises associated with the accumulation state and inflow demand, respectively, n_k and q_k are the accumulation state and inflow demand vectors internal to the MHE, respectively, whereas $\hat{p}$ is the vector of model parameters obtained via MBPE as the solution of (3.8).

3.3.3 Model predictive control

The problem of finding the control inputs that minimize total time spent (TTS) for a finite horizon can be formulated as the following economic nonlinear MPC problem (extending the work in [13], [58], and [59]):

$$\underset{u_k}{\text{minimize}} \quad T \cdot \sum_{k=1}^{N_\text{c}} \mathbf{1}^T n_k \tag{3.24}$$

$$\text{subject to} \quad n_0 = \hat{n}_t(t) \tag{3.25}$$

$$|u_0 - u(t - T)| \leq \Delta_u \tag{3.26}$$

$$\text{for } k = 0, \ldots, N_\text{c} - 1: \tag{3.27}$$

$$n_{k+1} = F(n_k, \hat{q}_t(t), u_k, \hat{p}) \tag{3.28}$$

$$\underline{u} \leq u_k \leq \bar{u} \tag{3.29}$$

$$\text{for } k = 1, \ldots, N_\text{c}: \tag{3.30}$$

$$n_{i,k} \leq n_{i,\text{jam}} \quad \forall i \in \mathcal{R}, \tag{3.31}$$

where k is the time interval counter of the MPC, N_c is the prediction horizon, n_k and u_k are the state and control input vectors internal to the MPC, respectively, $\hat{n}_\tau(t)$ and $\hat{q}_\tau(t)$ are estimates of the accumulation state $n(t)$ and inflow demand $q(t)$ for time τ available at current time t (obtained via MHE as the solution of (3.16)), Δ_u is the rate limiting

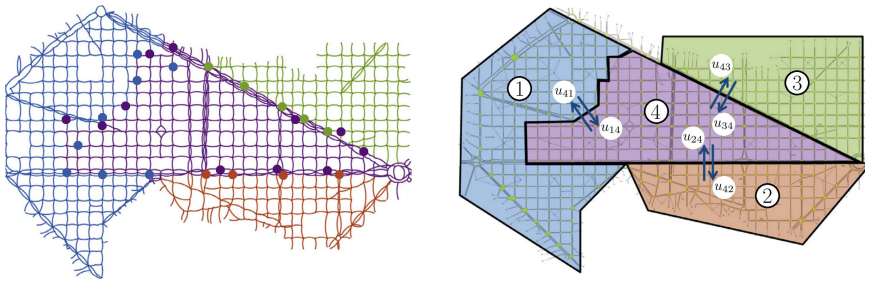

(a) (b)

Figure 3.2 – (a) Microscopic (Aimsun) model of the network, with clustering results as links (region 1 in blue, 2 in red, 3 in green, and 4 in purple) and controlled intersections as circles (intersections belonging to u_{14} in blue, u_{24} in red, u_{34} in green, and u_{4j} (with $j = 1, 2, 3$) in purple). (b) Network schematic showing the partitioning into four regions and the perimeter control inputs (figures adapted from [14]).

parameter on control inputs, $\underline{u}$ and $\bar{u}$ are the control input constraints, whereas $n_{i,k}$ is the total accumulation in region i.

Due to the nonlinear dynamics (3.5), the MHE and MPC problems given in eqs. (3.16) and (3.24), respectively, are nonconvex nonlinear optimization problems, which can be solved efficiently via, e.g., sequential quadratic programming or interior point solvers (for details, see [69]).

3.4 Results

An urban road network consisting of roughly 1500 links and 600 intersections is replicated as a computer model using the microscopic simulation package Aimsun (see fig. 3.2a). The model represents a portion of the urban network of the city of Barcelona in Spain, covering an area of 12 km^2. The network is partitioned into four regions (see fig. 3.2b) using the optimization-based clustering method of [24], where minimizing heterogeneity is considered in the objective function and cluster contiguity is enforced via constraints. The network model is taken from [14]; the reader is referred to that study for further details on the network setup.

3.4.1 Identification results

Accumulation state and inflow demand trajectories $n(t)$ and $q(t)$ are obtained by simulating a congested scenario for the network in fig. 3.2 using the Aimsun microscopic simulation framework. To reflect measurement noise, random noise terms $v_n(t)$ and $v_q(t)$ are added to the true trajectories to obtain the noisy measurements $y_n(t)$ and $y_q(t)$.

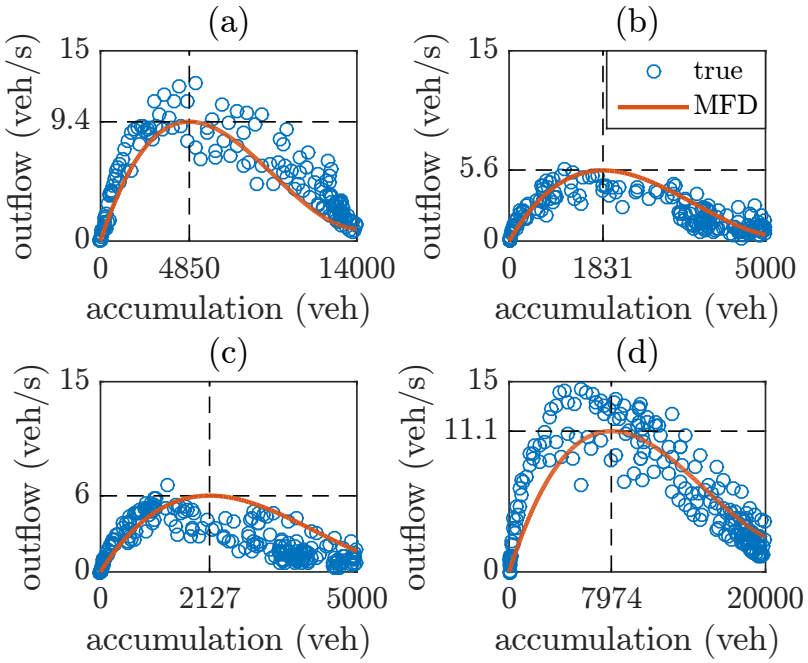

Figure 3.3 – Outflow as a function of regional accumulation for (a) region 1, (b) region 2, (c) region 3, (d) region 4, comparing the true outflow (blue), with the MFDs obtained by the MBPE method (red).

Covariances of the noise terms are chosen as $\Sigma_{v_n} = I\sigma_{v_n}$ and $\Sigma_{v_q} = I\sigma_{v_q}$, with $\sigma_{v_n} = 250$ veh and $\sigma_{v_q} = 0.1$ veh/s, representing moderate amount of noise. A no control scenario is considered, which employs well-tuned fixed perimeter control input values. The network is empty at the beginning and faces increasing inflow demands. The demands are nonzero for the first 2 hours of the simulation, while the total simulation length is 8 hours to ensure that the network is empty also at the end of the simulation (to be able to compare different cases). With a sampling time of $T = 90$ s, the simulation length is $K = 320$ time steps. Given the measurements on accumulation and inflow demand trajectories, the optimization problem (3.8) is solved to obtain the MFD parameters.

The MFDs obtained by the proposed MBPE method are shown in fig. 3.3, where they are compared with the true values of the outflow as a function of regional accumulation $g_i(n_i(t))$ (i.e., those obtained from microscopic simulation).

Overall, these results suggest that the proposed MBPE method is able to obtain MFDs that make physical sense, as they have a good qualitative match with the true outflows. However, the ultimate test for the obtained MFDs is usage in traffic estimation and control for improving mobility, which is examined in the following sections.

3.4.2 Estimation and control results

The MFDs (i.e., the model parameters vector $\hat{p}$) obtained by the MBPE method are used in the MHE and MPC schemes to control the urban network via perimeter control actuation for improving mobility under situations with noisy measurements. The MHE and MPC scheme is built using direct multiple shooting [70], while the dynamics are discretized with the Runge–Kutta method with a sampling time of $T = 90$ s. The implementation is done using MPCTools [71], which is an interface to CasADi [72], with IPOPT [73] as solver, in MATLAB 8.5.0 (R2015a), on a 64-bit Windows PC with 3.6-GHz Intel Core i7 processor and 16-GB RAM. Estimation and prediction horizons are chosen as $N_\mathrm{e} = 20$ and $N_\mathrm{c} = 20$, following the tuning results of [59] and [13], respectively. The perimeter controls are bounded via $\underline{u} = 0.1$ and $\bar{u} = 0.9$, with a rate limit of $\Delta_u = 0.1$. Simulation length is $K = 320$ in number of time steps, corresponding to 8 hours of real time, as in the no control case. The combined estimation and control scenario is simulated using the Aimsun microscopic simulation framework together with stand-alone MHE and MPC executable generated using MATLAB. The simulation operates by evolving traffic conditions through Aimsun, where the MHE-MPC code is called every 90 seconds. The MHE code, given recent measurements of accumulation $y_n(t)$ and inflow demands $y_q(t)$, solves 3.16 to find the accumulation state and inflow demand estimates $\hat{n}(t)$ and $\hat{q}(t)$. Then the MPC code, given $\hat{n}(t)$ and $\hat{q}(t)$, solves 3.24 to find the perimeter control inputs u_k^* (with $k = 0, \ldots, N_\mathrm{c} - 1$). Only the first one of these (i.e., u_0^*) is applied, which is realized in Aimsun by changing the duration of the green phases of the 28 predefined signalized intersections (out of about 600 in the network; see the circles in fig. 3.2a). The whole procedure is repeated at the next time step for 320 time steps.

The estimation results are shown in fig. 3.4 and fig. 3.5, which depict accumulation state and inflow demand trajectories (with measured, true, and estimated values) for a single Aimsun simulation with the combined MHE-MPC scheme. These figures suggest that the MHE scheme is able to obtain decent estimation performance, as indicated by the good match between the true and estimated accumulation state trajectories. Moreover, the regional accumulations for the no control case and the combined MHE-MPC scheme are shown in fig. 3.7. From the figure it is seen that the MHE-MPC scheme is able to decrease accumulations (and thus, the total time spent by vehicles in the network) and clear the network much faster, yielding an improvement of 31% over the no control case. These results indicate that the proposed traffic control framework carries strong potential of improving mobility in perimeter controlled city-scale urban networks. Moreover, the total CPU time of the MHE-MPC scheme is around 3 s (which is roughly negligible with respect to the sampling time of 90 s), indicating real-time feasibility of the proposed scheme.

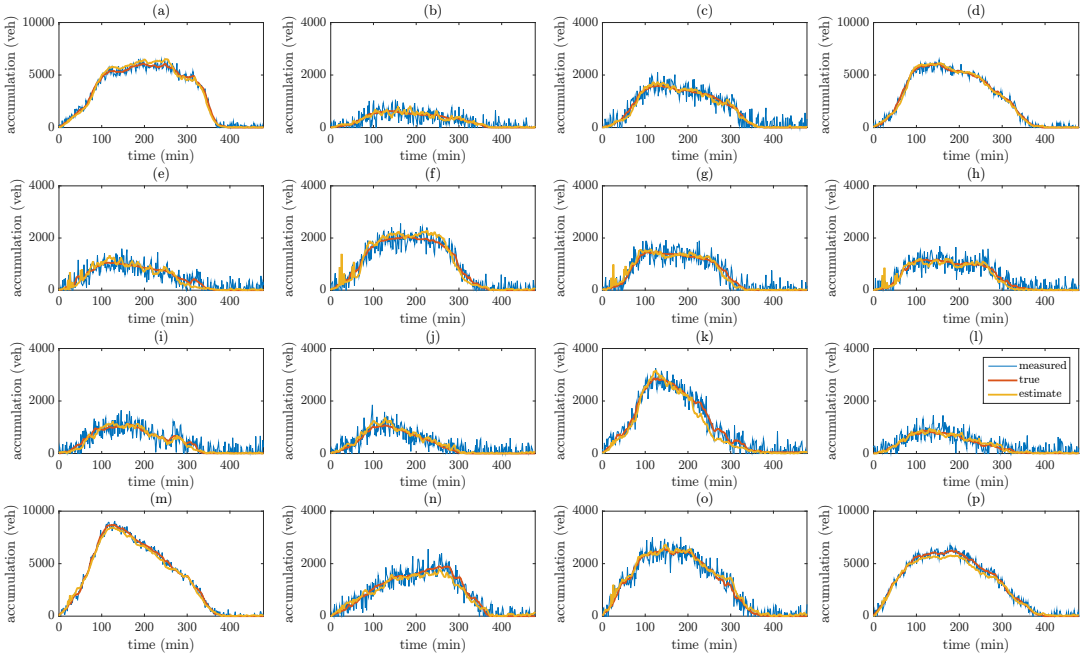

Figure 3.4 – Accumulation state $n_{ij}(t)$ trajectories with combined MHE-MPC scheme, showing the measured (blue), true (red), and estimated (yellow) values of: (a) $n_{11}(t)$, (b) $n_{12}(t)$, (c) $n_{13}(t)$, (d) $n_{14}(t)$, (e) $n_{21}(t)$, (f) $n_{22}(t)$, (g) $n_{23}(t)$, (h) $n_{24}(t)$, (i) $n_{31}(t)$, (j) $n_{32}(t)$, (k) $n_{33}(t)$, (l) $n_{34}(t)$, (m) $n_{41}(t)$, (n) $n_{42}(t)$, (o) $n_{43}(t)$, (p) $n_{44}(t)$.

3.5 Conclusion

A large-scale traffic management framework is proposed, consisting of optimization-based identification, estimation, and control methods employing macroscopic traffic models. The identification method, considering an MFD-based dynamical model of urban traffic, is based on the least squares prediction error approach. In this approach the parameter estimation problem is cast as an optimization problem aiming to minimize the weighted least squares difference between the measurements and model predictions. Furthermore, nonlinear MHE and economic MPC formulations are presented, intended for use together with the identification method for obtaining the MFD parameters, for alleviating congestion in perimeter controlled large-scale urban road networks. The proposed methods are tested in microscopic simulation experiments considering an urban network modeled as a perimeter controlled four region MFDs system. Showing good estimation and control performance, the results indicate strong potential of the proposed large-scale traffic control framework for improving mobility in city-scale urban networks.

Ongoing work involves evaluating the proposed methods on more scenarios (i.e., inflow demand patterns) in microscopic simulation experiments. Furthermore, the proposed identification method can be compared with the standard technique of obtaining MFD parameters via fitting polynomials to historical data on accumulations and outflows, and

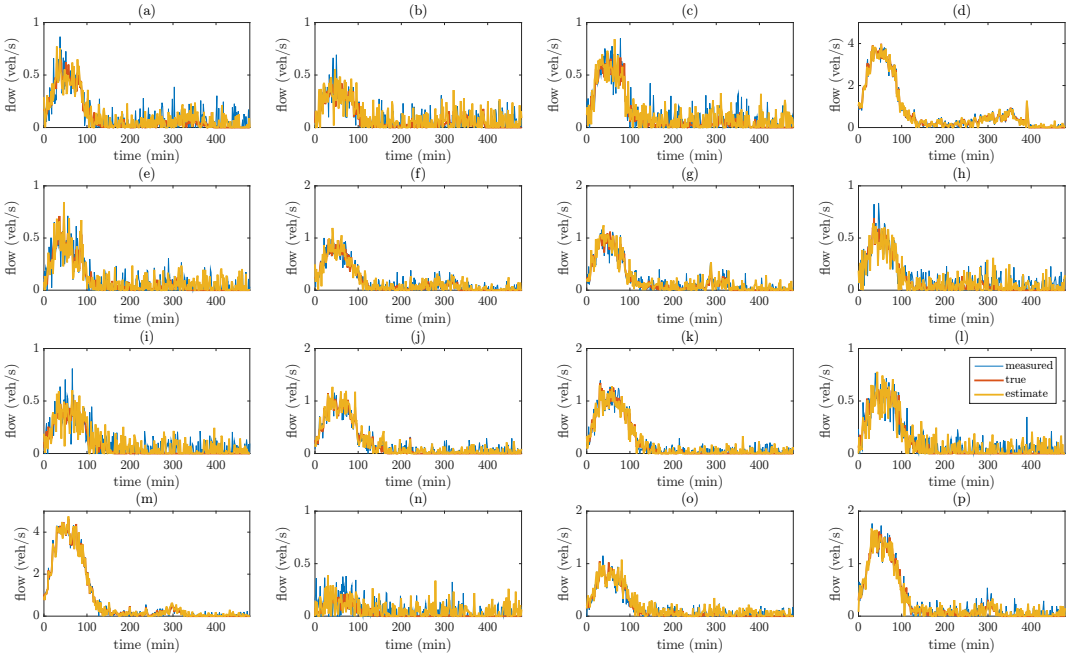

Figure 3.5 – Inflow demand $q_{ij}(t)$ trajectories with combined MHE-MPC scheme, showing the measured (blue), true (red), and estimated (yellow) values of: (a) $q_{11}(t)$, (b) $q_{12}(t)$, (c) $q_{13}(t)$, (d) $q_{14}(t)$, (e) $q_{21}(t)$, (f) $q_{22}(t)$, (g) $q_{23}(t)$, (h) $q_{24}(t)$, (i) $q_{31}(t)$, (j) $q_{32}(t)$, (k) $q_{33}(t)$, (l) $q_{34}(t)$, (m) $q_{41}(t)$, (n) $q_{42}(t)$, (o) $q_{43}(t)$, (p) $q_{44}(t)$.

sensitivity of estimation and control performance of the proposed methods to varying levels of measurement noise can be examined. Another direction currently under investigation is establishing the relationship between practical measurements involving loop detectors and those required by the MFD-based models (i.e., number of vehicles in a region with a certain destination). For progress towards practicable state estimation and perimeter control, proper sensor models and associated signal uncertainty need to be examined. A journal article considering some of the aforementioned directions is currently under preparation.

With this chapter we conclude part I, which focused on model-based estimation and control for perimeter controlled urban networks. Being a practically viable macroscopic actuation method, perimeter control carries strong potential for field applications of city-level urban traffic control. However, more advanced methods for actuation, such as route guidance, are expected to enable further improvements in mobility for large-scale traffic management. In part II, we focus on the design of optimization-based control methods employing regional route guidance.

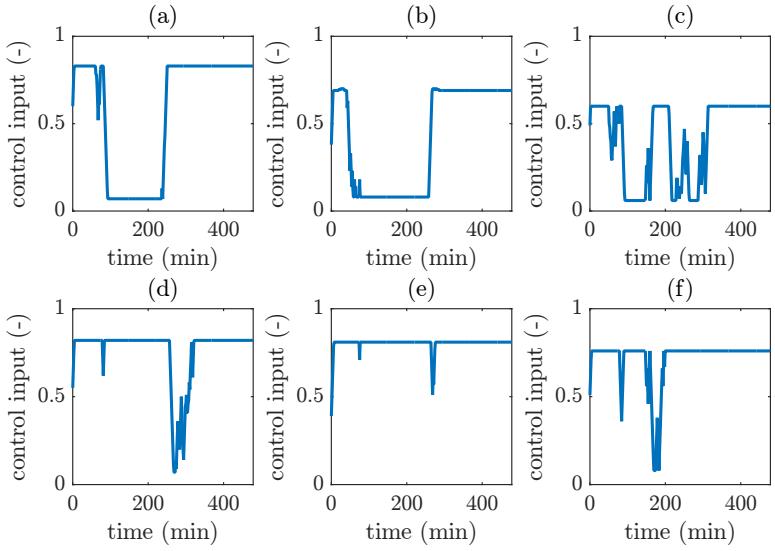

Figure 3.6 – Control input $u_{ih}(t)$ trajectories with combined MHE-MPC scheme: (a) $u_{14}(t)$, (b) $u_{24}(t)$, (c) $u_{34}(t)$, (d) $u_{41}(t)$, (e) $u_{42}(t)$, (f) $u_{43}(t)$.

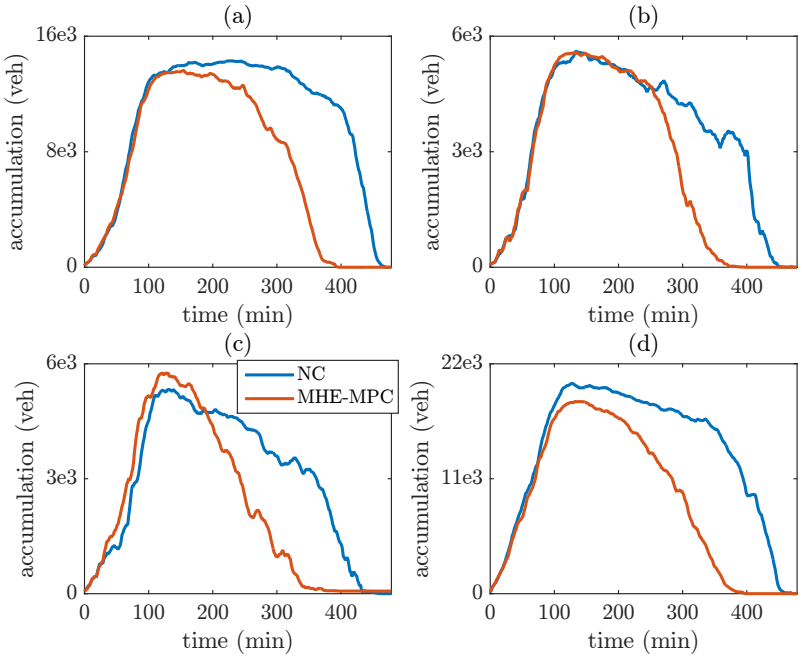

Figure 3.7 – Regional accumulation $n_i(t)$ trajectories comparing the no control case (blue) with the combined MHE-MPC scheme (red): (a) $n_1(t)$, (b) $n_2(t)$, (c) $n_3(t)$, (d) $n_4(t)$.

Part II

Large-scale traffic management via regional route guidance

Chapter 4

Integration of route guidance and perimeter control

4.1 Introduction

This chapter is dedicated to the development of network-level economic MPC schemes integrating perimeter control and regional route guidance for alleviating congestion in large-scale urban networks. Firstly, a novel MFD-based urban network model with cyclic behavior avoidance property is described. The model is expected to enable more accurate simulations including regional route guidance-based controllers, as route guidance might otherwise cause cyclic routes. Furthermore, the problem of finding the perimeter control and route guidance inputs for a multi-region urban network to minimize total time spent (TTS) is formulated as an economic MPC problem, along with various actuator configurations. The analysis in this work sheds some light to the demand conditions for which coupling of perimeter control and route guidance can prove beneficial. Macroscopic simulations are used to examine mobility improvements for the proposed economic MPC schemes, and the effect of driver compliance to route guidance on network performance.

Literature review is not included here; it is given for the whole dissertation in chapter 1.

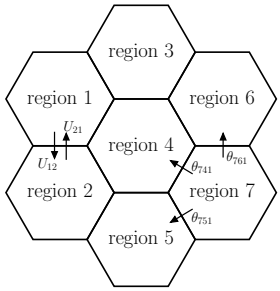

Figure 4.1 – Schematic of an urban network with 7 regions.

4.2 Modeling of a multi-region urban network

4.2.1 MFD-based modeling with route guidance

We consider an urban network $\mathcal{R}$ with heterogeneous distribution of accumulation, consisting of R homogeneous regions, i.e., $\mathcal{R} = \{1, 2, \ldots, R\}$, each with a well-defined outflow MFD, defined via $G_I(N_I(t))$ (veh/s) expressing the trip completion flow (i.e., outflow) at accumulation $N_I(t)$. A network consisting of 7 regions is schematically shown in fig. 4.1. The exogenous inflow demand generated in region I with destination J is $Q_{IJ}(t)$ (veh/s), whereas $N_{IJ}(t)$ (veh) is the accumulation in region I with destination J, and $N_I(t)$ (veh) the total accumulation in region I, at time t; $I, J \in \mathcal{R}$; $N_I(t) \triangleq \sum_{J\in\mathcal{R}} N_{IJ}(t)$. Between each pair of neighboring regions I and H ($I \in \mathcal{R}$, $H \in \mathcal{N}_I$, where $\mathcal{N}_I$ is the set of regions neighboring region I) there exists perimeter controls $U_{IH}(t)$ and $U_{HI}(t)$ $\in [0, 1]$ that can manipulate the transfer flows. Furthermore, each region is equipped with regional route guidance controls $\theta_{IHJ}(t)$ ($I \in \mathcal{R}$, $H \in \mathcal{N}_I$, $J \in \mathcal{R} \setminus \{I\}$), that can distribute the transfer flows exiting a region over its neighboring regions. Dynamics of an R-region MFDs network are [36], [52]:

$$\dot{N}_{II}(t) = Q_{II}(t) - M_{II}(t) + \sum_{H\in\mathcal{N}_I} U_{HI}(t) M_{HII}(t) \tag{4.1a}$$

$$\dot{N}_{IJ}(t) = Q_{IJ}(t) - \sum_{H\in\mathcal{N}_I} U_{IH}(t) M_{IHJ}(t) + \sum_{H\in\mathcal{N}_I; H\neq J} U_{HI}(t) M_{HIJ}(t), \tag{4.1b}$$

for $I, J \in \mathcal{R}$, where $M_{II}(t)$ (veh/s) is the exit (i.e., internal trip completion) flow from region I to destination I:

$$M_{II}(t) = \frac{N_{II}(t)}{N_I(t)} G_I(N_I(t)) \tag{4.2}$$

and $M_{IHJ}(t)$ (veh/s) is the transfer flow from region I to destination J through the next immediate region H:

$$M_{IHJ}(t) = \theta_{IHJ}(t) \frac{N_{IJ}(t)}{N_I(t)} G_I(N_I(t)), \tag{4.3}$$

with $M_{HII}(t)$ and $M_{HIJ}(t)$ defined similarly, expressing the transfer flows from H through I with destinations I and J, respectively. It is assumed that trips inside a region have similar lengths (i.e., the distance traveled per vehicle inside a region does not depend on the origin and destination of the trip). Simulation and empirical results [16] suggest that the MFD can be approximated by an asymmetric unimodal curve skewed to the right (i.e., the critical accumulation N_I^{cr}, which maximizes $G_I(N_I(t))$, is less than half of the jam accumulation N_I^{jam}, which puts the region in gridlock). Thus, $G_I(N_I(t))$ can be expressed with a third-degree polynomial in the variable $N_I(t)$, i.e., $G_I(N_I(t)) = A_I N_I^3(t) + B_I N_I^2(t) + C_I N_I(t)$, where A_I, B_I, and C_I are estimated parameters.

Transfer flows are influenced by the boundary capacity between regions I and H, as high accumulation in region H might restrict the reception of inflows from the boundary, which can be formalized through the following equation expressing capacity-restricted transfer flow $\hat{M}_{IHJ}(t)$ [36], [52]:

$$\hat{M}_{IHJ}(t) = \min\left(M_{IHJ}(t), C_{IH}(N_H(t))\frac{M_{IHJ}(t)}{\sum_{K\in\mathcal{R}} M_{IHK}(t)}\right) \tag{4.4}$$

where $C_{IH}(N_H(t))$ (veh/s) is the boundary capacity between regions I and H that depends on N_H as follows [36]:

$$C_{IH}(N_H) = \begin{cases} C_{IH}^{\max} & \text{if } 0 \le N_H < \alpha \cdot N_{H,\text{jam}} \\ \frac{C_{IH}^{\max}}{1-\alpha}\left(1 - \frac{N_H}{N_H^{\text{jam}}}\right) & \text{if } \alpha \cdot N_H^{\text{jam}} \le N_H \le N_H^{\text{jam}}, \end{cases} \tag{4.5}$$

where $C_{IH}^{\max}$ (veh/s) is the maximum boundary capacity, N_H^{jam} (veh) is the jam accumulation of the receiving region H, whereas $\alpha \cdot N_H^{\text{jam}}$ (with $0 < \alpha < 1$) specifies the point where $C_{IH}(N_H)$ starts decreasing with increasing accumulation.

The boundary capacity constraint can be omitted in the prediction model of MPC for computational advantage. The physical reasoning of this omission is that (i) the boundary capacity decreases for accumulations much larger than the critical accumulation, and (ii) the controller will not allow the regions to have accumulations close to gridlock [34]. The effect of tightening boundary capacity is studied in section 4.4.5.

The assumption of a low-scatter regional outflow MFD is based on the equivalent assumption of a time-invariant regional trip length. While an adequate model for control design with simplified system dynamics without delays (i.e., it considers outflows equal to the ratio of production over constant trip length), and although there are empirical verifications about its validity via aggregated data (e.g.,[16]), the MFD should not be considered as a universal law. For example, strong fluctuations in the demand that create fast evolving transients can influence the trip length distribution in a region at a specific time, potentially causing the ratio of production over trip length approximation

of outflow to have inaccuracies. While we consider this a valid assumption for a range of cases, further research would be useful to study under what conditions more complex dynamics (with delays) are required (see, e.g., some analysis in [76]), which is a research priority.

4.2.2 Cyclic behavior prohibiting urban network model

The urban network model (4.1) has no memory of the region the vehicles were previously, thus does not prohibit vehicles from flowing back and forth between neighboring regions (i.e., it permits cyclic behavior). While this memoryless choice of routes is not crucial when only perimeter control actuation is applied, it is physically important for route guidance based schemes, where the controller may try to emulate perimeter control actuation via cyclic routes. We also need to be able to compare travel times and trip lengths for inflow demands $Q_{IJ}(t)$ and for various control strategies and driver compliance levels. Thus, instead of N_{IJ} and M_{IHJ} we have to introduce more detailed states. With N_{OGIJ} and M_{OGIHJ} denoting the accumulation and flow, respectively, with origin O, previous region G, current region I, destination region J, and immediate next region H, the dynamics keeping memory of origin and previous regions can be written as:

$$\dot{N}_{IIII}(t) = Q_{II}(t) - M_{IIIII}(t), \quad \forall I \in \mathcal{R} \tag{4.6a}$$

$$\dot{N}_{IIIJ}(t) = Q_{IJ}(t) - \sum_{H \in \mathcal{N}_I} U_{IH}(t) M_{IIIHJ}(t), \quad \forall I, J \in \mathcal{R},\ J \neq I, \tag{4.6b}$$

$$\dot{N}_{OGII}(t) = \sum_{F \in \mathcal{N}_G^* \setminus \{I\}} U_{GI}(t) M_{OFGII}(t) - M_{OGIII}(t),$$
$$\forall O, G, I \in \mathcal{R},\ G \in \mathcal{N}_I,\ O \neq I, \tag{4.6c}$$

$$\dot{N}_{OGIJ}(t) = \sum_{F \in \mathcal{N}_G^* \setminus \{I,J\}} U_{GI}(t) M_{OFGIJ}(t) - \sum_{H \in \mathcal{N}_I \setminus \{O,G\}} U_{IH}(t) M_{OGIHJ}(t)$$
$$\forall O, G, I, J \in \mathcal{R},\ G \in \mathcal{N}_I,\ O \neq I,\ O \neq J,\ G \neq J,\ J \neq I, \tag{4.6d}$$

where $\mathcal{N}_G^*$ is the set containing the neighboring regions of G and region G itself. Note that if the last two indices of a flow term are identical, then this denotes an exit flow (as next and final region are the same); it denotes a transfer flow otherwise. Note that in (4.6a) there are no control inputs as flows are internal and uncontrolled. Note also that in (4.6c)–(4.6d) the positive terms of the right hand side are controlled transfer flows from the neighboring regions to the current region. The exit and transfer flow terms can be calculated as follows:

$$M_{OGIHJ}(t) = \theta_{OGIHJ}(t) \frac{N_{OGIJ}(t)}{N_I(t)} G_I(N_I(t)), \tag{4.7}$$

where θ_{OGIHJ} denotes the fraction of flows in an identical way with the flow terms, having the same 5 indices.

Using (4.6) as the simulation model (i.e., the *plant* representing reality) with MPC controllers having (4.1) as the prediction model requires the transfer of variables between the two models as follows:

$$\sum_{O\in\mathcal{R}\setminus\{J\}}\sum_{G\in\mathcal{R}\setminus\{J\}} N_{OGIJ}(t) = N_{IJ}(t),\ \forall I,J\in\mathcal{R} \tag{4.8}$$

for the accumulations states and

$$\theta_{OGIHJ}(t) = \begin{cases} \theta_{IHJ}(t) & \text{if } H\neq G, \\ 0 & \text{otherwise} \end{cases} \tag{4.9}$$
$$\forall O,G,I,J\in\mathcal{R},$$
$$G\in\mathcal{N}_I,\ H\in\mathcal{N}_I\setminus\{O\}$$
$$O\neq I,\ O\neq J,\ G\neq J,\ J\neq I$$

for the fraction of flows, where cycle-inducing θ_{OGIHJ} terms (i.e., those with $H=G$) are forced to be 0. Owing to this, the model (4.6) can prohibit cycles of length 2, and is thus a more realistic representation of urban network dynamics. For prohibiting longer cycles, (4.6) should be extended with longer route memory, but this is not considered in this work since cycles longer than two are assumed to be negligible.

4.3 Optimal control via perimeter control and route guidance

4.3.1 Model predictive control

We formulate the problem of finding the U_{IH} and θ_{IHJ} values that minimize TTS (for a finite horizon) as the following discrete time economic nonlinear MPC problem:

$$\begin{aligned}
\underset{U,\theta}{\text{minimize}} \quad & T_c \cdot \sum_{k=0}^{N_p-1} \mathbf{1}^T N(k) && (4.10)\\
\text{subject to} \quad & N(0) = \hat{N}(t_c) && (4.11)\\
& |U(0) - \hat{U}(t_c-1)| \le \Delta_U && (4.12)\\
& |\theta(0) - \hat{\theta}(t_c-1)| \le \Delta_\theta && (4.13)\\
& \text{for } k = 0, \dots, N_p - 1 : && (4.14)\\
& \quad N(k+1) = f(N(k), Q(k), U(k), \theta(k)) && (4.15)\\
& \quad 0 \le \sum_{j \in \mathcal{R}} N_{IJ}(k) \le N_I^{\text{jam}},\ \forall I \in \mathcal{R} && (4.16)\\
& \quad U_{\min} \le U_{IH}(k) \le U_{\max},\ \forall I \in \mathcal{R}, H \in \mathcal{N}_I && (4.17)\\
& \quad 0 \le \theta_{IHJ}(k) \le 1,\ \forall I, J \in \mathcal{R}, I \ne J, H \in \mathcal{N}_I && (4.18)\\
& \quad \sum_{H \in \mathcal{N}_I} \theta_{IHJ}(k) = 1,\ \forall I, J \in \mathcal{R}, I \ne J && (4.19)\\
& \quad \text{if } k \ge N_c : && (4.20)\\
& \quad\quad U(k) = U(k-1) && (4.21)\\
& \quad\quad \theta(k) = \theta(k-1), && (4.22)
\end{aligned}$$

where T_c is the control sampling time, $N(k)$, $Q(k)$, $U(k)$, and $\theta(k)$ are vectors containing all $N_{IJ}(k)$, $Q_{IJ}(k)$, $U_{IH}(k)$, and $\theta_{IHJ}(k)$ terms, respectively, with k being the control interval counter, f is the time discretized version of eq. (4.1)–(4.3), t_c is the current control time step and $\hat{N}(t_c)$ is the measurement taken at t_c, $\hat{U}(t_c-1)$ and $\hat{\theta}(t_c-1)$ are the control inputs applied to the plant previously, N_p and N_c are the prediction and control horizons, whereas Δ_U and Δ_θ are the rate limits on perimeter control and route guidance inputs, respectively.

The problem (4.10) is a nonconvex nonlinear program (NLP), which can be solved efficiently via, e.g., sequential quadratic programming (SQP) or interior point solvers.

We propose three MPC schemes: (i) perimeter control MPC (PC) has U_{IH} as control input, while drivers are free to choose their own routes (i.e., θ_{IHJ}), which are assumed fixed to their measured value, at t_c, for the prediction horizon. (ii) For route guidance MPC (RG) θ_{IHJ} is the control input, while U_{IH} is fixed to $U_{\max}$. (iii) Perimeter control and route guidance MPC (PCRG) has access to both actuators. While $\theta_{IHJ}(t_c)$ is difficult to estimate with fixed location sensors, use of mobile sensors with advanced estimation

techniques provide strong potential in this direction (see, e.g., [77]).

Performance metrics for evaluating the MPC schemes are TTS and *total traveled distance* (TTD):

$$\mathrm{TTS} = T_s \cdot \sum_{t=1}^{T_{\mathrm{exp}}} \sum_{I \in \mathcal{R}} N_I(t), \tag{4.23}$$

$$\mathrm{TTD} = T_s \cdot \sum_{t=1}^{T_{\mathrm{exp}}} \sum_{I \in \mathcal{R}} L_I \cdot \Big(M_{II}(t) + \sum_{H \in \mathcal{N}_I} \sum_{J \in \mathcal{R} \setminus I} \bar{M}_{IHJ}(t) \Big), \tag{4.24}$$

where the flow $\bar{M}_{IHJ}(t)$ (veh/s) is defined as $\bar{M}_{IHJ}(t) = U_{IH}(t)\theta_{IHJ}(t)M_{IJ}(t)$. It is important to look at both performance metrics, as route guidance might enforce some drivers to take significantly longer routes for the system benefit. Such a result would be difficult to be acceptable in practice as drivers would follow the proposed routes only if their individual travel time is not significantly worse.

For a single-region city governed by an outflow MFD, minimizing TTS will result in maximizing outflow (which is equivalent to maximizing TTD), as the objective is to let vehicles finish their trips as soon as possible. Thus, as proven in [8], the best strategy is to keep the region at its critical accumulation if the delays of vehicles waiting outside the network (i.e., the virtual queues) are considered.

For a multi-region city (as is the case in the chapter), however, it might be impossible to keep all regions under or at critical accumulation. Then, control via tracking regional accumulation setpoints is difficult, as it is not straightforward to find those setpoints that minimize TTS (since these might be time-varying and depend on the demand pattern). Maximizing TTD, on the other hand, might create very long routes for some vehicles especially under uncongested conditions due to detouring, which would decrease network outflow.

4.3.2 Controller tuning and computational efficiency

MPC performance is strongly influenced by the prediction horizon N_p. Computational effort is affected also by the chosen direct method and NLP solver (see [69] for details). To study the relations between all of the above, a series of simulation experiments (based on the congested scenario in section 4.4.1) is conducted with varying values of N_p (with N_c fixed to 2 and a control sampling time of $T_c = 240$ s) and various direct methods (see [78] for details). Direct multiple shooting (DMS, [70]) and direct collocation (DC) (solved with the solver IPOPT [73]) results for all three MPC schemes[1] are included together with direct single shooting (DSS) (solved with an SQP solver) for PC. Using

[1] Implementation is done via the CasADi toolbox [72] in MATLAB 8.5.0 (R2015a), on a 64-bit Windows PC with 3.6-GHz Intel Core i7 processor and 16-GB RAM.

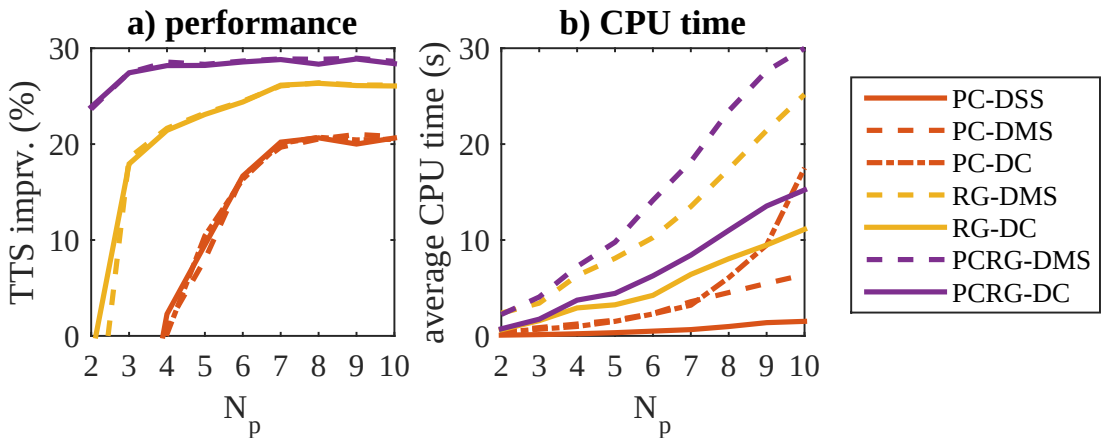

Figure 4.2 – (a) Percent improvement in TTS over NC and (b) average CPU times for the MPC schemes with various direct methods as a function of N_p.

SQP for DMS and DC is computationally disadvantageous, since SQP favors small and dense NLPs (such as those arising from DSS), while DMS and DC yield large and sparse NLPs (which are amenable to efficient solutions via e.g. IPOPT). The results, given in fig. 4.2, show the TTS performance and the average CPU times, which indicate that: (a) TTS performance is fairly insensitive to the choice of N_p for $N_p \geq 7$, (b) DSS is favorable for PC, whereas DC is favorable for RG and PCRG, (c) even for short horizons PCRG is able to yield high improvements.

4.4 Results

All simulations are conducted on a 7 region urban network (see fig. 4.1), with the simulation model given in (4.6) for representing the reality. A unit MFD is considered with the parameters $\bar{A} = 4.133 \cdot 10^{-11}$, $\bar{B} = -8.282 \cdot 10^{-7}$, $\bar{C} = 0.0042$, jam accumulation $\bar{N}^{\text{jam}} = 10^4$ (veh), critical accumulation $\bar{N}^{\text{cr}} = 3.4 \cdot 10^3$ (veh), maximum outflow $G(\bar{N}^{\text{cr}}) = 6.3$ (veh/s), with an average trip length of $\bar{L} = 3600$ m, which are consistent with the MFD observed in a part of downtown Yokohama (see [16]). Each region is assumed to have a different MFD that is a (within $\pm 10\%$) scaled version of the unit MFD. Boundary capacity effect is included, with values $\bar{C}_{IH}^{\max} = 3.2$ veh/s and $\bar{\alpha} = 0.64$ for the unit MFD.

Based on the results in section 4.3.2, the prediction and control horizons are chosen as $N_p = 7$ and $N_c = 2$ for the MPC schemes. Simulation sampling time is 30 s while the length of the simulation experiment is $T_{\text{exp}} = 240$ (in number of simulation steps), giving an effective length of 120 minutes. Bounds of U_{IH} are $U_{\min} = 0.1$ and $U_{\max} = 0.9$, whereas the rate limits are $\Delta_U = 0.2$ and $\Delta_\theta = 0.1$, to reflect the fact that it is more difficult to cause abrupt changes in routing.

For capturing the effect of measurement noise in accumulation states (as accumulations have to be measured from fixed and mobile sensors, which invariably have noise), we add random noise terms with normal distribution:

$$\tilde{N}_{IJ}(t) = N_{IJ}(t) + N_{IJ}(t) \cdot \mathcal{N}(0, \sigma^2_{N_{IJ}}),\ \forall I, J \in \mathcal{R}, \tag{4.25}$$

where the noise has zero mean and its variance is chosen as $\sigma^2_{N_{IJ}} = 0.25$ in the simulations. Demand uncertainty is also considered, with the MPC having access to average demand profiles, while the actual inflow demands have random noise:

$$\tilde{Q}_{IJ}(t) = Q_{IJ}(t) + Q_{IJ}(t) \cdot \mathcal{N}(0, \sigma^2_{Q_{IJ}}),\ \forall I, J \in \mathcal{R}, \tag{4.26}$$

with the variance chosen as $\sigma^2_{Q_{IJ}} = 0.25$ in the simulations, representing presence of large noise.

The MPC controllers are compared with a *no control* (NC) case, in which U_{IH} are fixed to $U_{\max}$, while drivers are free to choose their routes. In simulations this is captured by calculating θ_{IHJ} by a logit model (see [79]) using the current travel times from I to destination J through a predefined finite number of shortest sequences of regions connecting the two, calculated with Dijkstra's algorithm for K-shortest paths ($K = 3$ for this chapter). As drivers adapt to traffic conditions in real time, the θ_{IHJ} values are updated at each control time step. The logit model relaxes the assumption that drivers always choose the physical shortest path. Simulations using logit model thus tend to be more realistic as drivers rarely have perfect information and do not always behave as rational actors. Parameters of the logit model can be adjusted to reflect the amount of information available to drivers or their sensitivity to travel time differences between routes.

An interesting point to investigate is about deciding what the preferred actuation scheme is (i.e., PC, RG, or PCRG) under different demand conditions, given that there is a nonnegligible installation cost. While in principle the regions of the city that attract most of the trips should operate at the critical accumulation that maximizes flow (e.g., [8] proves this for single region systems), this might not be the case for multiple regions with competing objectives. Our objective is also to investigate the attractivity of the regions of a city with respect to (i) destinations and (ii) crossing zones. While point (i) is clear, with respect to point (ii) a region might attract a lot of trips simply because many shortest paths are passing from this region (even if destinations are elsewhere). Thus, two simulation parameters are defined to construct various scenarios: (a) The ratio of demands with destination region 4 (i.e., city center) to demands from periphery to periphery, denoted by ρ and (b) driver compliance level, denoted by γ. The ratio ρ, expressing the relative intensity of the inflow demands towards city center, is defined as

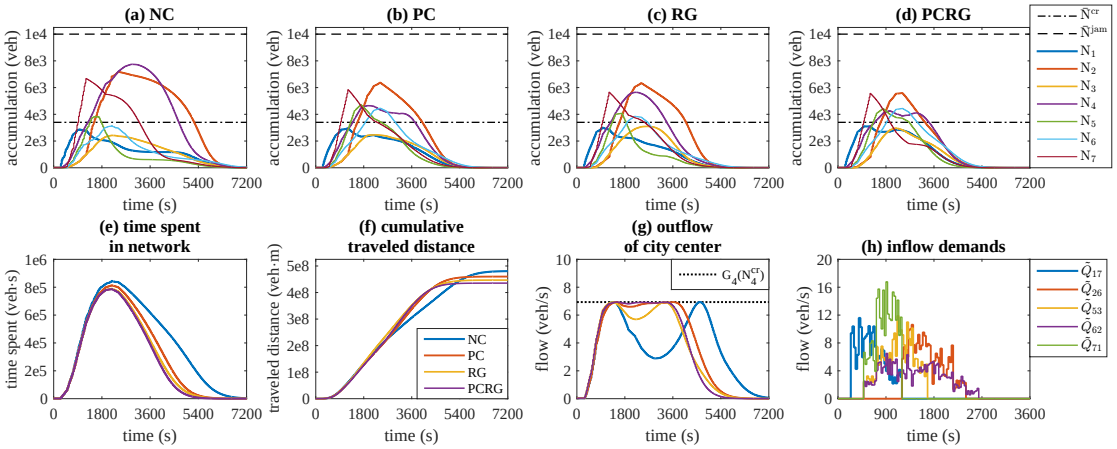

Figure 4.3 – Results of the congested scenario for the no control (NC) case and the three MPC schemes. Regional accumulations for (a) NC, (b) PC, (c) RG, (d) PCRG. Comparison of the four cases for (e) time spent in network, (f) standard deviation of regional accumulations, (g) outflow of city center. (h) Noisy inflow demand profiles, expressing demands for trips between 5 origin-destination region pairs.

follows:

$$\rho = \frac{\sum_{t=1}^{T_{\text{exp}}} \sum_{I \in \mathcal{R}} Q_{I4}(t)}{\sum_{t=1}^{T_{\text{exp}}} \sum_{I \in \mathcal{R}\setminus\{4\}} \sum_{J \in \mathcal{R}\setminus\{4\}} Q_{IJ}(t)}, \tag{4.27}$$

whereas the driver compliance level γ (also defined as a constant for a single simulation experiment) indicates the percentage of drivers following the route guidance recommendations of the traffic control scheme (i.e., either RG and PCRG), which is used in obtaining the route guidance command θ_{IHJ} value for the control step t_c as follows:

$$\theta^{\text{real}}_{IHJ}(t_c) = \gamma \theta^{\text{MPC}}_{IHJ}(t_c) + (1-\gamma)\theta^{\text{logit}}_{IHJ}(t_c), \tag{4.28}$$

where $\theta^{\text{real}}_{IHJ}(t_c)$ is the realized route guidance command (i.e., the value used in simulation), whereas $\theta^{\text{MPC}}_{IHJ}(t_c)$ and $\theta^{\text{logit}}_{IHJ}(t_c)$ are the outputs of the MPC and the logit model, respectively.

4.4.1 Congested scenario

Let us describe the base case scenario: The network is uncongested at the beginning, but faces increased inflow demands as time progresses. The driver compliance level γ is 100% and ratio of demands ρ is equal to 0, meaning no trips have city center as destination–nevertheless this is an important region of attraction as many trips prefer to cross the center due to short distance. The results are given in fig. 4.3, where the evolution of regional accumulations (fig. 4.3a to 4.3d) are shown alongside graphs of time spent in network (fig. 4.3e), cumulative traveled distance (fig. 4.3f), outflow of city

center (i.e., region 4) (fig. 4.3g), and the noisy inflow demands $\tilde{Q}_{IJ}(t)$ (fig. 4.3h), all as a function of simulation time, for the no control (NC) case and the three MPC schemes (please refer to the legends in fig. 4.3 for descriptions of each figure). A summary of the results is given in table 4.1, which shows the two performance metrics about time and distance (i.e., TTS and TTD), improvement over the NC case for TTS, increase in TTD over the theoretically possible minimum TTD (which is calculated by considering that all vehicles are able to take the physical shortest path to their destinations under free flow conditions, and is equal to $3.87 \cdot 10^8$ veh·m), and the CPU times for the MPC schemes. The results indicate that all MPC schemes are capable of improving mobility in the urban network, as they have decreased values of both the TTS and TTD metrics, in comparison to the NC case. Noting that control sampling time T_c is chosen as 240 s, the CPU time results given in table 4.1 suggest that the schemes are computationally tractable, as their CPU times are negligible in comparison to T_c.

PCRG is superior in distributing the vehicle flows efficiently over the whole network, which translates to efficient usage of the network capacity, leading to less congestion and also decreased values of TTS. This is clearly seen in the regional accumulation plots (b)–(d) in fig. 4.3, where PCRG can suppress congestion evenly in all regions. Note also that for all three strategies not all regions are able to operate below the critical value of accumulation, so even the best control scheme still experiences some congestion for some regions, notably for smaller durations. This highlights the importance of using prediction and aggregated future O-D information via MPC. For example, PI type controllers without demand information (see [9], [12], [80]) are successful when all regions can operate close to their critical accumulations. But if this is not possible due to high demand, aggregated O-D information is expected to further improve network performance.

The NC case cannot avoid severe congestion close to gridlock, leading to drastic decrease in outflow for the city center (as seen in fig. 3g) and thus inefficient use of the city center capacity for transferring flows from periphery to periphery. This is crucial for both TTS and TTD metrics, since routes through the city center are generally the physical shortest paths connecting two opposing peripheral regions. The MPC schemes, on the

Table 4.1 – Performance Evaluation for Congested Scenario

Control scheme	TTS ($\times 10^7$ veh·s)	TTS decrease over NC (%)	TTD ($\times 10^8$ veh·m)	TTD increase over theo. min. (%)	Avg. CPU time (s)	Max. CPU time (s)
NC	9.50	–	4.81	25	–	–
PC	7.58	20	4.60	19	0.66	1.59
RG	7.02	26	4.47	16	6.43	8.22
PCRG	6.76	29	4.35	13	8.45	10.18

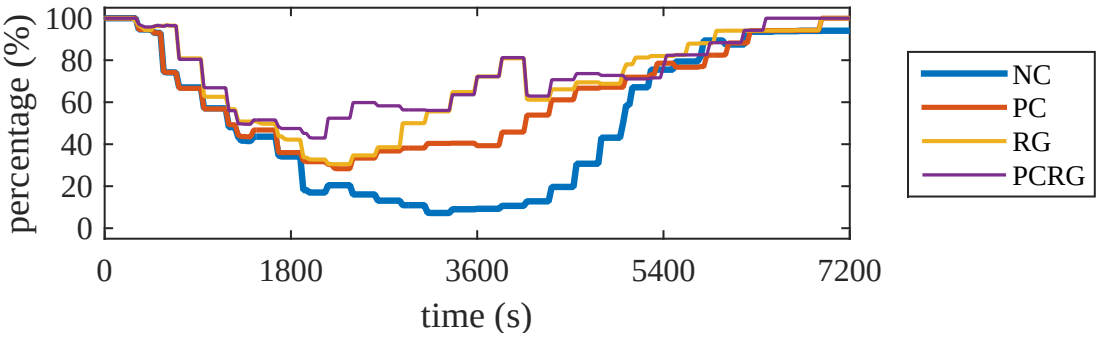

Figure 4.4 – Usage of physical shortest path for the congested scenario.

other hand, make efficient use of the city center as seen in the city center outflow (i.e., $G_4(N_4(t))$) plot in fig. 4.3g, which shows their success in keeping the city center close to critical accumulation N_4^{cr} until network starts to unload. It is interesting that city center remains severely congested even if drivers are adaptive and update their routes based on travel time information (i.e., the NC case), which is not the case when control is applied.

Route guidance based schemes can improve both TTS and TTD metrics compared to the PC scheme due to their authority over routing, increasing the percentage of drivers using the physical shortest path. Thus, vehicles spend less time and travel for shorter distances before exiting the network. The percentage of drivers that are momentarily using the physical shortest path to their destinations is given in fig. 4.4 for NC and the three MPC schemes. This result shows that route guidance based schemes succeed in making more drivers use the physical shortest path, explaining the improvement in TTD. The fact that regional route guidance (which tries to develop conditions close to system optimum) might create worse travel times for some users is analyzed later in the chapter.

4.4.2 Effect of cyclic behavior prohibition

To examine the effect of absence of cyclic behavior prohibition in the proposed model, given in section 4.2.2, a series of simulation experiments are conducted based on the scenario in section 4.4.1. The model formulation is changed via relaxing the condition $H \neq G$ in eq. (4.9) so as to allow cyclic flows. To summarize the presence of cyclic behavior, the percentage of vehicle flows that are returning to the region they came from among the total vehicle flows is considered:

$$\frac{\sum_{O\in\mathcal{R}}\sum_{K\in\mathcal{R}\setminus G}\sum_{G\in\mathcal{R}\setminus K}\sum_{K\in\mathcal{R}\setminus G}\sum_{J\in\mathcal{R}}\bar{M}_{OKGKJ}(t)}{\sum_{O\in\mathcal{R}}\sum_{G\in\mathcal{R}}\sum_{I in\mathcal{R}}\sum_{H\in\mathcal{R}}\sum_{J\in\mathcal{R}}\bar{M}_{OGIHJ}(t)}, \tag{4.29}$$

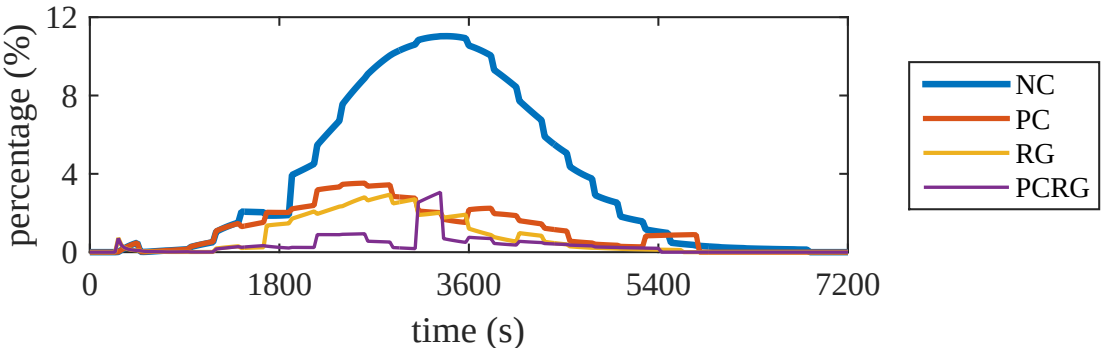

Figure 4.5 – Ratio of cyclic to total flows for NC and the three MPC schemes.

where the vehicle flow $\bar{M}_{OGIHJ}(t)$ is defined as follows

$$\bar{M}_{OGIHJ}(t) = U_{IH}(t)\theta_{OGIHJ}(t)M_{OGIJ}(t). \tag{4.30}$$

The results are given in fig. 4.5, showing this percentage as a function of simulation time. There are substantial cyclic flows occurring in the simulation, which can be avoided with the use of the proposed model, supporting the use of such a model with more detailed states to represent the plant.

4.4.3 Driver compliance and demand ratio analysis

In an ideal case with route guidance actuation, all drivers would follow θ_{IHJ} exactly, but this may not be the case in reality as some drivers might prefer choosing their own routes. To analyze how driver compliance affects route guidance performance, a series of simulations with four different values of ρ are conducted by varying compliance level γ from 0% to 100%, which are summarized in fig. 4.6. Interestingly, the results differ with varying ratio of demand that has the city center as a destination: For low values of ρ, i.e., for the case with most of the trips from periphery to periphery, these results show that: (a) PC is not very successful in decreasing TTS, while RG performs well for high compliance; thus, PC is not very appropriate when destinations are distributed all over the city and the city center is used mainly for crossing trips, (b) there is no difference between RG and PCRG schemes. For high ρ values, on the other hand, the results indicate: (a) Increasing γ, especially for RG, yields in larger performance improvements, (b) there are substantial differences between RG and PCRG. Specifically, for the case with $\rho = 0.35$, RG cannot prevent gridlock for γ lower than 0.8, whereas PCRG is able to prevent it for γ higher than 0.5, showcasing the superiority of PCRG over RG in improving network performance even in difficult demand conditions (i.e., high ρ) and low compliance. Besides the performance improvement aspect of these results, an intuition with respect to field implementations can be developed: When a small number of destinations is within the city center, a route guidance system would be sufficient

and perimeter control is not necessary. This might happen if the city center has high quality public transport and expensive parking, discouraging people to travel by car in the center. If the number of destinations in the center is higher, then perimeter control is beneficial as it can prevent the center from overcrowding even for low levels of compliance. Furthermore, while RG and PCRG have similar performance for high compliance (with the exception of many city center trips, i.e., for $\rho = 0.35$), the difference is highly pronounced for lower compliance levels. This highlights the importance of coupling PC with RG for realistic implementations, as γ might not be very high due to issues of acceptance by the whole population of drivers and lack of smart technologies in some vehicles.

4.4.4 Detailed analysis of travel time benefits

Control via route guidance may cause some drivers to experience longer travel times compared to cases with no route guidance, leading to lower compliance and finally in less efficient schemes due to low user acceptance. To examine the travel time benefit of drivers under the RG and PCRG schemes, compared to the PC scheme, a series of simulation experiments are conducted with four different values of ρ and γ. For each MPC scheme, the travel times of each group of users with a certain regional O-D are estimated as a function of time based on the horizontal distance between the cumulative departure-arrival curves. Figure 4.7 provides the cumulative curves for the three schemes (departure curve is the same, as each scheme is tested with the same demand) for O-D pair 1–7. While for small ρ and in the beginning of each case the three schemes are very similar, when a higher number of trips has the center as destination (i.e., for high values of ρ), PCRG performs better than PC and RG. Based on these estimations the distribution of travel time benefits of RG and PCRG are compared to PC, which does not have any ability to control individual O-D movements. The distributions, given in fig. 4.8, consist of all O-D pairs and times, and are for 4 different values of ρ, each case having a constant value of γ (for each case separately, this corresponds to the γ value for which PC and RG have the same TTS performance). The distributions are skewed and contain both positive and negative values indicating the influence of the schemes for different users. These results indicate the superiority of PCRG over RG, as it keeps almost all drivers better off in terms of experienced travel times: In all cases, roughly 90% of drivers benefit from PCRG, and in general only 2-3% experience travel times extended longer than 5 minutes, suggesting substantial potential for practice.

4.4.5 Sensitivity to changes in boundary capacity

To study the effect of the boundary capacity, a series of simulation experiments are conducted via scaling the parameters $C_{IH}^{\max}$ (maximum capacity) and α (specifies the accumulation for which the capacity starts decreasing) used for the congested scenario

in 4.4.1 by factors varying from 0.3 to 1.1 (capacities are non-binding above 1.1). The results, given in fig. 4.9, show that the MPC schemes are fairly insensitive to changes in boundary capacity for factors larger than 0.6, supporting the initial conjecture that boundary capacity can be ignored in the MPC prediction model. Interestingly, boundary capacity seems to provide benefits similar to perimeter control for those cases without actual perimeter control, as seen from the decreased TTS for factors around 0.5 for NC and 0.6 for RG.

4.5 Conclusion

The chapter includes contributions in two aspects: (a) For traffic modeling, a novel cyclic behavior prohibiting dynamic urban network model is proposed, with the potential of yielding more realistic simulation results for route guidance scenarios compared to current MFD-based urban network models in the literature, (b) for the control design aspect, integrating perimeter control and route guidance type actuators, economic nonlinear MPC schemes are developed for improving mobility in urban networks. Macroscopic simulation studies indicate the potential for substantial improvement in mobility through the use of route guidance, in comparison to control via perimeter control only. A further observation is that since route guidance actuation cannot restrict flows, unlike perimeter control, it is unable to protect urban regions from severe congestion especially for cases with imperfect driver compliance. Highest performance is obtained by using both types of actuators.

This chapter focused on the combined use of two macroscopic traffic actuation methods, namely perimeter control and route guidance, in an optimization-based control framework. Although perimeter control is expected to be relatively easily applicable in field implementations since it requires instrumenting a set of traffic lights, realizing route guidance actuation is potentially more involved due to the need for sending routing commands to drivers. In the next chapter we examine how a hierarchical traffic management scheme can be designed for realizing macroscopic route guidance actions by a lower-level path assignment mechanism.

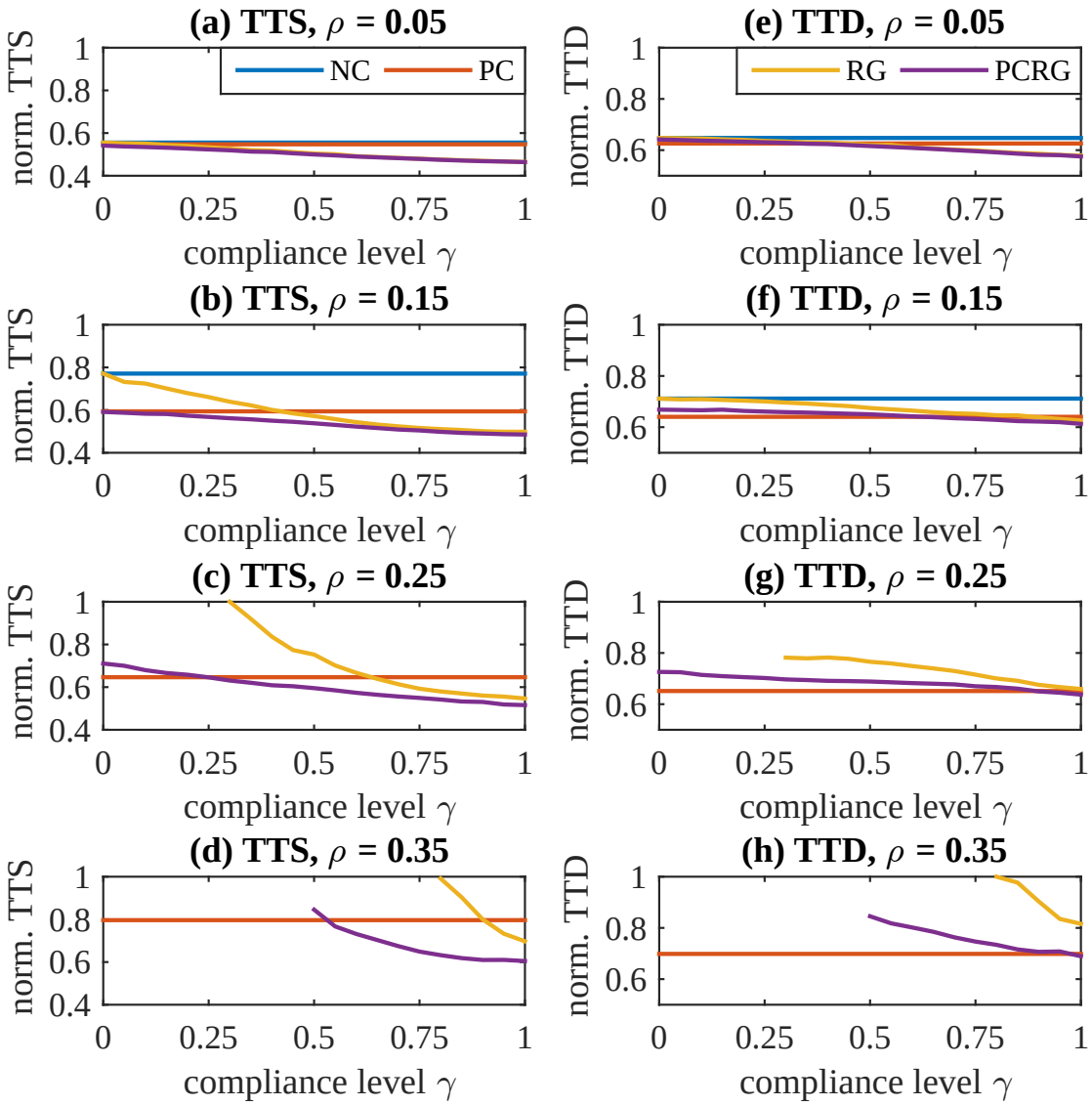

Figure 4.6 – Performance comparison of the NC case and the three MPC schemes, for different values of ρ, as a function of driver compliance level γ: (a)–(d) normalized TTS, (e)–(h) normalized TTD.

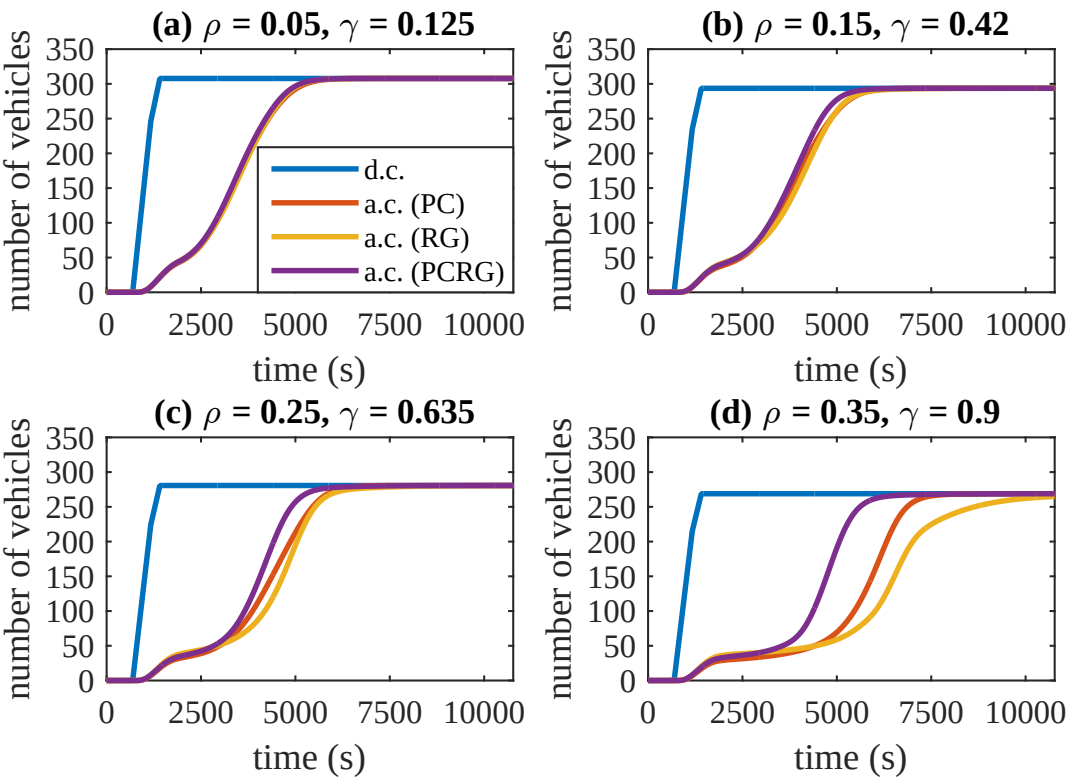

Figure 4.7 – Departure curve (d.c.) and arrival curves (a.c.) for the three MPC schemes, for the O-D pair 1–7.

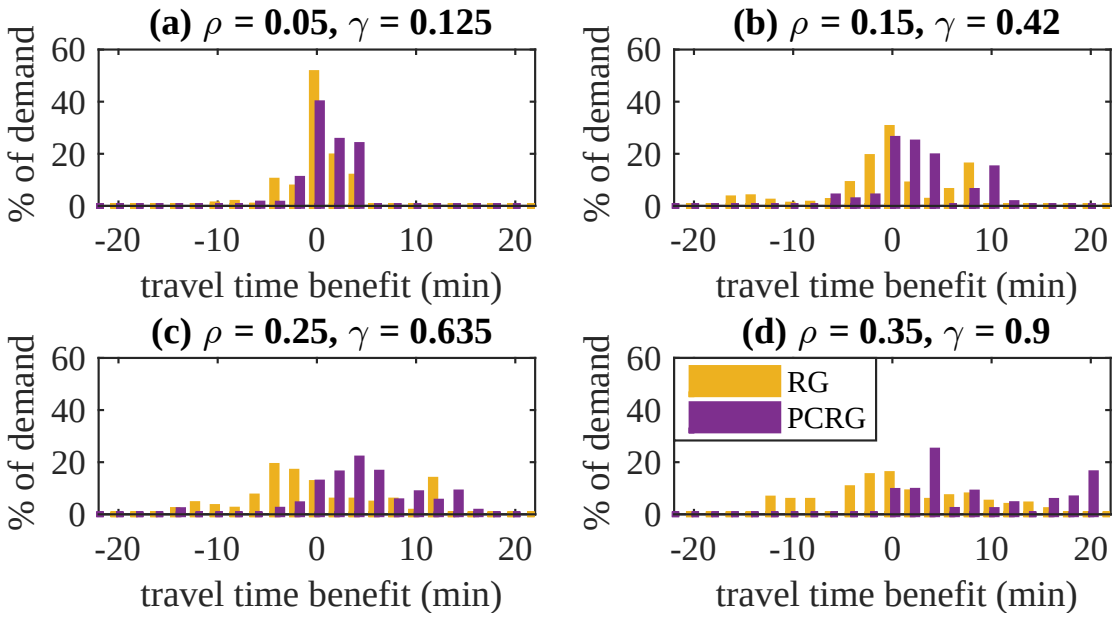

Figure 4.8 – Travel time benefit of drivers in RG and PCRG schemes with respect to PC scheme, for ρ values of 0.05, 0.15, 0.25, and 0.35, for a constant γ separately for each ρ value.

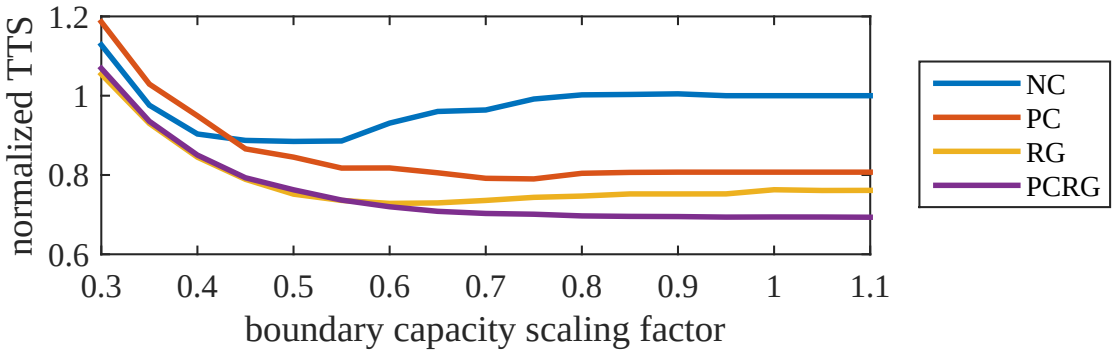

Figure 4.9 – Sensitivity of TTS performance to changes in boundary capacity.

Chapter 5

Integration of route guidance and path assignment

5.1 Introduction

In this chapter a hierarchical traffic management scheme is proposed, integrating path assignment with route guidance control. Considering MFD-based dynamics with heterogeneity terms, the route guidance-based economic MPC scheme optimizes network performance by actuation via split ratios of interregional transfer flows (i.e., route guidance commands). The lower-level path assignment mechanism recommends sub-regional paths for vehicles to follow, satisfying the route guidance commands in order to achieve said performance. Performance of the proposed hierarchical scheme is evaluated via macroscopic simulation experiments on an urban network with 7 regions and 49 sub-regions.

Literature review is not included here; it is given for the whole dissertation in chapter 1.

5.2 Two-level modeling of a multi-region urban network

In this section, we introduce two traffic models: (i) a region model considering an urban network partitioned into a small number of regions, and (ii) a sub-region model defining dynamics for a far more detailed network representation where the above regions are

divided into smaller sub-regions. A network consisting of 7 regions and 49 sub-regions is schematically shown in Figure 5.1.

To build a hierarchical control scheme, we use the approach of [36] with two modeling levels; sub-region model representing the traffic reality and region model representing the operation or prediction model. In the sub-regional representation, the network is actually not partitioned into 49 sub-regions, but simply this collection of 49 sub-regions is the network itself. In other words, the sub-regions, for the purposes of this work, are the smallest particles and represent the network itself. The sub-region dynamics, together with the presumed sub-regional MFD parameters, are considered to represent the reality of the urban network, where we assume that: (1) There is no internal routing inside a sub-region (as details beyond the sub-region are not modeled), (2) there are no interactions between the sub-regional average trip lengths and the path assignment decisions (the average distance the vehicles cross in a sub-region is assumed constant and same for everyone), (3) the traffic performance is represented by a stable MFD (note that we also test the proposed model later with some scatter in sub-region MFD). In a more detailed representation (e.g., microscopic simulation), sub-regions can be replaced with links (sections between intersections), where also there is no route choice (the only option is to cross the whole link), trip distance is the same for all users and fundamental diagram is stable. Therefore, one can make an analogy between sub-regions and links. In contrast to this, in the region model, we assume that the network (as represented by the 49 sub-regions) is partitioned into 7 regions for control purposes, and this is the actual partitioning considered in the chapter. Region sizes are important in the sense that partitioning the network into a large number of regions could potentially lead to computational problems regarding the route guidance MPC. In [63], the computational efficiency results suggest that for a network partitioned into 7 regions, the MPC schemes retain real-time feasibility, whereas a number much more than 7 could be expected to yield intractability problems.

5.2.1 Region model

Consider an urban network $\mathcal{R}$ with heterogeneous distribution of accumulation, with a given partition into R regions, i.e., $\mathcal{R} = \{1, 2, \ldots, R\}$. Inflow demand generated in region I with destination J is $Q_{IJ}(t)$ (veh/s), whereas $N_{IJ}^{H}(t)$ (veh) is the accumulation in region I with destination J that is going to transfer from I to H, with $N_I(t)$ (veh) expressing the total regional accumulation in I, at continuous time t; $I, J \in \mathcal{R}$; $N_I(t) \triangleq \sum_{J\in\mathcal{R}} \sum_{H\in\mathcal{V}_I} N_{IJ}^{H}(t)$, where $\mathcal{V}_I$ is the set of regions adjacent to I. For each region we consider regional split ratios $\theta_{IJ}^{H}(t)$ (for $I, J \in \mathcal{R}$, $H \in \mathcal{V}_I$), that can distribute the transfer flows entering region I with destination J over neighboring regions $H \in \mathcal{V}_I$. Note here that in contrast to previous works [52], [63], where the regional split ratio $\theta_{IJ}^{H}(t)$ expresses a distribution of the flow exiting region I over its neighbors, in the present work it distributes the flow *entering* region I. This definition of $\theta_{IJ}^{H}(t)$ is consistent with

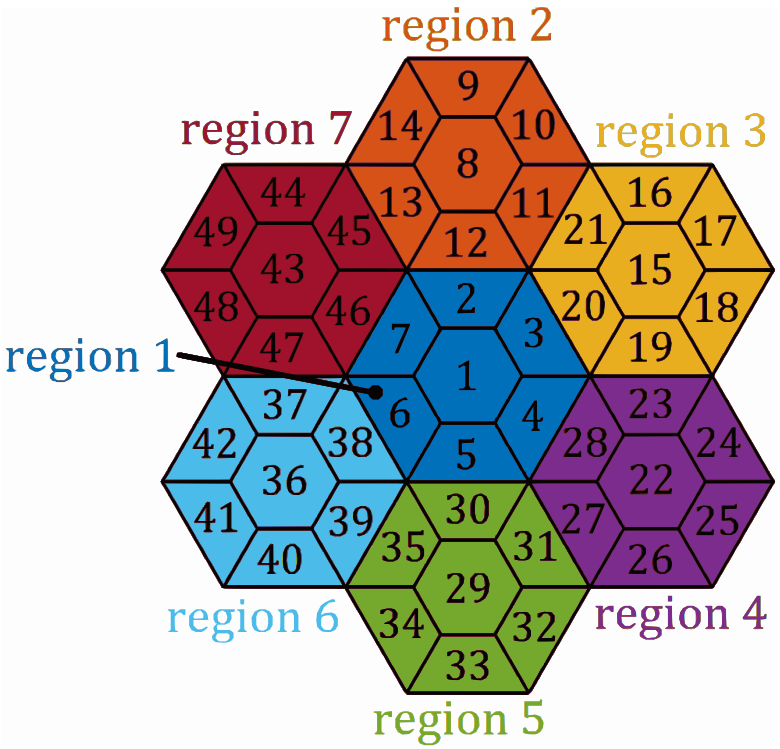

Figure 5.1 – Schematic of a multi-region urban network, consisting of 7 regions each with 7 sub-regions (region 1 contains sub-regions 1 to 7, region 2 contains 8 to 14, etc.).

the definition of the path assignment control inputs for the sub-regional model, which will be described in the next sections.

Mass conservation equations for an R-region MFDs network are:

$$\dot{N}_{II}^{H}(t) = \theta_{II}^{H}(t)\left(Q_{II}(t) + \sum_{G\in\mathcal{V}_I} M_{GI}^{I}(t)\right) - M_{II}^{H}(t) \quad H \in \mathcal{V}_I \cup I \tag{5.1a}$$

$$\dot{N}_{IJ}^{H}(t) = \theta_{IJ}^{H}(t)\left(Q_{IJ}(t) + \sum_{G\in\mathcal{V}_I} M_{GJ}^{I}(t)\right) - M_{IJ}^{H}(t) \quad H \in \mathcal{V}_I,\ I \neq J, \tag{5.1b}$$

for $I, J \in \mathcal{R}$. $M_{II}^{I}(t)$ (veh/s) is the exit (i.e., internal trip completion) flow from region I to destination I (exiting without leaving region I), whereas $M_{IJ}^{H}(t)$ (veh/s) is the flow transferring from I to H with destination J. The exit and transfer flows can be expressed as follows (following [36]):

$$M_{II}^{I}(t) = \frac{N_{II}^{I}(t)}{N_I(t)}\frac{F_I(N_I(t))}{L_{II}(t)}\rho_I(N_I(t),\sigma(N_I(t))) \tag{5.2a}$$

$$M_{IJ}^{H}(t) = \frac{N_{IJ}^{H}(t)}{N_I(t)}\frac{F_I(N_I(t))}{L_{IH}(t)}\rho_I(N_I(t),\sigma(N_I(t))), \tag{5.2b}$$

where $F_I(\cdot)$ (veh.m/s) is the production MFD of region I as a function of regional accumulation $N_I(t)$ (for a 3rd degree polynomial approximation, the MFD is of the form $F_I(N_I(t)) = A\, N_I(t)^3 + B\, N_I(t)^2 + C\, N_I(t)$, where A, B, and C are the MFD parameters estimated from data), $L_{II}(t)$ and $L_{IH}(t)$ are the average trip lengths for internal trips inside region I and transferring trips from I to H, respectively, whereas $\rho_I(\cdot) \in [0,\, 1]$ is the heterogeneity coefficient of region I expressing the decrease in production due to heterogeneity ($\rho_I(\cdot) = 1$ if region I is perfectly homogeneous and it decreases with increasing heterogeneity), which can be formulated as follows (see [36] for details):

$$\rho_I(N_I(t), \sigma(N_I(t))) = \beta \cdot (\mathrm{e}^{\gamma \cdot (\sigma(N_I(t)) - \sigma_{\mathrm{h}})} - 1) + 1 \quad \forall I \in \mathcal{R}, \tag{5.3}$$

where $\sigma(N_I(t))$ is the heterogeneity variance of region I, σ_{h} is the standard deviation of summation of negative binomial distributions of the sub-regions of region I with mean occupancy $N_I(t)/|\mathcal{I}|$ (with $\mathcal{I}$ the set of sub-regions in region I and $|\mathcal{I}|$ its size), whereas β and γ are estimated parameters describing the effect of heterogeneity in link density on the production of the region. Analyses based on real data demonstrate that the negative binomial distribution can provide accurate estimations for mean and standard deviation of occupancies for the Yokohama network [36]. That means, one can accurately estimate the production in a region using two terms; (i) an upper bound (low-scatter) MFD (i.e. $F_I(N_I(t))$) and (ii) the heterogeneity degradation (i.e. ρ_I). While $F_I(N_I(t))$ can be represented with a 3^{rd}-degree polynomial function, ρ_I is modeled with an exponential function. The parameters of these functions are network-specific values and might exhibit changes in different applications; however, it is important that one uses a consistent set of parameters based on the same network and data set.

The regional split ratios $\theta^H_{IJ}(t)$ are control inputs which are to be computed by the network-level route guidance MPC, the design of which is studied in the next section. Note that recently there are efforts to address in heterogeneous trip lengths in more detail by considering a trip based formulation (see for example [81], [82] and [83]). While these models might provide a better estimation of outflow, they are more tedious to be integrated in a control framework. This is an ongoing research direction.

5.2.2 Sub-region model

Sub-region model presented in this section builds on [51], and it is necessary to develop the path assignment mechanism which will be introduced in the next section. Consider an urban network $\mathcal{SR}$ with heterogeneous distribution of accumulation and a given partition into SR sub-regions, i.e., $\mathcal{SR} = \{1, 2, \ldots, SR\}$. Now, consider a sub-region $r \in \mathcal{SR}$ with homogeneous distribution of congestion whose traffic performance is well described by MFD, $f_r(n_r(t))$, representing the sub-region production (veh.m/s) corresponding to the accumulation $n_r(t)$ (veh) at continuous time t. The average sub-region r speed is $v_r(t) = f_r(n_r(t))/n_r(t)$ (m/s), and trip completion rate is $m_r(t) = f_r(n_r(t))/l_r$ (veh/s),

considering a constant sub-regional average trip length l_r (m) independent of time, destination or next region.

Let $n_{o,d}^{p,r}(t)$ denote the number of vehicles in sub-region r at time t with first sub-region o in a given region I, destination sub-region d and path p, i.e. the sequence of sub-regions from o to the last sub-region $\bar{d}$ in I; $o, \bar{d}, r \in \mathcal{I}$, $d \in \mathcal{SR}$, $\sum_o \sum_d \sum_p n_{o,d}^{p,r}(t) = n_r(t)$. Note that r belongs to p, and all sub-regions along p are in region I. That means, $n_{o,d}^{p,r}(t)$ tracks the vehicles from the time they enter region I or start their trip until they leave it or reach their destination. Therefore, o is either the origin sub-region where the demand is generated or the boundary sub-region that receives flows from other regions. Similarly, $\bar{d}$ is either the destination sub-region (i.e. $d = \bar{d}$) or the boundary sub-region that sends flows to other regions. Trip completion rate or the transfer flow $m_{o,d}^{p,r}(t)$ for the same group of vehicles reads as follows:

$$m_{o,d}^{p,r}(t) = \frac{n_{o,d}^{p,r}(t)}{n_r(t)} \cdot m_r(t) = \frac{f_r(n_r(t))}{n_r(t)} \cdot \frac{n_{o,d}^{p,r}(t)}{l_r} = v_r(t) \cdot \frac{n_{o,d}^{p,r}(t)}{l_r}. \tag{5.4}$$

If $d = r$, the above equation refers to flow leaving the network at sub-region d. Otherwise, it represents the transfer flow from sub-region r to sub-region $p^+(r)$, i.e. the sub-region following r in the path p. However, as the transfer flow is also subject to the boundary capacity between the sub-regions, we denote the actual transfer flow by $\hat{m}_{o,d}^{p,r}(t)$. Note that, in a similar way, $p^-(r)$ is the sub-region preceding r in path p. Sub-region traffic dynamics are then defined as follows:

$$\frac{\mathrm{d}n_{o,d}^{p,r}}{\mathrm{d}t} = \begin{cases} q_{o,d}^p - m_{o,d}^{p,r} & \text{(i) if } r = o \;\&\; r = d, \\ q_{o,d}^p - \hat{m}_{o,d}^{p,r} & \text{(ii) if } r = o \;\&\; r \neq d, \\ \hat{m}_{o,d}^{p,p^-(r)} - m_{o,d}^{p,r} & \text{(iii) if } r \neq o \;\&\; r = d, \\ \hat{m}_{o,d}^{p,p^-(r)} - \hat{m}_{o,d}^{p,r} & \text{(iv) otherwise.} \end{cases} \tag{5.5}$$

where

$$\hat{m}_{o,d}^{p,r} = \min[m_{o,d}^{p,r}, c_r^p(n_{p^+(r)}) \cdot a_{o,d}^{p,r}] \quad \forall\, r \neq d \tag{5.6}$$

$q_{o,d}$ denotes the sum of the exogenous demand generated in o or the flow transferred to o at time t with destination d, and $q_{o,d}^p$ represents the assigned flow to path p; $\sum_p q_{o,d}^p = q_{o,d}$. Note that time t is omitted from the above equations for the sake of notational simplicity. Additionally, $q_{o,d}^p$ is equal to $q_{o,d} \cdot \alpha_{o,d}^p$, where $\alpha_{o,d}^p$ is the path fraction and the decision variable to be computed by ILP-based path assignment scheme that will be described in the next section. Equation 5.5 defines the change in accumulation $n_{o,d}^{p,r}$ based on four cases. In (i), we deal with internal demand within the same sub-region; therefore, the rate is simply the newly assigned flow minus the trip completion rate which is not bounded by any capacity function. The sub-regional model assumes that internal sub-regional demand never leaves the sub-region; therefore, in this case the sub-regional path p consists of

only one sub-region. In (ii), r is the first sub-region in the region but not the destination. So, the rate is simply the assigned flow minus the transfer flow to the next sub-region in path p. (iii) If r is destination but not the first sub-region, then the rate is defined as the transfer flow from the previous sub-region minus the trip completion rate which is again not bounded by any capacity function. In other cases (iv), the rate is equal to the transfer flow from the previous sub-region minus the transfer flow to the next sub-region.

Equation 5.6 defines the actual transfer flow from r to the next sub-region $p^+(r)$ in path p for all sub-regions except destination sub-region d. It is the minimum of two terms: (i) the sending flow from sub-region r and (ii) the receiving capacity of sub-region $p^+(r)$ that is a function of two terms; $c_r^p(n_{p^+(r)})$ and $a_{o,d}^{p,r}$. Capacity at boundary between r and $p^+(r)$, i.e. $c_r^p(n_{p^+(r)})$, is a decreasing function of accumulation, which represents the resistance of the sub-region to absorb more traffic with increasing congestion. Additionally, $a_{o,d}^{p,r}$ is the fraction of boundary capacity that can be allocated to $\hat{m}_{o,d}^{p,r}$. Using $m_{o,d}^{p,r}$ values, we calculate the total number of vehicles heading for a particular boundary between two sub-regions. As not all the vehicles may be allowed to pass the boundary due to the finite capacity, we calculate the fraction of $m_{o,d}^{p,r}$ to the total flow heading for the same boundary and assign the corresponding fraction of the capacity to $\hat{m}_{o,d}^{p,r}$. Equation 5.6 suggests that only the minimum of the sending flow, i.e. $m_{o,d}^{p,r}$, and the allocated capacity, i.e. $c_r^p(n_{p^+(r)}) \cdot a_{o,d}^{p,r}$ can cross the boundary. This calculation follows the definition of [84].

5.3 Hierarchical traffic management of large-scale urban networks

In this section, we develop an integrated hierarchical route guidance system. The flowchart in Figure 5.2 summarizes the proposed hierarchical framework. On the upper level, the MPC scheme computes optimum regional split ratios based on the accumulation, average trip length and heterogeneity measurements taken from the sub-region model. MPC assumes that average trip length and heterogeneity measures remain constant over the prediction horizon and minimizes the network delay by predicting the evolution of region accumulations. The optimum split ratios are then transferred to ILP-based path assignment scheme, which produces sub-regional path decisions in accordance with the aggregated split values within each region. This procedure assigns the transfer flow and the exogenous demand to the paths between the sub-region they appear in (or the boundary sub-region) and their destination (or the boundary sub-region). The resulting path decisions calculated by the ILP-based path assignment scheme are then applied to the sub-region model.

While the sub-region and region models are defined based on the continuous time t, the hierarchical control framework operates on a discrete-time basis. The lower-level, consisting of the sub-region model (i.e., the *plant*) and the ILP mechanism, is operated

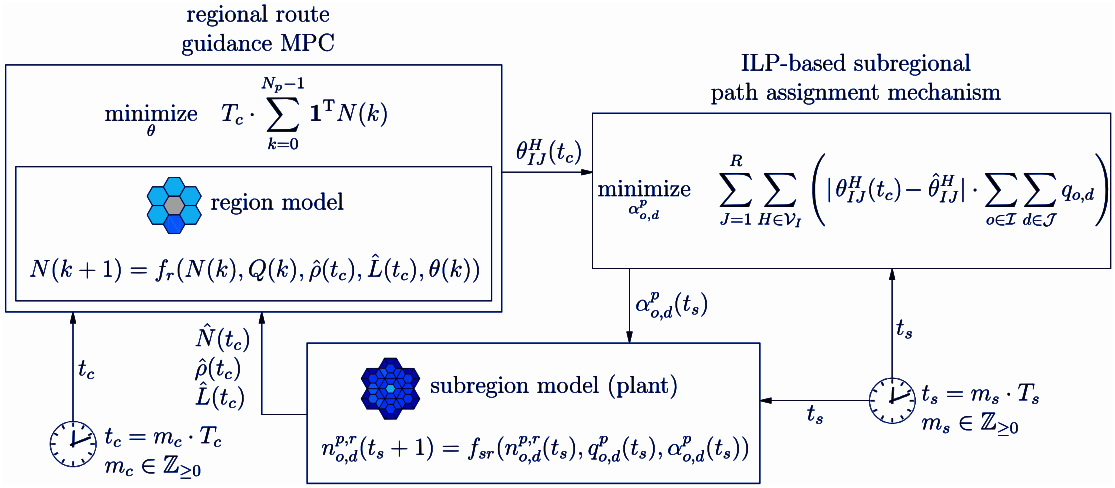

Figure 5.2 – Structure of the proposed path assignment and regional route guidance based hierarchical traffic management scheme.

according to the simulation time step t_s (see the clock at lower right of Figure 5.2). The simulation time step t_s is an integer multiple of the simulation sampling time T_s (s), i.e., $t_s = m_s \cdot T_s$ with $m_s \in \mathbb{Z}_{\geq 0}$. In other words, the ILP commands $\alpha^p_{o,d}(t_s)$ are updated at each simulation time step t_s (i.e., each T_s seconds). The MPC scheme at the upper-level, on the other hand, is operated according to the control time step t_c (see the clock at lower left of figure 5.2). The control time step t_c is an integer multiple of the control sampling time T_c (s), i.e., $t_c = m_c \cdot T_c$ with $m_c \in \mathbb{Z}_{\geq 0}$. Thus, the MPC scheme receives the traffic state information, and updates its decisions $\theta^H_{I,J}$ based on this information, at each control sampling time t_c (i.e., each T_c seconds). Note that control time step T_c is usually chosen as an integer multiple of T_s for convenience. Hence, the MPC command $\theta^H_{IJ}(t_c)$ is updated at each control time step t_c and kept constant between consecutive control time steps, while the ILP mechanism uses this constant value to compute the $\alpha^p_{o,d}(t_s)$ command until the control step ends (thus, using the same value for T_c/T_s times). The whole procedure is repeated in the next control time step in the receding horizon fashion.

5.3.1 Sub-regional path assignment

In this section, we formulate an ILP problem in order to assign the flows in the sub-region network so that they satisfy θ^H_{IJ} values ordered by route guidance MPC and produce L_{IH} values within a tolerance range. The formulation, which is repeated for each region

I, reads as follows:

$$\underset{\alpha^p_{o,d}}{\text{minimize}} \quad \sum_{J=1}^{R} \sum_{H \in \mathcal{V}_I} \left(|\theta^H_{IJ}(t_c) - \hat{\theta}^H_{IJ}| \cdot \sum_{o \in \mathcal{I}} \sum_{d \in \mathcal{J}} q_{o,d} \right) \tag{5.7}$$

$$\text{subject to} \quad \sum_{p \in \mathcal{P}^o} \alpha^p_{o,d} = 1, \quad \forall o \in \mathcal{I}, \forall d \tag{5.7a}$$

$$\alpha^p_{o,d} \in \{0, 1\} \quad \forall o \in \mathcal{I}, \forall d, \forall p \in \mathcal{P}^o \tag{5.7b}$$

$$\hat{\theta}^H_{IJ} = \frac{\sum_{o \in \mathcal{I}} \sum_{d \in \mathcal{J}} \sum_{p \in \mathcal{P}^o_H} \left(q_{o,d} \cdot \alpha^p_{o,d} \right)}{\sum_{o \in \mathcal{I}} \sum_{d \in \mathcal{J}} q_{o,d}} \quad \forall J, \forall H \in \mathcal{V}_I \tag{5.7c}$$

$$\hat{L}_{IH} = \frac{\sum_{o \in \mathcal{I}} \sum_{d} \sum_{p \in \mathcal{P}^o_H} \left(q_{o,d} \cdot \alpha^p_{o,d} \cdot l^p \right)}{\sum_{o \in \mathcal{I}} \sum_{d} \sum_{p \in \mathcal{P}^o_H} \left(q_{o,d} \cdot \alpha^p_{o,d} \right)} \quad \forall H \in \mathcal{V}_I \tag{5.7d}$$

$$(1 - \varepsilon) \cdot L_{IH}(t_c) \leq \hat{L}_{IH} \leq (1 + \varepsilon) \cdot L_{IH}(t_c) \quad \forall H \in \mathcal{V}_I, \tag{5.7e}$$

where $\theta^H_{IJ}(t_c)$ is the regional split ratio ordered by MPC at the control time step t_c and $L_{IH}(t_c)$ is the average trip length assumed to remain constant from the same control time step. $\hat{\theta}^H_{IJ}$ and $\hat{L}_{IH}$, on the other hand, are the corresponding variables that are reconstructed based on the trajectories of assigned flows. Also, denote $\mathcal{P}^o$ the set of all paths starting from o, $\mathcal{P}^o_H$ the subset of paths heading for neighboring region H, l^p the distance to be crossed along path p within region I and ε tolerance error between the observed and reconstructed trip lengths. Note that simulation time step t_s is omitted from the above equations for the sake of notational simplicity and the only static variables are the physical path distance l^p and tolerance error ε. The remaining variables, which are not followed by $.(t_c)$, should in fact be followed by $.(t_s)$.

Equation 5.7 minimizes the weighted average of the absolute difference between the ordered and reconstructed regional split ratios given the constraints presented from Equation 5.7a to 5.7e. The objective function considers the weighted average with respect to demand between regions (i.e. $\sum_{o \in \mathcal{I}} \sum_{d \in \mathcal{J}} q_{o,d}$) so as to attach more importance to high-volume pairs. Equation 5.7a guarantees that the demand between o and d is assigned to a path, while Equation 5.7b defines $\alpha^p_{o,d}$ as a binary variable and warrants an all-or-nothing assignment process. Considering the demand $q_{o,d}$ to be assigned between o and d (including the exogenous demand and the transfer flow), Equation 5.7c defines the regional split ratios based on the assigned flows. The denominator in Equation 5.7c is the total flow to be assigned between I and J, while the numerator is the portion allocated with the routes targeting neighboring region H. Similarly, Equation 5.7d computes the average trip lengths based on the assigned paths. The denominator represents the assigned flow heading for the boundary between I and H, and the numerator defines the total distance traveled by them. Finally, Equation 5.7e defines the tolerance bounds that the reconstructed trip length should fall into. Note that the above formulation is

repeated for each region I.

Since Equation 5.7d includes the decision variable $\alpha^p_{o,d}$ both in the numerator and the denominator, the resulting problem cannot be formulated as an ILP. Therefore, assuming that θ^H_{IJ} values ordered by MPC will be fully satisfied, we replace Equation 5.7d with the following:

$$\hat{L}_{IH} = \frac{\sum_{o\in\mathcal{I}}\sum_{d}\sum_{p\in\mathcal{P}^o_H}\left(q_{o,d}\cdot\alpha^p_{o,d}\cdot l^p\right)}{\sum_{o\in\mathcal{I}}\sum_{d}\left(q_{o,d}\cdot\delta_{dJ}\cdot\theta^H_{IJ}\right)} \quad \forall H\in\mathcal{V}_I \tag{5.8}$$

where δ_{dJ} is 1 if $d\in\mathcal{J}$, and 0 otherwise. We note that Equation 5.7d and Equation 5.8 are equal to each other if θ^H_{IJ} and $\hat{\theta}^H_{IJ}$ are the same. And, the above approximation does not affect the performance of the assignment scheme as long as θ^H_{IJ} and $\hat{\theta}^H_{IJ}$ are close to each other. Essentially, Equation 5.7d is replaced with Equation 5.8 relying on the assumption that the value of the objective function is zero. However, this does not force the objective function to be zero. The decision variables (i.e. $\alpha^p_{o,d}$) are still in the numerator of the formula presented in Equation 8, which allows the framework to test different values of $\hat{L}_{IH}$ and so $\hat{\theta}^H_{IJ}$. Obviously, the value of $\hat{L}_{IH}$ from Equation 5.7d will differ from that of Equation 5.8 in most cases where θ^H_{IJ} and $\hat{\theta}^H_{IJ}$ are not exactly the same. Nevertheless, this discrepancy should be minimal at the optimal solution where θ^H_{IJ} and $\hat{\theta}^H_{IJ}$ are expected to be similar. This replacement is crucial to keep the problem linear and tackle it with ILP solution methods. Nevertheless, we realize that Equation 5.8 does not account for dynamic conditions in the sub-regions; it only considers the distance to be crossed along the path, which is a static physical measure. In order to ensure homogeneity within the regions, we further modify Equation 5.8 and express the travel time from region I to region H with the below formula:

$$\frac{\hat{L}_{IH}}{V_I} = \frac{\sum_{o\in\mathcal{I}}\sum_{d}\sum_{p\in\mathcal{P}^o_H}\left(q_{o,d}\cdot\alpha^p_{o,d}\cdot\sum_{r\in p}\left(l_r/v_r\right)\right)}{\sum_{o\in\mathcal{I}}\sum_{d}\left(q_{o,d}\cdot\delta_{dJ}\cdot\theta^H_{IJ}\right)} \quad \forall H\in\mathcal{V}_I \tag{5.9}$$

where V_I denotes the average speed in region I (i.e. $F_I(N_I)/N_I$). Basically, we break the path distance l^p into sub-regions, and calculate the travel time in each sub-region r using the static average distance l_r and the dynamic speed v_r changing with time t_s (the actual notation should be $v_r(t_s)$, but t_s is omitted for simplicity). The sum of them gives us the travel time on the sub-regional path p. If actual traffic conditions are ignored, certain sub-regions within a given region might be more (or less) congested depending on the routing and the sub-regional paths. To avoid such cases and improve homogeneity within regions, we replace Equation 5.8 with Equation 5.9 where we account for both distance and current traffic conditions in the network. Note that the target measure in Equation 9 is the average travel time from I to H, not the average distance which is a static network attribute. This allows us to react to uneven distribution of congestion across the sub-regions and ensure homogeneity within the regions. In other words, Equation 5.9 enables ILP to control the region-to-region travel times and avoids overloading of

few sub-regions. We also note that we do not use Equation 5.9 the way it is presented; we take V_I to the right hand side of the equation to compute $\hat{L}_{IH}$ and substitute it into Equation 5.7e.

The path assignment mechanism could also be formulated as a linear programming problem, where $\alpha^p_{o,d}$ could be defined as a continuous variable between 0 and 1. Although this would significantly simplify the computation efforts, there may not always be enough demand to accommodate such split ratios. While we keep the formulation here as an ILP problem, we test the effects of this assumption later in Section 5.4.3.

The ILP problem is formulated using YALMIP [85], an optimization modeling toolbox for MATLAB, and solved with Gurobi. The optimization scheme is implemented using MATLAB 8.5.0 (R2015a), on a 64-bit Windows PC with 3.6-GHz Intel Core i7 processor and 16-GB RAM.

5.3.2 Regional route guidance MPC

We formulate the problem of finding the regional split ratio θ^H_{IJ} values that minimize total time spent (for a finite horizon) as the following discrete time economic nonlinear MPC problem (extending the work in [63]):

$$
\begin{aligned}
\underset{\theta}{\text{minimize}} \quad & T_c \cdot \sum_{k=0}^{N_p-1} \mathbf{1}^{\mathrm{T}} N(k) \\
\text{subject to} \quad & N(0) = \hat{N}(t_c) \\
& |\theta(0) - \hat{\theta}(t_c - 1)| \leq \Delta_\theta \\
& \text{for } k = 0, \ldots, N_p - 1 : \\
& \quad N(k+1) = f_r\left(N(k), Q(k), \rho(t_c), \hat{L}(t_c), \theta(k)\right) \\
& \quad 0 \leq N_I(k) \leq N_I^{\text{jam}}, \ \forall I \in \mathcal{R} \\
& \quad 0 \leq \theta^H_{IJ}(k) \leq 1, \ \forall I, J \in \mathcal{R}, H \in \mathcal{V}_I \cup I \\
& \quad \sum_{H \in \mathcal{V}_I \cup I} \theta^H_{IJ}(k) = 1, \ \forall I, J \in \mathcal{R} \\
& \quad \text{if } k \geq N_c : \\
& \quad\quad \theta(k) = \theta(k-1),
\end{aligned}
\tag{5.10}
$$

where T_c and t_c are the control sampling time and control time step, respectively (with $t_c = m_c \cdot T_c$ where $m_c \in \mathbb{Z}_{\geq 0}$), $N(k)$, $Q(k)$, $\hat{\rho}(t_c)$, $\hat{L}(t_c)$, and $\theta(k)$ are vectors containing all $N^H_{IJ}(k)$, $Q_{IJ}(k)$, $\hat{\rho}_I(t_c)$, $\hat{L}_{IH}(t_c)$ and $\theta^H_{IJ}(k)$ terms (with $\hat{\rho}_I(t_c) \triangleq \rho_I(\hat{N}_I(t_c), \sigma(\hat{N}_I(t_c)))$), respectively, with k being the control interval counter, f is the time discretized version of eq. (5.1)–(5.2), $\hat{N}(t_c)$, $\hat{\rho}(t_c)$, and $\hat{L}(t_c)$ are the measurements on accumulations, heterogeneity coefficient, and average trip lengths taken at the current control time

step, respectively, $\hat{\theta}(t_c - 1)$ is the control input applied to the plant at the previous control time step, N_p and N_c are the prediction and control horizons, whereas Δ_θ is the rate limit on regional split ratios. Within the prediction horizon N_p, we assume that heterogeneity coefficients $\hat{\rho}(t_c)$ and average trip lengths $\hat{L}(t_c)$ remain constant. To relax this assumption one needs to either estimate a vector of accumulations and trip lengths valid for a finite horizon into the future (same length as N_p) or model the dynamics that define heterogeneity and average trip length as a function of route guidance control inputs. We also consider that as trip length is a difficult quantity even to measure and estimate, it will be even more difficult to predict it. Assuming a quantity constant, when it is difficult to predict, is a well-established approach in MPC literature (it is better not to predict when errors are expected to be large). The prediction aspect is considered outside the scope of the chapter, and could be considered for future work.

The optimization problem (5.10) is a nonconvex nonlinear program (NLP), which can be efficiently solved via, e.g., sequential quadratic programming or interior point solvers (see [69] for details). Software implementation of the MPC scheme is done using the CasADi [72] toolbox in MATLAB 8.5.0 (R2015a), on a 64-bit Windows PC with 3.6-GHz Intel Core i7 processor and 16-GB RAM, using a direct collocation scheme (see, e.g., [78] for details) with the NLPs solved by the interior point solver IPOPT [73].

5.4 Results

The simulation case study is based on a network with 49 subregions partitioned into 7 regions (see Figure 5.1). The path-based subregion-level model given in Equations (5.4)-(5.6) is used as the simulation model (i.e., the *plant* representing reality), whereas the region-level model given in Equations (5.1)-(5.2) is used as the prediction model of the route guidance MPC. Each region is assumed to have a production MFD with the parameters $A = 9.98 \cdot 10^{-8}$, $B = -0.002$, $C = 9.78$, jam accumulation $N^{\text{jam}} = 10^4$ (veh), critical accumulation $N^{\text{cr}} = N^{\text{jam}}/3$ (veh), which are consistent with the MFD observed in a part of downtown Yokohama (see [16]). sub-regions are assumed to have well-defined production MFDs, the parameters of which are scaled versions of the region MFDs, whereas the associated average trip lengths are constant and there is assumed to be no heterogeneity affecting the sub-regions. Region MFDs, on the other hand, are exposed to variations in the outflow as they are affected by the average trip lengths $L_{IH}(t)$ and heterogeneity coefficient $\rho_I(t)$, which are dynamically changing with the traffic conditions at the sub-region level. Prediction and control horizons for the MPC are chosen as $N_p = 5$ and $N_c = 2$ (following the controller tuning results of [63] for a 7-region network as depicted in Figure 5.1). The traffic states in the plant are updated using a time discretized version of the sub-region model given in (5.5), with a simulation sampling time of $T_s = 60$ s. Path assignment decisions of the ILP mechanism are also updated together with the traffic states each $T_s = 60$ s, whereas the MPC operates with a control sampling time of $T_c = 240$ s. Thus, the ILP mechanism uses the same route

guidance decision coming from the MPC for the 4 simulation time steps belonging to the same control time step.

The sub-regional path assignment mechanism is essentially in charge of tracking two signal classes; split ratios (i.e. θ_{IJ}^{H}) and average trip lengths (i.e. L_{IH}). While the ILP formulation minimizes the difference between the ordered split ratios (i.e. θ_{IJ}^{H}) and reconstructed split ratios (i.e. $\hat{\theta}_{IJ}^{H}$) (Equation 5.7), it ensures that the reconstructed trip lengths (i.e. $\hat{L}_{IH}$) are close to the trip lengths observed from the plant (i.e. L_{IH}) and are within the bounds defined by ε (see Equation 5.7e). Regional route guidance MPC assumes that average trip length measures remain constant over the prediction horizon and minimizes the network delay by changing the split ratios. The sub-regional path assignment mechanism follows the same rationale and aims to match the reconstructed split ratios with the ordered ones (see Equation 5.7) while maintaining the reconstructed average trip lengths in the vicinity of observed ones (see Equation 5.7e). Accordingly, the objective function in the ILP is the sum of absolute difference between θ_{IJ}^{H} and $\hat{\theta}_{IJ}^{H}$ values, and the tolerance range of $\hat{L}_{IH}$ with respect to L_{IH} is added as a constraint in the optimization problem. The value of ε, in this study, is 0.05. And, it has been chosen such that the outflow from the regions is not largely affected by the changing trip length values, and yet the overall framework is flexible enough to follow the ordered split ratio signals. Note that the mismatch between ordered and reconstructed patterns can always be taken into account in the next time step by the feedback mechanism of the control framework, and we observe that the results are not very sensitive to the changes within the range $\varepsilon \in [0.025, 0.10]$.

Additionally, ILP formulation presented in Equation 5.7 includes the set of paths (i.e. $\mathcal{P}^{o}$) which requires the enumeration of alternatives between the sub-region pairs (in the same region). As the enumeration of all paths would present computational difficulties at a large-scale region and include unrealistic routes, we limit our analysis with the first 5 physical (distance-based) shortest paths between the sub-region pairs. Therefore, the resulting scheme does not offer a "perfectly optimal" solution where few agents are largely penalized to reach social equilibrium; instead, it considers limited willingness of travellers to switch to alternative routes and provides a constrained social equilibrium solution where no traveller is given an exceedingly long path (similar to [86]). While SO conditions might generate longer paths for a few users, with the above consideration, it is more likely that users follow and comply with the outcome of guidance strategy. To determine the shortest paths, we use the physical network properties (e.g., connectivity, distance) of the 49-sub-region representation, just like one would do with a link-level representation of a network. In other words, we build a graph where nodes are sub-regions and the neighboring nodes (as seen in Figure 5.1) are connected to each other with an edge whose value is equal to the sub-regional average trip length (i.e., l_r). We then identify the shortest paths between the sub-regions using this graph. An alternative to the static (distance-based) choice set we use here might be to consider dynamic traffic conditions and update the choice in every time step with the time-based shortest paths.

Nevertheless, our current framework, which builds on the YALMIP toolbox, does not allow such changes because of the coding-related limitations. While the toolbox makes development of optimization problems very simple, it requires the ILP-based mechanism to be built in advance with a choice set. Therefore, such dynamic changes in the choice set are not possible.

Note that the sub-region model that is used for testing the hierarchical control does not appear anywhere inside the two levels of the hierarchical control scheme. Hence, there is a significant difference between the models used for optimization and the model used for replicating reality; the "plant". The ILP-based path assignment mechanism does not use a dynamical model at all; it simply relies on the physical network properties (e.g., connectivity, distance, etc.) that are easy to be collated. On the other hand, the route guidance MPC uses the region model which is very different than the sub-region model in the following aspects: a) the region model considers the aggregated representation of 7 sub-regions as a single region and scrutinizes traffic flows between regions not sub-regions, b) the sub-regions have well-defined MFDs, whereas the region MFDs are subject to heterogeneity effects according to the congestion distribution at the sub-regional level (as modeled by Equation 5.3).

5.4.1 Congested scenario

To test the performance of the proposed hierarchical route guidance (RG) scheme (the structure of which is given as a block diagram in Figure 5.2) against a no control (NC) case, we conduct a simulation experiment based on a congested scenario for the two cases. In both NC and RG, drivers receive a path information when they enter the network or a new region, and the route choice terms are updated every control time step (i.e. 4 minutes) to have a fair comparison between the scenarios. Depending on trip to be made, the path consists of sequence of sub-regions from origin sub-region or region boundary to the destination sub-region or region boundary. In NC, the path decisions reflect the shortest path based on instantaneous traffic conditions, while RG assigns the vehicles to the paths produced by the hierarchical scheme. In both NC and RG scenarios, the network starts empty but is exposed to increased inflow demands as time progresses. As the vehicles are closer to their origin than to their destination in the beginning of the simulation, the first 20 minutes is considered the warm-up period and RG system is activated after that.

Figure 5.3 shows the regional accumulations (Figure 5.3a and 5.3b) and heterogeneity coefficients as described by Equation 5.3 (Figure 5.3c and 5.3d) for the two scenarios. The figure clearly indicates that the RG scheme is efficient in alleviating congestion, whereas in the NC case, congestion cannot be avoided in the city center (i.e. region 1). By comparing Figure 5.3a and 5.3b we observe that the peripheral regions (i.e., regions 2 to 7) carry slightly more traffic in RG scenario than in NC scenario, which

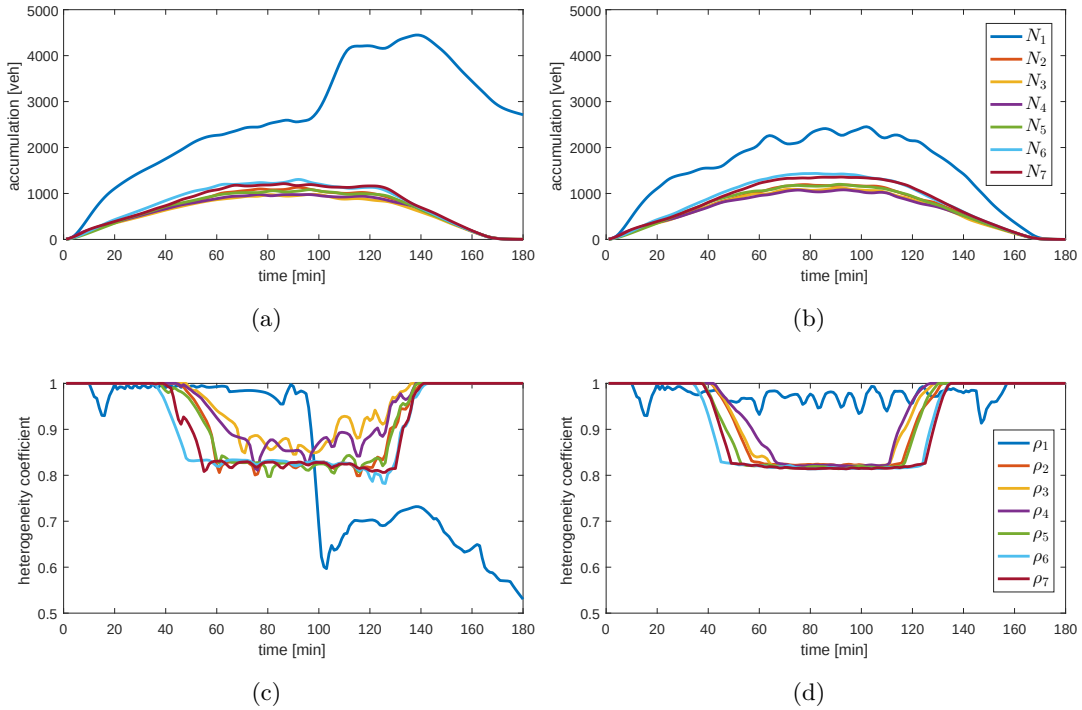

Figure 5.3 – Results of the congested scenario, showing region accumulations $N_I(t)$ (a)-(b) and heterogeneity coefficients $\rho_I(t)$ (c)-(d) as functions of time, for the no control case (a)-(c) and the hierarchical route guidance scheme (b)-(d).

in turn helps the central region stay uncongested. In NC scenario, the accumulation in the central region escalates to very high values at around 100 min, and the network is not emptied at the end of the 3-hour simulation. To have a fair comparison between the two scenarios, we run the simulation as long as there are vehicles in the system and calculate the total time spent when all the vehicles reach their destination. This calculation results in $2.32 \cdot 10^4(veh.h)$ and $1.72 \cdot 10^4(veh.h)$ for NC and RG scenarios, respectively, which corresponds to around 27% improvement with RG. An important reason that RG performs significantly better is not only a subset of vehicles does not cross the center region, but also the level of homogeneity is higher in the central region that further increases the outflow. Note that, as presented in Eq. 5.2, low ρ_I values lead to low outflows from the region. In NC scenario, a sharp decrease in the heterogeneity coefficient (i.e. ρ_1) signals the deterioration in the congestion distribution in region 1, which is followed by high accumulation values in the same region. On the other hand, RG strategy achieves to produce coefficient values close to 1 and guarantees that congestion distribution stays consistent throughout the simulation in the central region. Additionally, in both NC and RG, we observe that the heterogeneity coefficient in the peripheral regions seems to converge to a value around 0.8 as the simulation progresses. This is mainly due to the physical structure of the network; the sub-regions at the outer layer of the network (e.g. sub-regions 10, 16 and 25) are rarely used by through traffic. The traffic load they

carry is inherently low compared with other sub-regions in the region, which causes a lower heterogeneity coefficient for the region they belong to. While the homogenization of the regions is not considered as part of the objective function in the regional route guidance MPC, ILP-based sub-regional path assignment accounts for the sub-region speeds at the current time step and constraints the change in region-to-region travel time through Equation 5.9. This enables ILP to react to uneven distribution of congestion and homogenize the traffic across sub-regions. Therefore, as Figure 5.3 depicts, the improvement comes from both regional route discipline and increased homogeneity within the regions. In the RG scenario, the accumulation in the central region is significantly lower and the heterogeneity coefficient is substantially higher.

Figure 5.4(a) and (b) depict the sub-region accumulations of region 1 (i.e., the central region) in NC and RG scenarios, respectively. While accumulation values are comparable

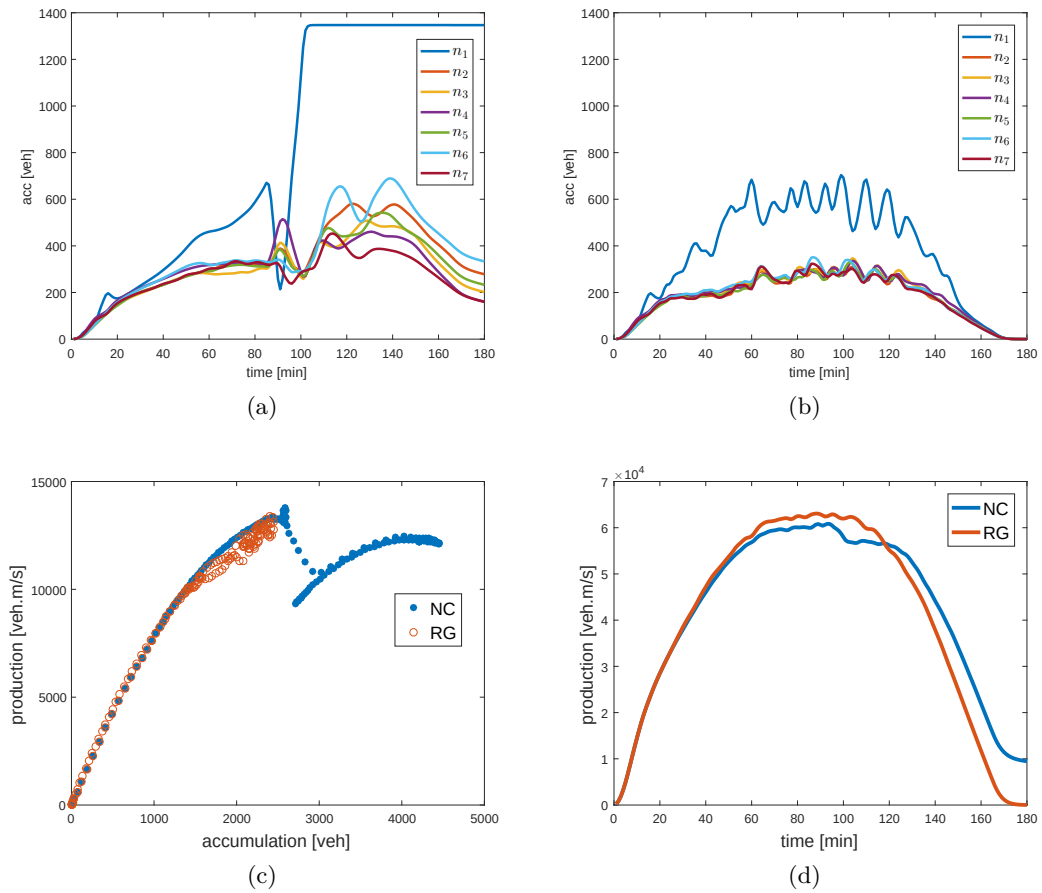

Figure 5.4 – Results of the congested scenario comparing sub-region accumulations of region 1 (a)-(b), production MFDs of region 1 (c), and the network production as a function of time (d), for the no control case (NC) (a) and the hierarchical route guidance scheme (RG) (b).

across the scenarios in the first half of the simulation, the central sub-region (i.e., sub-region 1) starts attracting significant demand at around 90 (min) and reaches gridlock state few minutes later. On the other hand, although central sub-region always carries a higher traffic, RG strategy ensures a greater level of homogeneity in the region and does not cause gridlock state in any sub-region. Figure 5.4(c) presents the production MFD of region 1 in two scenarios which results from the accumulations introduced in Figure 5.4(a) and (b). The city center suffers from a significant capacity drop in NC scenario, while RG scenario is able to keep region 1 in the uncongested regime and guarantee higher production values despite few scatter (see the red circles in Figure 5.4(c)). Note that the capacity drop we observe in NC scenario is due to the jump in the heterogeneity coefficient values presented in Figure 5.3(c). The difference in MFD patterns is also reflected in the overall network production; Figure 5.4(d) shows that RG is able to produce higher production during the peak hour and empty the network earlier than NC scenario. Note the non-zero production values in NC at the end of the simulation.

Figure 5.5 presents the average trip length values that result from NC and RG scenarios in region 5. As can be seen from Figure 5.1, region 5 has 3 neighboring regions. Hence, including the internal trips, Figure 5.5 depicts 4 curves separately for NC and RG scenarios. At the start of the simulation, most vehicles are closer to their origin than to their destination; therefore, the outflow values are very small and the average trip length values are very high. However, we note that, in all scenarios, they quickly converge to stable values (like a warm up period). The average trip lengths to neighboring peripheral regions (i.e. L_{54} and L_{56}) slightly increase after the activation of RG, while the one to the central region (i.e. L_{51}) and to itself (i.e. L_{55}) remain more or less the same. This is due

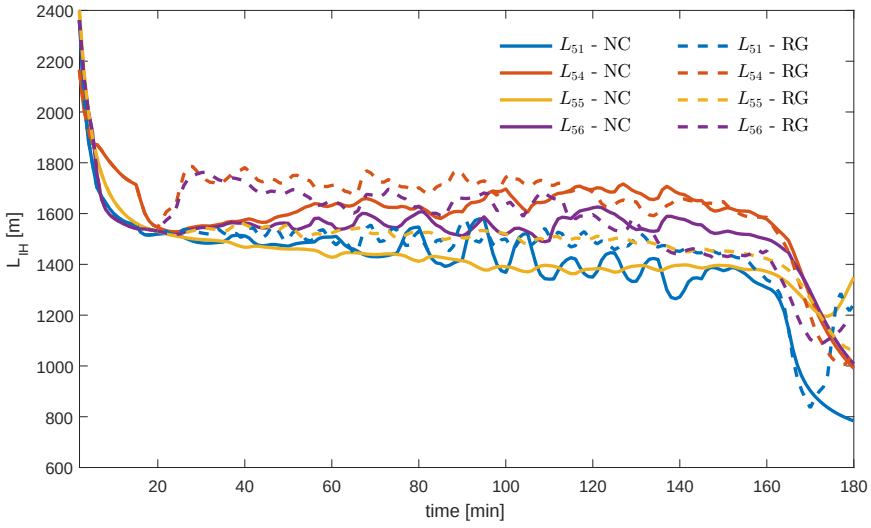

Figure 5.5 – Average trip length values in region 5.

to the change in the assignment patterns; as there are more vehicles using the peripheral network with the implementation of RG, it is not possible to keep the average trip length values at the low level observed in NC. However, both L_{54} and L_{56} quickly converge to slightly higher values and remain approximately stable until the network unloading stage. The simulation ends with relatively low distance values in both scenarios as a result of the region being emptied and most vehicles being closer to their destination. Trip length graphs for other peripheral regions are omitted due to space limitation. Nevertheless, they represent similar patterns.

Figure 5.6 compares NC with RG regarding the proportion of accumulations (i.e. N_{IJ}^{H}/N_{IJ}) and presents the ordered and reconstructed split ratios (i.e. θ and $\hat{\theta}$) in RG. Note that split ratios apply to transfer flows (between regions) and the newly generated exogenous demand, while the proportion of accumulation defines the route choice patterns for all circulating vehicles. For the illustration purposes, we choose the

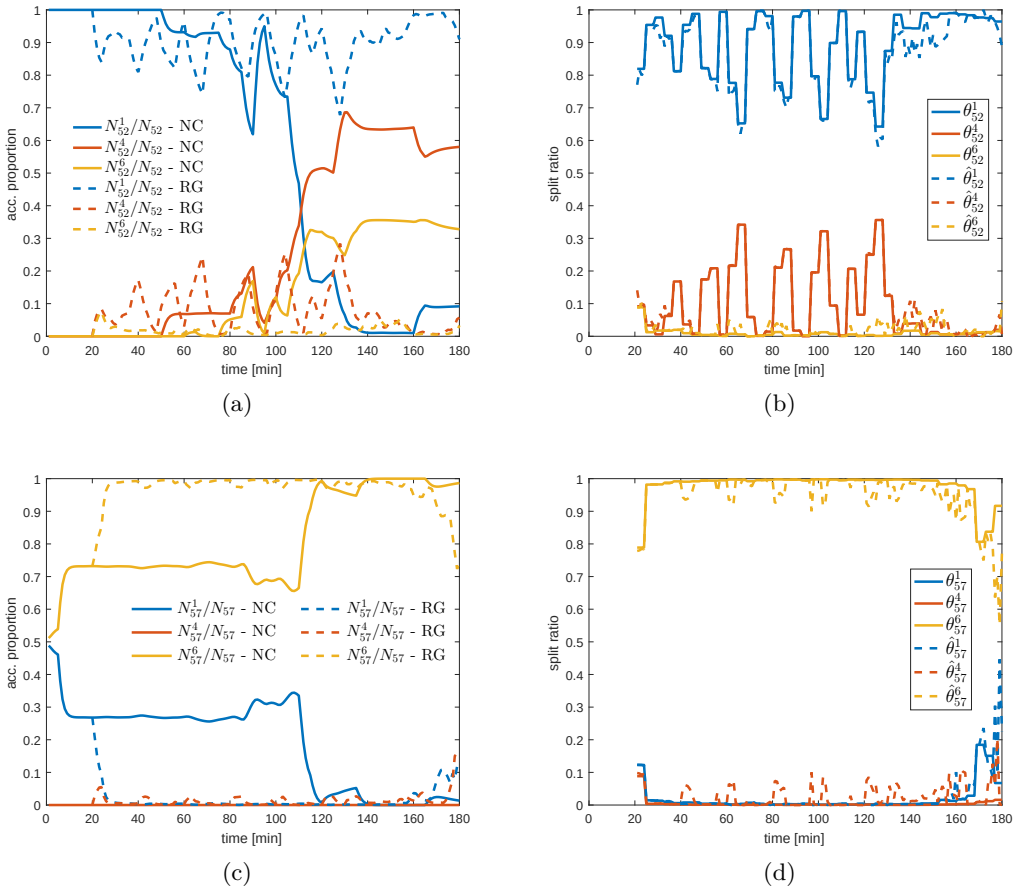

Figure 5.6 – (a), (c) Resulting accumulation proportions in NC and RG; (b), (d) Ordered and reconstructed split ratios, θ and $\hat{\theta}$, in RG for vehicles going from region 5 to regions 2 and 7.

vehicles traveling from region 5 to regions 2 and 7. As previously mentioned, the first 20 min of the simulation is considered the warm-up period during which RG is not active. That is why accumulation proportions are the same for NC and RG in the first 20 min (see Figure 5.6a and 5.6c).

Figure 5.6a and 5.6b introduce the accumulation proportions and split ratios, respectively, for the vehicles traveling from region 5 to 2. All vehicles start off by choosing region 1 in NC (see Figure 5.6a), as it provides the (physical) shortest alternative (see Figure 5.1). Due to changing traffic conditions, after $t = 50$(min), alternative paths that do not cross the central region become more appealing, and some vehicles start using the idle capacity at the periphery of the network. However, this does not save the central region from getting overly congested. On the contrary, RG, after being activated at $t = 20$(min), assigns 0-35% of the (newly entering) demand to the peripheral regions (see the red and yellow curves in Figure 5.6b) and ensures that the central region has a more balanced distribution of accumulation (see Figure 5.6a). Note that the ordered and reconstructed split ratios in Figure 5.6b are very close to each other for this particular demand pair throughout the simulation. Figure 5.6c and 5.6d present the split ratios and accumulation proportions, respectively, for the vehicles traveling from region 5 to 7. According to the regional representation of the network (see Figure 5.1), the central region 1 and the peripheral region 6 provide equally appealing alternatives (in terms of distance). In NC scenario, initially, approximately 30% of the accumulation crosses the central region; however, in response to hyper-congestion in the center, travelers switch to peripheral regions towards the end of the simulation. On the other hand, RG guides almost all the vehicles through the peripheral region 6 and protects the central region from congestion. Note that regional split ratios are rapidly changing in RG at the end of the simulation, which is due to the network being emptied. Turning RG off below a certain accumulation level could easily prevent this behavior, but is not expected to significantly change the results as there are very few vehicles in the network within this period.

Figure 5.7 and 5.8 provide a series of snapshots over time that depicts the evolution of regional and sub-regional accumulations in the network, respectively. In Figure 5.7, we see that congestion is rather evenly distributed across the regions in RG, while NC scheme is overloading the central region. Note that the central region has some residual accumulation at the end of the time horizon, while the network is completely emptied in RG. Figure 5.8 provides a zoom-in view of the accumulations in the network. We observe that the sub-regions at the outermost layer of the network are used at below their capacity throughout the simulation in both scenarios. As these sub-regions are not critical in terms of the network connectivity, they are mostly used by vehicles entering or leaving the network through them. In addition, we note that the sub-region at the core of the network (sub-region 1 in Figure 5.1) gets gridlocked (i.e. reaches jam accumulation) at around 120 min, and it cannot be rescued from that state until the simulation end. In overall, these results show that the RG scheme can distribute congestion evenly over

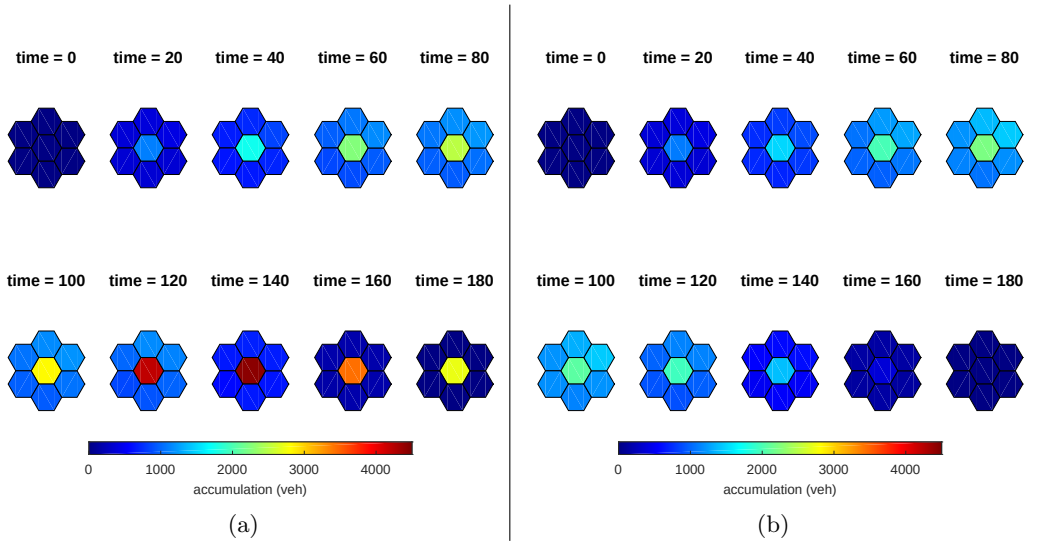

Figure 5.7 – Evolution of region accumulations over time (min). (a) NC, (b) RG.

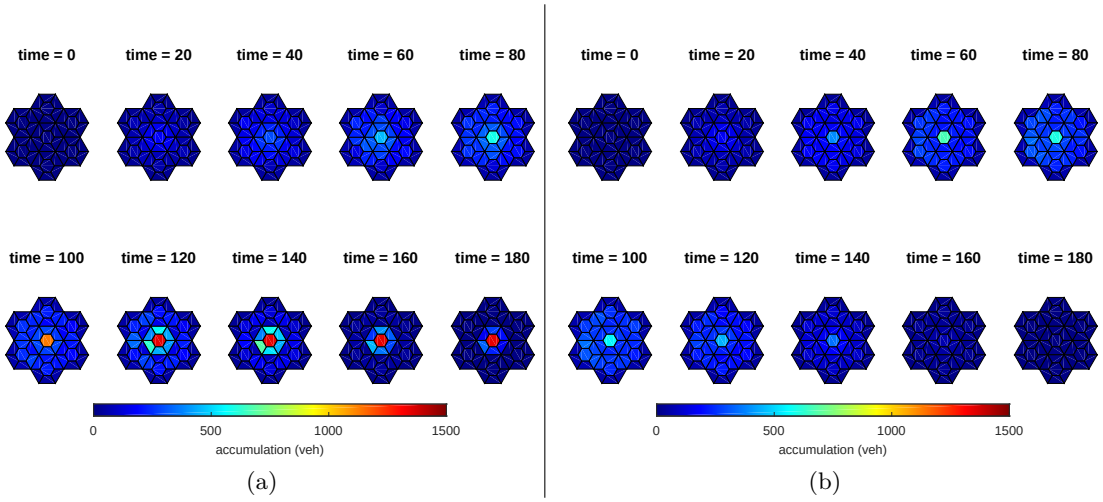

Figure 5.8 – Evolution of sub-region accumulations over time (min). (a) NC, (b) RG.

the network using the authority over path assignment and route guidance, leading to an efficient use of network capacity and ultimately to increased mobility.

5.4.2 Comparison with perimeter control-based MPC

To evaluate the performance of the proposed hierarchical control scheme in comparison with a perimeter control case, an MPC with only perimeter control type actuation is tested using the simulation experiment with the congested scenario. The perimeter control MPC is constructed in a similar vein with the proposed regional route guidance MPC: the multi-region MFDs network based MPC formulation from [63] is extended with heterogeneity variance and dynamic trip length terms as in equation (5.10), while perimeter control inputs (i.e. $U_{IJ}(t)$) are introduced into the formulation as decision variables and the regional split ratios $\theta^H_{IJ}(t)$ are defined as measurements (for the MPC) that are assumed constant for the prediction horizon. On the sub-region level the drivers are free to choose their own routes as in the no control case. As the perimeter control MPC could not cope with the gridlock-level congestion in sub-region 1 due to the increasing heterogeneity, it is supplemented with a simple bang-bang perimeter controller that protects this sub-region from severe congestion. Note that while the perimeter control MPC controls the boundaries between regions, the bang-bang controller restricts the inflow from sub-regions 2-7 to sub-region 1. In fact, incorporation of the bang-bang controller adds 6 new borders to be controlled in the network, and in a real-world context, it may not be always possible to control the intersections in the city center (represented by region 1). However, to conduct a fair comparison here, we design a perimeter control (PC) strategy that combines the MPC control inputs at the region boundaries and the bang-bang control inputs at the border of sub-region 1. A discussion on why the perimeter control MPC itself does not work properly will be provided in the following paragraph.

Figure 5.9(a) presents the accumulation of region 1 for NC, RG and PC (i.e. MPC+bang-bang) scenarios. We clearly see that although PC can improve over the NC scenario by protecting region 1, it is not as effective as RG in the alleviation of congestion. Figure 5.9(b) presents the perimeter control action at the boundary between regions 6 and 1, which corresponds to the border between sub-regions 38 and 6 at the plant. While the maximum outflow is maintained at the border until around 100 (min), the controller reacts to the increasing accumulation in region 1 in the following time steps and restricts the inflow to the region 1. However, PC is not able to clear the network until the end of the 3-hour simulation. As in NC scenario, we run the simulation until the network is empty in PC scenario and calculate the total time spent in the network. PC results in $2.12 \cdot 10^4 (veh.h)$, which presents around 9% improvement over NC scenario, while RG yields 27% reduction in the total time spent. Finally, Figure 5.9(c) compares the production MFDs of region 1 in three cases: observations from the plant, production model with heterogeneity coefficient presented in Equation 5.3 and production model with

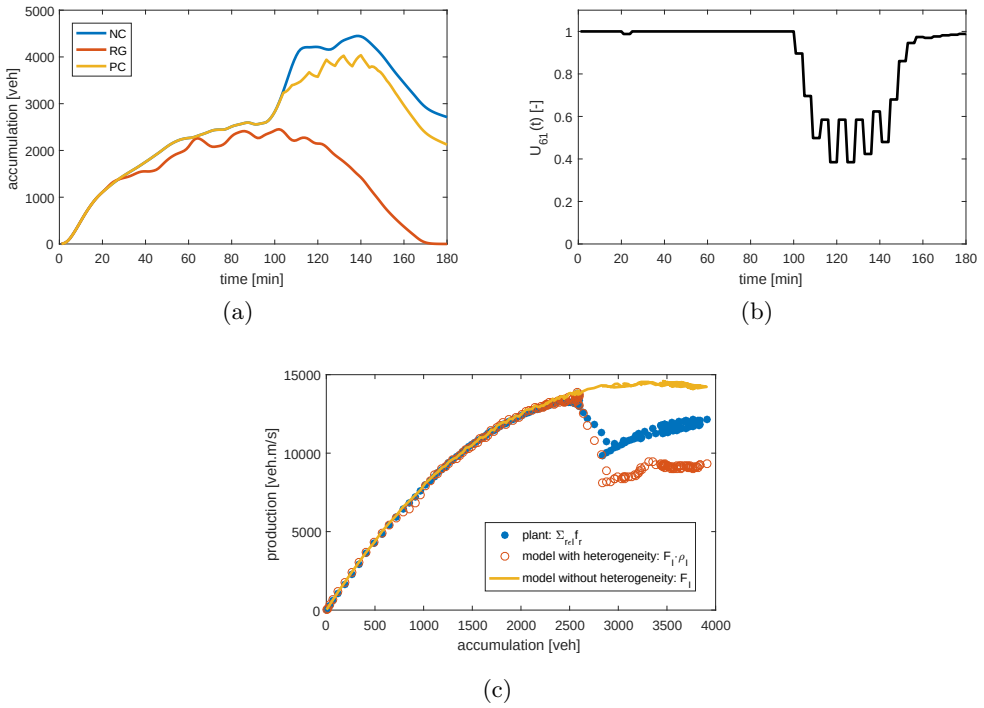

Figure 5.9 – (a) Accumulation of region 1 in the no control case (NC), the proposed route guidance (RG), and the perimeter control (PC), (b) Perimeter control input $U_{61}(t)$ for the PC case, (c) Production MFDs in region 1.

full homogeneity assumption (upper envelope for the production values). Note that this analysis represents a scenario where the perimeter control only consists of MPC control inputs. We clearly see that the production estimation with the heterogeneity model does not provide an accurate approximation for the plant measurements. As only one sub-region is very congested and the others are not, region 1 exhibits a highly imbalanced congestion scenario where the production model with heterogeneity coefficient fails to provide accurate estimations. We observe that the resulting heterogeneity coefficient values push the production estimations further down than the plant measurements. This is the main reason why perimeter control MPC itself cannot cope with the congested scenario in hand. On the other hand, RG strategy improves the homogeneity inside the regions, keeps the traffic states within the limit of trackable values and improves the traffic conditions in the network.

5.4.3 Sensitivity analyses

In this subsection, we test the sensitivity of our model with respect to certain design and scenario features; in particular (1) compliance rates of drivers to the guidance information, (2) path assignment characteristics (i.e., all-or-nothing vs. partial flows) and (3) noise in

the plant characteristics (i.e., randomness in the sub-region MFD).

First, we test our strategy with lower compliance rates. We keep the same formulation for the sub-regional path assignment and the regional route guidance, where we assume full compliance of users (note that the design of controller does not explicitly consider a given compliance rate). Nevertheless, at the testing stage, we provide the resulting $\alpha^p_{o,d}$ values only with the complying users and let the other users make route choice decisions in accordance with NC scenario. Figure 5.10a presents the accumulation values in region 1 (supposedly the most congested region) resulting from a number of compliance rates. Clearly, the higher the compliance rate is, the less congested region 1 becomes. Nevertheless, all the scenarios produce considerably better traffic conditions than NC scenario. Even with 25% compliance rate, traffic conditions are significantly improved and hyper-congestion (values higher than critical accumulation N^{cr}= 3333 veh) is avoided. That means, even a small percentage of users complying with the guidance information and avoiding potentially congested parts of the network, can bring major benefits to the system. The network performance with low compliance rates is similar to the full-compliance RG scenario, the resulting total time spent in the network is only 2-4% higher than that of 100% compliance scenario.

Second, assuming that there may not be always enough demand to accommodate continuous split ratios (between the boundary nodes), we have applied all-or-nothing assignment and defined $\alpha^p_{o,d}$ as a binary variable. To test the effects of this assumption, we now describe it as a continuous variable between 0 and 1 and reformulate the sub-region assignment mechanism as a linear programming (LP) problem. Figure 5.10b depicts the accumulation evolution in all regions for ILP and LP formulation. None of the regions exhibits a significant difference; however, we note minor changes particularly for region 1 between 60 min and 120 min. LP formulation leads to stable accumulation values within this period, while ILP formulation produces small up-and-downs. As LP can achieve a better tracking of signals (θ^H_{IJ} and L_{IH}) by adjusting continuous path flow distributions, it creates a more consistent accumulation profile even in the most congested period. Note that we do not observe a meaningful change in the performance measures across the two scenarios, which indicates that the model can as well be useful with all-or-nothing assumptions.

Third, we investigate the effect of additional noise in the plant characteristics. The purpose of the detailed 49-sub-region simulator is to create a significant difference between what the model knows during optimization (i.e. 7-region model) and what influence comprehensive plant characteristics might have. The sub-region model provides a simulation environment where many of the assumptions in the region model are released. For example, while routing is achieved with split ratios (θ^H_{IJ}) in the region model, sub-regional paths are incorporated into the plant in order to navigate the vehicles around the network. Nevertheless, we acknowledge that MFDs at the sub-regional level might experience scatter too (as link FDs do). Therefore, we release the assumption of

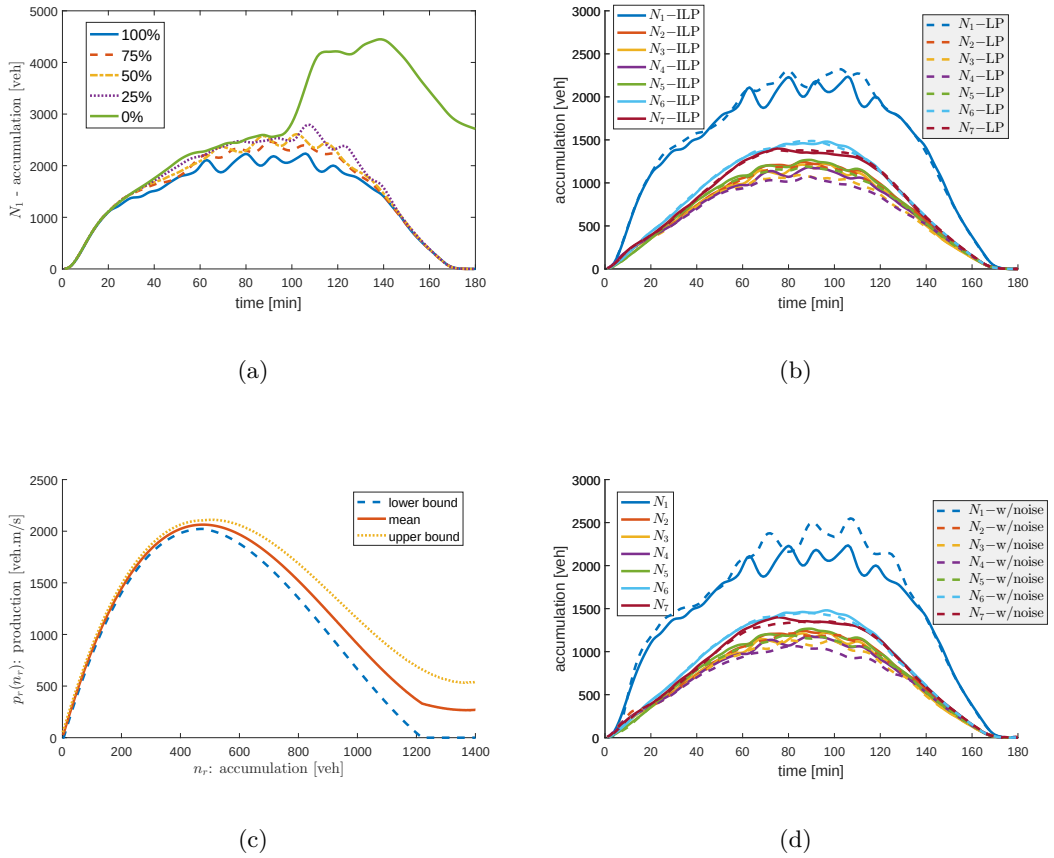

Figure 5.10 – (a) Accumulation in region 1 with varying compliance rates, (b) accumulation in all regions with continuous and integer decision variables in the sub-regional path assignment formulation, (c) sub-region MFD with uniformly distributed random noise between lower and upper bounds, (d) region accumulations resulting from the RG scenario with and without noise in sub-region MFD.

deterministic MFDs at the sub-regional level, and we incorporate noise into the sub-region MFD values. Figure 5.10c depicts the resulting sub-region MFD curve along with its mean, upper and lower bounds. We assume that the production value corresponding to a certain accumulation level is uniformly distributed between upper and lower bounds. Note that the noise increases with accumulation in the region, which is consistent with the observations from real data and microscopic simulation models. We then incorporate the random MFD curves into our framework and apply the proposed model to evaluate the impact of noise on the overall performance. Figure 5.10d compares the regional accumulation values resulting from the scenario with noise to the base scenario where we assume deterministic MFD curves for the sub-regions. While the new scenario with noise leads to higher accumulation values and greater variation in the central region (the most congested region), the framework is capable of mitigating the congestion. Total time spent in the two scenarios is very similar, which indicates the robustness of the proposed algorithm to the noise involved in estimations.

5.5 Conclusion

In this chapter a hierarchical traffic management scheme is proposed, integrating a path assignment mechanism with route guidance-based economic MPC. Firstly, MFD-based regional and sub-regional dynamical traffic models are described, intended as prediction model (for MPC) and simulation model, respectively. The contributions of the chapter are in two aspects: (1) Development of an ILP-based path assignment mechanism that can translate macroscopic route guidance commands into low-level, path-based traffic decisions, (2) integration of heterogeneity effects and variable trip lengths in the prediction model of the regional route guidance-based economic MPC scheme. Performance of the proposed hierarchical scheme is evaluated on macroscopic simulations in a network with 49 sub-regions. Results indicate potential in making efficient use of network capacity via actuation over paths for improved mobility.

Chapter 6

Conclusion and future research

With this dissertation we developed optimization-based control and estimation methods in part I (chapters 2 and 3), together with regional route guidance-based traffic management schemes in part II (chapters 4 and 5), for improving mobility in heterogeneously congested large-scale urban road networks. This final chapter contains summaries of the results and main contributions of each chapter, alongside discussions on potential practical applications and possible directions for future research. Detailed conclusions are also provided at the end of each chapter.

Part I Optimal Perimeter Control and Estimation for Urban Networks

Chapter 2 Nonlinear MHE for a two-region MFDs system The main contributions can be listed as follows:

- A state estimation method is proposed for estimating accumulation states and inflow demands for a two-region urban network using a macroscopic traffic model.
- Specifying the first attempt at MFD-based state estimation design, the method enables model-based large-scale traffic control in situations of noisy and limited measurements.

The proposed nonlinear MHE scheme is capable of OD inflow demand and accumulation state estimation for a two-region large-scale urban network model with MFD-based dynamics. Observability tests involving four practically motivated measurement compositions revealed that observability is retained even for compositions with limited or no measurements on OD-based information. Extensive simulations show that the estimation performance of the proposed MHE scheme is fairly insensitive to increasing noise intensity, and is superior to an EKF. Further simulations revealed that assuming constant future demands in the MPC formulation yields control performances practically

identical to the case with perfect demand information. Overall, the results indicate a strong potential towards implementation of MFD-based perimeter control, since the proposed MHE-MPC scheme is capable of high performance congestion management under severe conditions of measurement noise, limited or no OD-based information, and unknown future inflow demands.

Future research could investigate more sophisticated MFD-based models, such as those considering aggregated trip lengths as state variables, and the design of associated state estimation and feedback perimeter control methods. Strong demand fluctuations inducing fast evolving transient states, route choice effects, and spatially heterogeneous distribution of congestion can influence the trip length distribution in the network. These can result, for rapidly evolving traffic conditions, in accumulation-based models relying on the outflow MFD (as approximated by production over trip length) to exhibit inaccuracies due to the MFD ignoring traffic history of the network (i.e., it is memoryless). For example, in case of an inflow demand discontinuity in uncongested conditions, outflow and accumulation predicted by the outflow MFD-based model increase instantaneously, although they should increase only after a delay related to the duration of the shortest trip. Trip-based MFD models (see [83]) and their extensions (see [87]) involving average distance remaining to be traveled as a state specify strong candidates for addressing such concerns associated with accumulation-based model relying exclusively on outflow MFD with production over trip length approximation. Development of control-oriented trip-based models of MFDs networks, and testing their performance in model-based prediction, estimation, and control with detailed microscopic simulations and real-world experiments against accumulation-based models is an important research priority. Furthermore, preliminary investigations suggest that the favorable situation for the two-region MFDs system case, where even measurement compositions without OD-based information yield observability, does not directly carry over to multi-region dynamics with more than two regions. More research is needed to reveal the measurement compositions that are required to yield observability for multi-region MFD-based models.

Chapter 3 Identification, estimation, and control for large-scale networks We can summarize the main contributions as follows:

- A traffic control framework, consisting of optimization-based identification, estimation, and control methods, is proposed for large-scale urban networks.
- The proposed methods, employing an MFD-based dynamical model with accumulation states having current and destination region indices, are applied for the first time in detailed microscopic simulations.

In this chapter a system identification method is proposed for obtaining MFD

parameters from data considering a macroscopic dynamical model of large-scale urban traffic. Based on the least squares prediction error approach, the identification problem is formulated as an optimization problem involving minimization of the weighted least squares difference between the measurements and model predictions. Furthermore, nonlinear MHE and economic MPC formulations are presented, which employ the MFD parameters obtained by the identification method. The traffic control framework, consisting of the proposed identification, state estimation, and control methods, is applied to a four region urban network using detailed microscopic simulations. Results indicate strong potential of the framework for improving mobility in city-scale traffic with macroscopic model-based estimation and control methods.

Future research could focus on testing the proposed methods under various measurement noise conditions to evaluate their sensitivity to noise intensity and comparing them to standard estimation and control methods in the literature. Such analyses are expected to reveal the limits of noise that can be tolerated in measurements for feedback perimeter control. Another important point is to investigate how the results obtained by the proposed MBPE method compare to other MFD extraction methods (for example, the standard method of fitting a polynomial to regional accumulation against outflow data). Design of estimation and control methods using MFD-based models with heterogeneity (as introduced by [36]) and hysteresis, is also an interesting future research direction, as it is expected that such models can result in improved performance. Development of more detailed MFD-based dynamical models considering state variables representing aggregated trip lengths, alongside associated identification, estimation, and control methods is a research priority. Some of these directions are currently under investigation in ongoing work. Finally, as the ultimate test for the proposed methods, field implementations carried out in real networks will shed more light on the potential of MFD-based modeling, estimation, and control for improving mobility in congested city-level road transport systems.

Part II Large-scale Traffic Management via Regional Route Guidance

Chapter 4 Integration of route guidance and perimeter control We can list the main contributions as follows:

- Based on macroscopic traffic models, economic MPC schemes employing route guidance and perimeter control actuation are designed for alleviating congestion in large-scale networks.
- Macroscopic simulations reveal that using route guidance alongside perimeter control yields improvements in mobility.

In this chapter route guidance-based economic MPC schemes are proposed for large-scale traffic management. The contributions are in two aspects:

(a) In the traffic modeling side a novel cyclic behavior prohibiting dynamic urban network model is proposed, with the potential of yielding more realistic simulation results compared to current MFD-based urban network models in the literature, (b) in the control design aspect, integrating perimeter control and route guidance type actuators, economic nonlinear MPC schemes are developed for improving mobility in urban networks. Simulation studies show the potential for substantial improvement in mobility through the use of route guidance, in comparison to control via perimeter control only. A further observation is that since route guidance actuation cannot restrict flows, unlike perimeter control, it is unable to protect urban regions from severe congestion especially for cases with imperfect driver compliance. Highest performance is obtained by using both types of actuators.

Future research could include comparison of the proposed MPC schemes with feedback perimeter control approaches from the literature (such as [12], [14]). Such investigations can reveal the extent to which having route guidance actuation can improve over high-performance perimeter control methods. Another important point is to evaluate the proposed schemes on detailed microscopic simulations to establish the performannce improvements in a more realistic manner. Although feedback perimeter control is already successfully implemented in microscopic simulation-based studies (see [12], [14] and chapter 3), testing MFD-based control methods employing route guidance remains unexplored. Design of MFD-based route guidance actuated control schemes for mixed urban-freeway networks specifies another promising future direction. Efficient usage of the combined urban-freeway capacity for serving both urban trips and highway traffic passing through the urban area can be expected to improve overall network performance.

Chapter 5 Integration of route guidance and path assignment The main contributions can be summarized as follows:

- Using a path assignment mechanism with route guidance-based economic MPC, a hierarchical traffic management scheme is proposed for congestion control.
- Integrating path assignment with route guidance is shown to yield mobility improvements in macroscopic simulations.

A hierarchical traffic management scheme based on path assignment and route guidance is developed in this chapter. Regional and sub-regional MFD-based dynamical traffic models are described, which are employed as prediction model (in MPC) and simulation model, respectively. The contributions of the chapter are twofold: (1) An ILP-based path assignment mechanism is designed, which can translate macroscopic route guidance-based control actions into low-level sub-regional path decisions, (2) heterogeneity effect and variable trip lengths are incorporated into the prediction model of the regional route

guidance MPC scheme. Efficiency of the proposed hierarchical scheme is tested on a network with 49 sub-regions in macroscopic simulations. The results indicate a great potential in making efficient use of network capacity via actuation over paths and achieving improved mobility. Such a hierarchical traffic management scheme can be implemented in real life applications, if data from global positioning system and loop detectors are combined to obtain real-time measurements of the detailed accumulation states.

Future research could study the integration of the route guidance system with the perimeter control strategy, which is expected to further improve network performance. Although this is already investigated at the region level without path assignment (see chapter 4), more detailed experiments considering sub-regional dynamics are expected to shed more light on the capabilities of combined perimeter control and route guidance actuators. Moreover, testing the proposed scheme with microscopic simulations is expected to reveal the performance improvements in a more realistic setting. In addition, replacing the sub-regional representation of traffic dynamics at the lower level with more detailed link-level modeling is an interesting future direction, as such models are expected to yield higher accuracy and thus better path assignment decisions. Investigating how the lower level can support the network-level controller is also a promising point for future work. Similar to the approach taken in [36], lower level controllers considering both higher resolution (i.e., sub-regional) perimeter control and path assignment can be used to increase regional homogeneity in distribution of congestion and track network-level route guidance setpoints, potentially resulting in improved mobility.

In conclusion, it is possible to improve mobility in large-scale urban road networks using traffic control systems employing perimeter control and route guidance actuation. For progress towards practicable design and implementation of such traffic control systems, in this dissertation we developed optimization-based control, estimation, and identification methods employing MFD-based dynamical traffic models, and evaluated them on macroscopic and microscopic simulations. Overall, the results suggest that the proposed methods carry strong potential for improving mobility in urban traffic.

Bibliography

[1] M. Papageorgiou, C. Diakaki, V. Dinopoulou, A. Kotsialos, and Y. Wang, "Review of road traffic control strategies", *Proceedings of the IEEE*, vol. 91, no. 12, pp. 2043–2067, 2003. DOI: 10.1109/JPROC.2003.819610.

[2] C. Diakaki, M. Papageorgiou, and K. Aboudolas, "A multivariable regulator approach to traffic-responsive network-wide signal control", *Control Engineering Practice*, vol. 10, no. 2, pp. 183–195, 2002. DOI: 10.1016/S0967-0661(01)00121-6.

[3] K. Aboudolas, M. Papageorgiou, A. Kouvelas, and E. Kosmatopoulos, "A rolling-horizon quadratic-programming approach to the signal control problem in large-scale congested urban road networks", *Transportation Research Part C: Emerging Technologies*, vol. 18, no. 5, pp. 680–694, 2010. DOI: 10.1016/j.trc.2009.06.003.

[4] A. Kouvelas, K. Aboudolas, M. Papageorgiou, and E. B. Kosmatopoulos, "A hybrid strategy for real-time traffic signal control of urban road networks", *IEEE Transactions on Intelligent Transportation Systems*, vol. 12, no. 3, pp. 884–894, 2011. DOI: 10.1109/TITS.2011.2116156.

[5] L. Tassiulas and A. Ephremides, "Stability properties of constrained queueing systems and scheduling policies for maximum throughput in multihop radio networks", *IEEE Transactions on Automatic Control*, vol. 37, no. 12, pp. 1936–1948, 1992. DOI: 10.1109/9.182479.

[6] A. Kouvelas, J. Lioris, S. A. Fayazi, and P. Varaiya, "Maximum pressure controller for stabilizing queues in signalized arterial networks", *Transportation Research Record: Journal of the Transportation Research Board*, vol. 2421, no. 1, pp. 133–141, 2014. DOI: 10.3141/2421-15.

[7] T. Wongpiromsarn, T. Uthaicharoenpong, Y. Wang, E. Frazzoli, and D. Wang, "Distributed traffic signal control for maximum network throughput", in *15th IEEE Conference on Intelligent Transportation Systems*, IEEE, 2012, pp. 588–595. DOI: 10.1109/ITSC.2012.6338817.

[8] C. F. Daganzo, "Urban gridlock: Macroscopic modeling and mitigation approaches", *Transportation Research Part B: Methodological*, vol. 41, no. 1, pp. 49–62, 2007. DOI: 10.1016/j.trb.2006.03.001.

[9] M. Keyvan-Ekbatani, A. Kouvelas, I. Papamichail, and M. Papageorgiou, "Exploiting the fundamental diagram of urban networks for feedback-based gating", *Transportation Research Part B: Methodological*, vol. 46, no. 10, pp. 1393–1403, 2012. DOI: 10.1016/j.trb.2012.06.008.

[10] J. Haddad and A. Shraiber, "Robust perimeter control design for an urban region", *Transportation Research Part B: Methodological*, vol. 68, pp. 315–332, 2014. DOI: 10.1016/j.trb.2014.06.010.

[11] J. Haddad and N. Geroliminis, "On the stability of traffic perimeter control in two-region urban cities", *Transportation Research Part B: Methodological*, vol. 46, no. 9, pp. 1159–1176, 2012. DOI: 10.1016/j.trb.2012.04.004.

[12] K. Aboudolas and N. Geroliminis, "Perimeter and boundary flow control in multi-reservoir heterogeneous networks", *Transportation Research Part B: Methodological*, vol. 55, pp. 265–281, 2013. DOI: 10.1016/j.trb.2013.07.003.

[13] N. Geroliminis, J. Haddad, and M. Ramezani, "Optimal perimeter control for two urban regions with macroscopic fundamental diagrams: A model predictive approach", *IEEE Transactions on Intelligent Transportation Systems*, vol. 14, no. 1, pp. 348–359, 2013. DOI: 10.1109/TITS.2012.2216877.

[14] A. Kouvelas, M. Saeedmanesh, and N. Geroliminis, "Enhancing model-based feedback perimeter control with data-driven online adaptive optimization", *Transportation Research Part B: Methodological*, vol. 96, pp. 26–45, 2017. DOI: 10.1016/j.trb.2016.10.011.

[15] J Godfrey, "The mechanism of a road network", *Traffic Engineering & Control*, vol. 8, no. 8, 1969.

[16] N. Geroliminis and C. F. Daganzo, "Existence of urban-scale macroscopic fundamental diagrams: Some experimental findings", *Transportation Research Part B: Methodological*, vol. 42, no. 9, pp. 759–770, 2008. DOI: 10.1016/j.trb.2008.02.002.

[17] C. Buisson and C. Ladier, "Exploring the impact of homogeneity of traffic measurements on the existence of macroscopic fundamental diagrams", *Transportation Research Record: Journal of the Transportation Research Board*, vol. 2124, no. 1, pp. 127–136, 2009. DOI: 10.3141/2124-12.

[18] A. Mazloumian, N. Geroliminis, and D. Helbing, "The spatial variability of vehicle densities as determinant of urban network capacity", *Philosophical Transactions of the Royal Society A: Mathematical, Physical and Engineering Sciences*, vol. 368, no. 1928, pp. 4627–4647, 2010. DOI: 10.1098/rsta.2010.0099.

[19] N. Geroliminis and J. Sun, "Properties of a well-defined macroscopic fundamental diagram for urban traffic", *Transportation Research Part B: Methodological*, vol. 45, no. 3, pp. 605–617, 2011. DOI: 10.1016/j.trb.2010.11.004.

[20] V. Knoop, S. Hoogendoorn, J. Van Lint, *et al.*, "Routing strategies based on macroscopic fundamental diagram", *Transportation Research Record: Journal of the Transportation Research Board*, vol. 1, no. 2315, pp. 1–10, 2012. DOI: 10.3141/2315-01.

[21] N. Geroliminis and J. Sun, "Hysteresis phenomena of a macroscopic fundamental diagram in freeway networks", *Transportation Research Part A: Policy and Practice*, vol. 45, no. 9, pp. 966–979, 2011. DOI: 10.1016/j.tra.2011.04.004.

[22] M. Saberi and H. S. Mahmassani, "Exploring properties of networkwide flow–density relations in a freeway network", *Transportation Research Record: Journal of the Transportation Research Board*, vol. 2315, no. 1, pp. 153–163, 2012. DOI: 10.3141/2315-16.

[23] Y. Ji and N. Geroliminis, "On the spatial partitioning of urban transportation networks", *Transportation Research Part B: Methodological*, vol. 46, no. 10, pp. 1639–1656, 2012. DOI: 10.1016/j.trb.2012.08.005.

[24] M. Saeedmanesh and N. Geroliminis, "Clustering of heterogeneous networks with directional flows based on "Snake" similarities", *Transportation Research Part B: Methodological*, vol. 91, pp. 250–269, 2016. DOI: 10.1016/j.trb.2016.05.008.

[25] C. Lopez, P. Krishnakumari, L. Leclercq, N. Chiabaut, and H. Van Lint, "Spatiotemporal partitioning of transportation network using travel time data", *Transportation Research Record: Journal of the Transportation Research Board*, vol. 2623, no. 1, pp. 98–107, 2017. DOI: 10.3141/2623-11.

[26] C. E. Garcia, D. M. Prett, and M. Morari, "Model predictive control: Theory and practice–A survey", *Automatica*, vol. 25, no. 3, pp. 335–348, 1989. DOI: 10.1016/0005-1098(89)90002-2.

[27] D. Q. Mayne, J. B. Rawlings, C. V. Rao, and P. O. Scokaert, "Constrained model predictive control: Stability and optimality", *Automatica*, vol. 36, no. 6, pp. 789–814, 2000. DOI: 10.1016/S0005-1098(99)00214-9.

[28] C. V. Rao, J. B. Rawlings, and D. Q. Mayne, "Constrained state estimation for nonlinear discrete-time systems: Stability and moving horizon approximations", *IEEE Transactions on Automatic Control*, vol. 48, no. 2, pp. 246–258, 2003. DOI: 10.1109/TAC.2002.808470.

[29] I. Papamichail, A. Kotsialos, I. Margonis, and M. Papageorgiou, "Coordinated ramp metering for freeway networks–A model-predictive hierarchical control approach", *Transportation Research Part C: Emerging Technologies*, vol. 18, no. 3, pp. 311–331, 2010. DOI: 10.1016/j.trc.2008.11.002.

[30] J. R. D. Frejo, A. Núñez, B. De Schutter, and E. F. Camacho, "Hybrid model predictive control for freeway traffic using discrete speed limit signals", *Transportation Research Part C: Emerging Technologies*, vol. 46, pp. 309–325, 2014. DOI: 10.1016/j.trc.2014.06.005.

[31] A. Hegyi, B. De Schutter, and J. Hellendoorn, "Optimal coordination of variable speed limits to suppress shock waves", *IEEE Transactions on Intelligent Transportation Systems*, vol. 6, no. 1, pp. 102–112, 2005. DOI: 10.1109/TITS.2004.842408.

[32] L. D. Baskar, B. De Schutter, and H. Hellendoorn, "Traffic management for automated highway systems using model-based predictive control", *IEEE Transactions on Intelligent Transportation Systems*, vol. 13, no. 2, pp. 838–847, 2012. DOI: 10.1109/TITS.2012.2186441.

[33] S. Lin, B. De Schutter, Y. Xi, and H. Hellendoorn, "Fast model predictive control for urban road networks via milp", *IEEE Transactions on Intelligent Transportation Systems*, vol. 12, no. 3, pp. 846–856, 2011. DOI: 10.1109/TITS.2011.2114652.

[34] J. Haddad, M. Ramezani, and N. Geroliminis, "Cooperative traffic control of a mixed network with two urban regions and a freeway", *Transportation Research Part B: Methodological*, vol. 54, pp. 17–36, 2013. DOI: 10.1016/j.trb.2013.03.007.

[35] M. Hajiahmadi, J. Haddad, B. De Schutter, and N. Geroliminis, "Optimal hybrid perimeter and switching plans control for urban traffic networks", *IEEE Transactions on Control Systems Technology*, vol. 23, no. 2, pp. 464–478, 2015. DOI: 10.1109/TCST.2014.2330997.

[36] M. Ramezani, J. Haddad, and N. Geroliminis, "Dynamics of heterogeneity in urban networks: Aggregated traffic modeling and hierarchical control", *Transportation Research Part B: Methodological*, vol. 74, pp. 1–19, 2015. DOI: 10.1016/j.trb.2014.12.010.

[37] A. Csikós, T. Charalambous, H. Farhadi, B. Kulcsár, and H. Wymeersch, "Network traffic flow optimization under performance constraints", *Transportation Research Part C: Emerging Technologies*, vol. 83, pp. 120–133, 2017. DOI: 10.1016/j.trc.2017.08.002.

[38] K. Yang, N. Zheng, and M. Menendez, "Multi-scale perimeter control approach in a connected-vehicle environment", *Transportation Research Part C: Emerging Technologies*, vol. 94, pp. 32–49, 2018. DOI: 10.1016/j.trc.2017.08.014.

[39] Z. Zhou, B. De Schutter, S. Lin, and Y. Xi, "Two-level hierarchical model-based predictive control for large-scale urban traffic networks", *IEEE Transactions on Control Systems Technology*, vol. 25, no. 2, pp. 496–508, 2017. DOI: 10.1109/TCST.2016.2572169.

[40] X. Sun, L. Muñoz, and R. Horowitz, "Highway traffic state estimation using improved mixture Kalman filters for effective ramp metering control", in *42nd IEEE Conference on Decision and Control (CDC)*, IEEE, vol. 6, 2003, pp. 6333–6338. DOI: 10.1109/CDC.2003.1272322.

[41] Y. Wang and M. Papageorgiou, "Real-time freeway traffic state estimation based on extended Kalman filter: A general approach", *Transportation Research Part B: Methodological*, vol. 39, no. 2, pp. 141–167, 2005. DOI: 10.1016/j.trb.2004.03.003.

[42] A. Messmer and M. Papageorgiou, "METANET: A macroscopic simulation program for motorway networks", *Traffic Engineering & Control*, vol. 31, no. 9, 1990.

[43] L. Mihaylova, R. Boel, and A. Hegyi, "Freeway traffic estimation within particle filtering framework", *Automatica*, vol. 43, no. 2, pp. 290–300, 2007. DOI: 10.1016/j.automatica.2006.08.023.

[44] Y. Yuan, J. van Lint, R. E. Wilson, F. van Wageningen-Kessels, and S. P. Hoogendoorn, "Real-time Lagrangian traffic state estimator for freeways", *IEEE Transactions on Intelligent Transportation Systems*, vol. 13, no. 1, pp. 59–70, 2012. DOI: 10.1109/TITS.2011.2178837.

[45] R. Pueboobpaphan and T. Nakatsuji, "Real-time traffic state estimation on urban road network: The application of unscented Kalman filter", in *9th International Conference on Applications of Advanced Technology in Transportation*, 2006, pp. 542–547. DOI: 10.1061/40799(213)86.

[46] Q.-J. Kong, Z. Li, Y. Chen, and Y. Liu, "An approach to urban traffic state estimation by fusing multisource information", *IEEE Transactions on Intelligent Transportation Systems*, vol. 10, no. 3, pp. 499–511, 2009. DOI: 10.1109/TITS.2009.2026308.

[47] A. Nantes, D. Ngoduy, A. Bhaskar, M. Miska, and E. Chung, "Real-time traffic state estimation in urban corridors from heterogeneous data", *Transportation Research Part C: Emerging Technologies*, vol. 66, pp. 99–118, 2016. DOI: 10.1016/j.trc.2015.07.005.

[48] L. Leclercq and N. Geroliminis, "Estimating MFDs in simple networks with route choice", *Transportation Research Part B: Methodological*, vol. 57, pp. 468–484, 2013. DOI: 10.1016/j.trb.2013.05.005.

[49] M. Ramezani and M. Nourinejad, "Dynamic modeling and control of taxi services in large-scale urban networks: A macroscopic approach", *Transportation Research Part C: Emerging Technologies*, vol. 94, pp. 203–219, 2018. DOI: 10.1016/j.trc.2017.08.011.

[50] C. Menelaou, P. Kolios, S. Timotheou, C. Panayiotou, and M. Polycarpou, "Controlling road congestion via a low-complexity route reservation approach", *Transportation Research Part C: Emerging Technologies*, vol. 81, pp. 118–136, 2017. DOI: 10.1016/j.trc.2017.05.005.

[51] M. Yildirimoglu and N. Geroliminis, "Approximating dynamic equilibrium conditions with macroscopic fundamental diagrams", *Transportation Research Part B: Methodological*, vol. 70, pp. 186–200, 2014. DOI: 10.1016/j.trb.2014.09.002.

[52] M. Yildirimoglu, M. Ramezani, and N. Geroliminis, "Equilibrium analysis and route guidance in large-scale networks with MFD dynamics", *Transportation Research Part C: Emerging Technologies*, vol. 59, pp. 404–420, 2015. DOI: 10.1016/j.trc.2015.05.009.

[53] I. I. Sirmatel and N. Geroliminis, "Hybrid modeling and predictive control of bus transport systems", in *Transportation Research Board 96th Annual Meeting*, 2017. [Online]. Available: https://trid.trb.org/view/1439090.

[54] ——, "Dynamical modeling and predictive control of bus transport systems: A hybrid systems approach", *IFAC-PapersOnLine*, vol. 50, no. 1, pp. 7499 –7504, 2017, Proceedings of the 20th IFAC World Congress. DOI: 10.1016/j.ifacol.2017.08.1067.

[55] ——, "Hybrid model predictive control of bus transport systems", in *17th European Control Conference (ECC)*, IEEE, 2018, pp. 1660–1665. DOI: 10.23919/ECC.2018.8550489.

[56] ——, "Mixed logical dynamical modeling and hybrid model predictive control of public transport operations", *Transportation Research Part B: Methodological*, vol. 114, pp. 325–345, 2018. DOI: 10.1016/j.trb.2018.06.009.

[57] ——, "Moving horizon estimation for model predictive perimeter control of multi-region MFD networks", in *Transportation Research Board 98th Annual Meeting*, 2019. [Online]. Available: https://trid.trb.org/view/1572773.

[58] ——, "Moving horizon demand and state estimation for model predictive perimeter control of large-scale urban networks", in *18th European Control Conference (ECC)*, IEEE, 2019, pp. 3650–3655. DOI: 10.23919/ECC.2019.8795828.

[59] ——, "Nonlinear moving horizon estimation for large-scale urban road networks", *IEEE Transactions on Intelligent Transportation Systems*, 2019. DOI: 10.1109/TITS.2019.2946324.

[60] ——, "Model-based identification, estimation, and control for large-scale urban road networks", in *19th European Control Conference (ECC)*, IEEE, under review.

[61] ——, "Model predictive control of large-scale urban networks via perimeter control and route guidance actuation", in *55th IEEE Conference on Decision and Control (CDC)*, IEEE, 2016, pp. 6765–6770. DOI: 10.1109/CDC.2016.7799311.

[62] ——, "Integration of perimeter control and route guidance in large-scale urban networks via model predictive control", in *Transportation Research Board 96th Annual Meeting*, 2017. [Online]. Available: https://trid.trb.org/view/1438872.

[63] ——, "Economic model predictive control of large-scale urban road networks via perimeter control and regional route guidance", *IEEE Transactions on Intelligent Transportation Systems*, vol. 19, no. 4, pp. 1112–1121, 2018. DOI: 10.1109/TITS.2017.2716541.

[64] M. Yildirimoglu, I. I. Sirmatel, and N. Geroliminis, "Hierarchical management of heterogeneous large-scale urban networks via path assignment and regional route guidance", in *Transportation Research Board 97th Annual Meeting*, 2018. [Online]. Available: https://trid.trb.org/view/1495726.

[65] ——, "Hierarchical control of heterogeneous large-scale urban road networks via path assignment and regional route guidance", *Transportation Research Part B: Methodological*, vol. 118, pp. 106–123, 2018. DOI: 10.1016/j.trb.2018.10.007.

[66] R. Hermann and A. Krener, "Nonlinear controllability and observability", *IEEE Transactions on Automatic Control*, vol. 22, no. 5, pp. 728–740, 1977. DOI: 10.1109/TAC.1977.1101601.

[67] H. G. Kwatny and G. Blankenship, *Nonlinear Control and Analytical Mechanics: A Computational Approach*, ser. Control Engineering. Birkhäuser Basel, 2000. [Online]. Available: https://www.springer.com/gp/book/9780817641474.

[68] M. N. Chatzis, E. N. Chatzi, and A. W. Smyth, "On the observability and identifiability of nonlinear structural and mechanical systems", *Structural Control and Health Monitoring*, vol. 22, no. 3, pp. 574–593, 2015. DOI: doi.org/10.1002/stc.1690.

[69] M. Diehl, H. J. Ferreau, and N. Haverbeke, "Efficient numerical methods for nonlinear MPC and moving horizon estimation", in *Nonlinear Model Predictive Control: Towards New Challenging Applications*, L. Magni, D. M. Raimondo, and F. Allgöwer, Eds. Berlin, Heidelberg: Springer Berlin Heidelberg, 2009, pp. 391–417. DOI: 10.1007/978-3-642-01094-1_32.

[70] H. G. Bock and K.-J. Plitt, "A multiple shooting algorithm for direct solution of optimal control problems*", *IFAC Proceedings Volumes*, vol. 17, no. 2, pp. 1603–1608, 1984, 9th IFAC World Congress: A Bridge Between Control Science and Technology, Budapest, Hungary, 2-6 July 1984. DOI: 10.1016/S1474-6670(17)61205-9.

[71] M. J. Risbeck and J. B. Rawlings, *MPCTools: nonlinear model predictive control tools for CasADi (Octave interface)*, 2016. [Online]. Available: https://bitbucket.org/rawlings-group/octave-mpctools.

[72] J. A. Andersson, J. Gillis, G. Horn, J. B. Rawlings, and M. Diehl, "CasADi: a software framework for nonlinear optimization and optimal control", *Mathematical Programming Computation*, pp. 1–36, 2018. DOI: 10.1007/s12532-018-0139-4.

[73] A. Wächter and L. T. Biegler, "On the implementation of an interior-point filter line-search algorithm for large-scale nonlinear programming", *Mathematical Programming*, vol. 106, no. 1, pp. 25–57, 2006. DOI: 10.1007/s10107-004-0559-y.

[74] E. L. Haseltine and J. B. Rawlings, "Critical evaluation of extended Kalman filtering and moving-horizon estimation", *Industrial & Engineering Chemistry Research*, vol. 44, no. 8, pp. 2451–2460, 2005. DOI: 10.1021/ie034308l.

[75] L. Ljung, "Prediction error estimation methods", *Circuits, Systems and Signal Processing*, vol. 21, no. 1, pp. 11–21, 2002. DOI: 10.1007/BF01211648.

[76] R. Lamotte and N. Geroliminis, "The morning commute in urban areas: Insights from theory and simulation", in *Transportation Research Board 95th Annual Meeting*, 2016. [Online]. Available: https://trid.trb.org/view/1392730.

[77] L. Ambühl and M. Menendez, "Data fusion algorithm for macroscopic fundamental diagram estimation", *Transportation Research Part C: Emerging Technologies*, vol. 71, pp. 184–197, 2016. DOI: 10.1016/j.trc.2016.07.013.

[78] M. Diehl, H. Bock, H. Diedam, and P.-B. Wieber, "Fast direct multiple shooting algorithms for optimal robot control", in *Fast Motions in Biomechanics and Robotics: Optimization and Feedback Control*, M. Diehl and K. Mombaur, Eds. Berlin, Heidelberg: Springer Berlin Heidelberg, 2006, pp. 65–93. DOI: 10.1007/978-3-540-36119-0_4.

[79] M. Ben-Akiva and M. Bierlaire, "Discrete choice methods and their applications to short term travel decisions", in *Handbook of Transportation Science*, R. W. Hall, Ed. Boston, MA: Springer US, 1999, pp. 5–33. DOI: 10.1007/978-1-4615-5203-1_2.

[80] M. Keyvan-Ekbatani, M. Yildirimoglu, N. Geroliminis, and M. Papageorgiou, "Multiple concentric gating traffic control in large-scale urban networks", *IEEE Transactions on Intelligent Transportation Systems*, vol. 16, no. 4, pp. 2141–2154, 2015. DOI: 10.1109/TITS.2015.2399303.

[81] L. Leclercq, C. Parzani, V. L. Knoop, J. Amourette, and S. P. Hoogendoorn, "Macroscopic traffic dynamics with heterogeneous route patterns", *Transportation Research Part C: Emerging Technologies*, vol. 59, pp. 292–307, 2015. DOI: 10.1016/j.trc.2015.05.006.

[82] G. Mariotte, L. Leclercq, and J. A. Laval, "Macroscopic urban dynamics: Analytical and numerical comparisons of existing models", *Transportation Research Part B: Methodological*, vol. 101, pp. 245–267, 2017. DOI: 10.1016/j.trb.2017.04.002.

[83] R. Lamotte and N. Geroliminis, "The morning commute in urban areas with heterogeneous trip lengths", *Transportation Research Part B: Methodological*, vol. 117, pp. 794 –810, 2018. DOI: 10.1016/j.trb.2017.08.023.

[84] J. D. Little, "A proof for the queuing formula: L = λW", *Operations Research*, vol. 9, no. 3, pp. 383–387, 1961. DOI: 10.1287/opre.9.3.383.

[85] J. Löfberg, "YALMIP: a toolbox for modeling and optimization in MATLAB", in *IEEE International Conference on Robotics and Automation*, 2004, pp. 284–289. DOI: 10.1109/CACSD.2004.1393890.

[86] O. Jahn, R. H. Möhring, A. S. Schulz, and N. E. Stier-Moses, "System-optimal routing of traffic flows with user constraints in networks with congestion", *Operations Research*, vol. 53, no. 4, pp. 600–616, 2005. DOI: 10.1287/opre.1040.0197.

[87] R. Lamotte, M. Murashkin, A. Kouvelas, and N. Geroliminis, "Dynamic modeling of trip completion rate in urban areas with MFD representations", in *Transportation Research Board 97th Annual Meeting*, 2018. [Online]. Available: https://trid.trb.org/view/1497158.

Işık İlber Sırmatel

Graduate researcher

GC C2 385 Station 18
1005 Lausanne
Switzerland
+41 76 671 50 18
+41 21 693 24 84
isik.sirmatel@gmail.com
sirmatel.github.io
⋆ 20.03.1987, İstanbul

Research Interests

Optimal control and estimation, intelligent transportation systems, traffic flow modeling and control, model predictive control, mathematical optimization.

Education

01.2020 **Ph.D., electrical engineering**, *Urban Transport Systems Laboratory (LUTS), École Polytechnique Fédérale de Lausanne (EPFL)*.
Thesis: Optimization-based control, estimation, and identification of urban road transport systems
Supervisor: Prof. Nikolas Geroliminis

06.2014 **M.Sc., mechanical engineering**, *Department of Mechanical and Process Engineering, Eidgenössische Technische Hochschule Zürich (ETH Zürich)*.
Thesis: Adaptive model predictive control of constrained multiple-input multiple-output systems and its application to the quad tank system
Advisor: Prof. Manfred Morari

02.2012 **B.Sc., control engineering**, *Control and Automation Engineering Department, Faculty of Electrical and Electronics Engineering, Istanbul Technical University*.

06.2010 **B.Sc., mechanical engineering**, *Mechanical Engineering Department, Faculty of Mechanical Engineering, Istanbul Technical University*.

Research Experience

since 06.2015 **Graduate student research assistant**, *École Polytechnique Fédérale de Lausanne*.

since 06.2015 **Master thesis supervisor**, *École Polytechnique Fédérale de Lausanne*.
Arseni Fedosseev, *Modeling and control of autonomous taxi fleets in multimodal large-scale urban road networks*, 2018.
Nathalie Sylvie Dufour, *Traffic control for bus bunching - Model formulation and empirical findings from a case study in the city of Fribourg*, 2016.

since 06.2015 **Semester project supervisor**, *École Polytechnique Fédérale de Lausanne*.
Valentin Chevallaz, Máximo Jara, *Simulation, estimation, and control of single line bus transport systems*, 2019.
José R. Rodríguez, Mohamed Detsouli, *Hierarchical optimization and control of heterogeneous large-scale urban networks via perimeter control actuation*, 2017.
Babak H. Bakhtiari, Vittorio Rossati, José R. Rodríguez, *Analysis and control of the bus bunching problem in transportation networks*, 2016.

11.2016– **Visiting researcher**, *University of Southern California*.
02.2017 Topic: Feedback control of freeway systems with variable speed limits
Advisor: Prof. Petros Ioannou

04.2013– **Research intern**, *ABB Corporate Research Center, Germany*.
09.2013 Topic: Advanced self-tuning controllers for motion control solutions

Teaching Experience

since 06.2015 **Graduate student instructor**, *École Polytechnique Fédérale de Lausanne*.
Course: Fundamentals of Traffic Operations and Control, Fall 2016-2017-2018

2018 **Contributor (MOOC development)**, *École Polytechnique Fédérale de Lausanne*.
Course: Introduction to Traffic Flow Modeling and Intelligent Transportation Systems

Honors and Awards

2012 Ranked 2nd/75 at graduation — *B.Sc., control engineering, Istanbul Technical University*

2010 Ranked 1st/160 at graduation — *B.Sc., mechanical engineering, Istanbul Technical University*

Publications

Peer-Reviewed Journal Articles

[J4] I. I. Sirmatel and N. Geroliminis, "Nonlinear moving horizon estimation for large-scale urban road networks," *IEEE Transactions on Intelligent Transportation Systems*, 2019. DOI: 10.1109/TITS.2019.2946324

[J3] M. Yildirimoglu, I. I. Sirmatel, and N. Geroliminis, "Hierarchical control of heterogeneous large-scale urban road networks via path assignment and regional route guidance," *Transportation Research Part B: Methodological*, vol. 118, pp. 106–123, 2018. DOI: 10.1016/j.trb.2018.10.007

[J2] I. I. Sirmatel and N. Geroliminis, "Mixed logical dynamical modeling and hybrid model predictive control of public transport operations," *Transportation Research Part B: Methodological*, vol. 114, pp. 325–345, 2018. DOI: 10.1016/j.trb.2018.06.009

[J1] I. I. Sirmatel and N. Geroliminis, "Economic model predictive control of large-scale urban road networks via perimeter control and regional route guidance," *IEEE Transactions on Intelligent Transportation Systems*, vol. 19, no. 4, pp. 1112–1121, 2018. DOI: 10.1109/TITS.2017.2716541

Journal Articles under Review

[R1] Y. Ren, Z. Hou, I. I. Sirmatel, and N. Geroliminis, "Data driven model free adaptive iterative learning perimeter control for large-scale urban road networks," *Transportation Research Part C: Emerging Technologies*, under review

Journal Articles in Preparation

[P2] I. I. Sirmatel, D. Tsitsokas, A. Kouvelas, and N. Geroliminis, *Modeling, estimation, and control in large-scale urban road networks with remaining travel distance dynamics (to be submitted in June 2020)*

[P1] Y. Zhang, I. I. Sirmatel, F. Alasiri, P. Ioannou, and N. Geroliminis, *Feedback linearization and model predictive control for variable speed limit control (to be submitted in July 2020)*

Refereed Conference Articles

[C9] I. I. Sirmatel and N. Geroliminis, "Moving horizon demand and state estimation for model predictive perimeter control of large-scale urban networks," in *18th European Control Conference (ECC)*, IEEE, 2019, pp. 3650–3655. DOI: 10.23919/ECC.2019.8795828

[C8] I. I. Sirmatel and N. Geroliminis, "Moving horizon estimation for model predictive perimeter control of multi-region MFD networks," in *Transportation Research Board 98th Annual Meeting*, 2019. [Online]. Available: https://trid.trb.org/view/1572773

[C7] Y. Zhang, I. I. Sirmatel, F. Alasiri, P. A. Ioannou, and N. Geroliminis, "Comparison of feedback linearization and model predictive techniques for variable speed limit control," in *21st International Conference on Intelligent Transportation Systems (ITSC)*, IEEE, 2018, pp. 3000–3005. DOI: 10.1109/ITSC.2018.8569430

[C6] I. I. Sirmatel and N. Geroliminis, "Hybrid model predictive control of bus transport systems," in *17th European Control Conference (ECC)*, IEEE, 2018, pp. 1660–1665. DOI: 10.23919/ECC.2018.8550489

[C5] M. Yildirimoglu, I. I. Sirmatel, and N. Geroliminis, "Hierarchical management of heterogeneous large-scale urban networks via path assignment and regional route guidance," in *Transportation Research Board 97th Annual Meeting*, 2018. [Online]. Available: https://trid.trb.org/view/1495726

[C4] I. I. Sirmatel and N. Geroliminis, "Integration of perimeter control and route guidance in large-scale urban networks via model predictive control," in *Transportation Research Board 96th Annual Meeting*, 2017. [Online]. Available: https://trid.trb.org/view/1438872

[C3] I. I. Sirmatel and N. Geroliminis, "Hybrid modeling and predictive control of bus transport systems," in *Transportation Research Board 96th Annual Meeting*, 2017. [Online]. Available: https://trid.trb.org/view/1439090

[C2] I. I. Sirmatel and N. Geroliminis, "Dynamical modeling and predictive control of bus transport systems: A hybrid systems approach," *IFAC-PapersOnLine*, vol. 50, no. 1, pp. 7499 –7504, 2017, Proceedings of the 20th IFAC World Congress. DOI: 10.1016/j.ifacol.2017.08.1067

[C1] I. I. Sirmatel and N. Geroliminis, "Model predictive control of large-scale urban networks via perimeter control and route guidance actuation," in *55th IEEE Conference on Decision and Control (CDC)*, IEEE, 2016, pp. 6765–6770. DOI: 10.1109/CDC.2016.7799311

Extended Abstracts

[E8] I. I. Sirmatel and N. Geroliminis, "Nonlinear model predictive variable speed limit control of freeway systems," in *19th Swiss Transport Research Conference*, Ascona, Switzerland, 2019

[E7] I. I. Sirmatel and N. Geroliminis, "Optimization-based state estimation for perimeter controlled large-scale urban road networks," in *7th symposium arranged by European Association for Research in Transportation*, Athens, Greece, 2018

[E6] I. I. Sirmatel and N. Geroliminis, "Hybrid model predictive control of public transport operations," in *18th Swiss Transport Research Conference*, Ascona, Switzerland, 2018

[E5] I. I. Sirmatel and N. Geroliminis, "Moving horizon estimation for large-scale urban networks," in *17th Swiss Transport Research Conference*, Ascona, Switzerland, 2017

[E4] I. I. Sirmatel and N. Geroliminis, "Combined estimation and control of large-scale urban road networks: A real-time optimization based approach," in *6th symposium arranged by European Association for Research in Transportation*, Haifa, Israel, 2017

[E3] I. I. Sirmatel and N. Geroliminis, "Nonlinear model predictive control of large-scale urban networks with perimeter control and route guidance systems," in *19th EURO Working Group on Transportation Meeting*, Istanbul, Turkey, 2016

[E2] I. I. Sirmatel and N. Geroliminis, "Model predictive control of urban networks with perimeter control and route guidance," in *16th Swiss Transport Research Conference*, Ascona, Switzerland, 2016

[E1] I. I. Sirmatel and N. Geroliminis, "Hybrid dynamical modeling and control of public transport systems," in *5th symposium arranged by European Association for Research in Transportation*, Delft, The Netherlands, 2016

Training Courses

11.2016 **Short Course on Dynamic Traffic Flow Modeling and Control**.
Technical University of Crete
Instructor: Prof. Markos Papageorgiou

01.2016 **Instructional/Teaching Skills Workshop**.
École Polytechnique Fédérale de Lausanne
Instructor: Dr. Siara Ruth Isaac

Research Projects

since 06.2015 **METAFERW - Modeling and controlling traffic congestion and propagation in large-scale urban multimodal networks**.
Sponsor: European Research Council

2016 **Modeling, demand calibration, and control of bus transport systems - A case study in the city of Fribourg**.
Sponsor: Fribourg Public Transportation Company (TPF)

Academic Services

Reviewer (Journals)

Control Engineering Practice

IEEE Access

IEEE/CAA Journal of Automatica Sinica

IEEE Transactions on Control Systems Technology
IEEE Transactions on Intelligent Transportation Systems
IEEE Intelligent Transportation Systems Magazine
Systems and Control Letters
Transportation Research Part B: Methodological
Transportation Research Part C: Emerging Technologies
Transportmetrica A: Transport Science

Reviewer (Conferences)

European Control Conference
IEEE International Conference on Intelligent Transportation Systems
IFAC Symposium on Control in Transportation Systems
IFAC IFAC Workshop on Control of Transportation Systems

Skills

language Turkish, English, German
software MATLAB, Mathematica, Aimsun, Python, LaTeX